8-2005

Influence of Uncorrelated Defects on the Vortex Phase Diagram in $YBA_2Cu_3O_{7-6}$ Superconducting System

Lucian M. Undreiu
Western Michigan University

INFLUENCE OF UNCORRELATED DEFECTS ON THE VORTEX PHASE DIAGRAM IN $YBA_2Cu_3O_{7-\delta}$ SUPERCONDUCTING SYSTEM

by

Lucian M. Undreiu

A Dissertation
Submitted to the
Faculty of The Graduate College
in partial fulfillment of the
requirements for the
Degree of Doctor of Philosophy
Department of Physics
Dr. Lisa Paulius, Advisor

Western Michigan University
Kalamazoo, Michigan
August 2005

INFLUENCE OF UNCORRELATED DEFECTS ON THE VORTEX PHASE DIAGRAM IN $YBA_2Cu_3O_{7-\delta}$ SUPERCONDUCTING SYSTEM

Lucian M. Undreiu, Ph.D.

Western Michigan University, 2005

The goal of our work is to gain more insight into the vortex dynamics in $YBa_2Cu_3O_{7-\delta}$ single crystals with point defects induced by 9MeV proton irradiation. The position of the critical points from the first order melting transition line can be shifted in a controlled manner with the induced disorder. In order to accomplish a comparative study, different crystals and irradiation doses were used. The results were correlated using both electrical transport and ac specific heat measurements. Special attention was given to investigating the nature of the vortex state below the lower critical point of the first order vortex melting transition.

Four $YBa_2Cu_3O_{7-\delta}$ single crystals were used in the investigation with the purpose of establishing how universal the response to proton irradiation is. While the initial conditions of the crystals varied, we were able to obtain a consistent picture of the evolution of the vortex matter behavior as a function of irradiation.

The introduction of a sufficiently high density of random point disorder is theoretically predicted to induce the presence of the vortex glass or a vortex molasses in the system. Vortices are predicted to become fixed in a random pattern with no long-range positional order. In this case, the first order melting transition is replaced by a second order phase transition and critical scaling behavior is expected in the

vicinity of transition.

One of the purposes of this study is to determine the nature of the vortex matter below lower critical point. To this end we searched for the signatures of the vortex glass and vortex molasses states. Although our specific heat results indicated the presence of a second order phase transition, our scaling attempts were not consistent with the presence of either the vortex glass or vortex molasses states. Therefore, the nature of vortex matter in this region of the vortex phase diagram remains elusive.

NOTE TO USERS

ACKNOWLEDGMENTS

First of all I would like to thank my research advisor, Dr. Lisa Paulius. As graduate student, I was fortunate to have the best support from my supervisor: a well defined equilibrium between guidance and help. Dr. Lisa Paulius always knew how to motivate me by presenting the research projects in an interesting manner and stimulating curiosity and scientific effervescence. The time I spent in the laboratory I was introduced to low temperature physics and low signal measurements. I have benefited greatly from the many useful discussions we have had. I have to show all my gratitude for the trust invested in me. I always had the second chance in case I did not succeed first time. I always received encouragements and with patience I was able to gain confidence, which is so precious in the difficult effort leading to a doctoral degree.

Having the privilege to travel and experience different cultures and scientific environments, being exposed to diverse educational systems as a researcher, I was fortunate to meet people with extraordinary abilities in their field of research, but nevertheless with exceptional human qualities. I would like to thank Dr. Wai Kwok and Dr. Christophe Marcenat for hosting me at their laboratories and for all their great help and advice.

I would like to express my appreciation to my committee members, Dr. Clement Burns, Dr. Arthur McGurn and Dr. Wai Kwok for many helpful discussions and for reviewing this dissertation.

I am grateful to Prof. Dean Halderson for his precious advice throughout my study years. Among others at our department I want to mention Dr. Steve Ferguson,

Mr. Rick Welch and Mr. Allan Kern for their friendly assistance in setting up the experimental apparatus.

I can not express in words enough gratitude to my mother, Valeria, to my wife, Adriana and to my son, Vlad, for their unconditional love and support.

Lucian M. Undreiu

TABLE OF CONTENTS

Table of Contents—Continued

Table of Contents—Continued

LIST OF TABLES

LIST OF FIGURES

List of Figures-Continued

CHAPTER I

INTRODUCTION

1.1 Superconductivity: Basic Concepts

When it was discovered in 1911[1], superconductivity was described as a phenomenon characterized by a sudden loss of the electrical resistivity for temperatures below what became known as the superconducting critical temperature, T_c. First observed in Hg with a $T_c = 4.2K$, it was later discovered in a wide range of other materials, including the shaded elements shown in Figure 1.

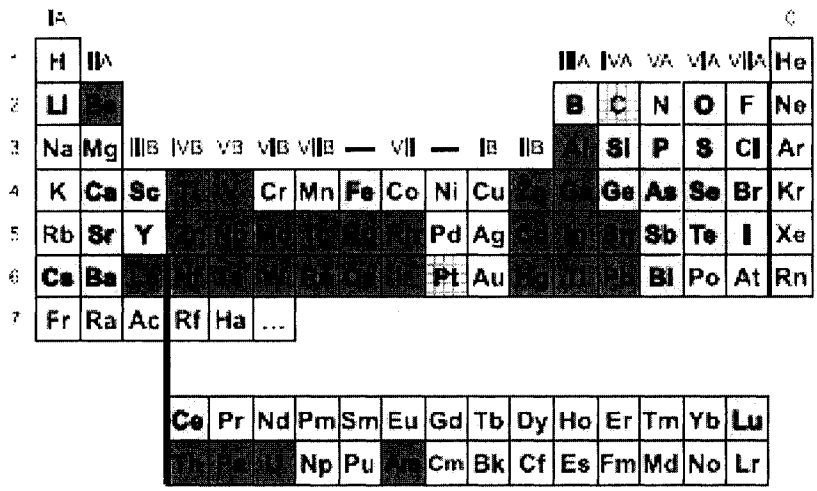

Figure 1 Periodic Table showing superconducting elements: the dark grey background denotes elements known to become superconducting, while the lighter grey background refers to those elements that need special conditions (such as higher pressure) to show superconductivity. All marked elements exhibit bulk superconductivity except platinum (compressed powder) and carbon (nanotubes). Good metals such as Cu, Ag and Au do not superconduct.

A major advance in understanding superconductivity was made by W. Meissner and R. Ochsenfeld[2] when they showed that a superconductor expels an applied magnetic field. This is known as the Meissner effect, sometimes referred to as perfect diamagnetism, and represents a basic property of the superconducting state. It marks the distinction between a perfect conductor and a superconductor. Unlike a perfect conductor, a superconductor can be described by thermodynamics. Because it takes energy to expel the external magnetic field, the superconducting state is destroyed if the applied magnetic field is larger than a critical value, H_c, known as the thermodynamic critical field. Superconductivity can also be destroyed by applying a high current density, larger than a critical value, J_c .The existence of a critical field directly implies the existence of a critical current because of the self field a current generates. Therefore, superconductivity is confined to a limited T-H-J space.

In applied magnetic fields, the superconducting transition is a first order phase transition and is accompanied by a jump in specific heat, an effect first observed in 1932[3]. The distinctive indication of a first order transition is a discontinuity in the first derivative of the free energy. Since the entropy is the negative of the derivative of the Gibbs free energy with respect to temperature, $s = -(\partial g/\partial T)$, a peak in the entropy at the transition signals its first order nature (here s and g denote the entropy and the Gibbs free energy per unit volume, respectively). In the absence of an applied magnetic field, there is no latent heat of transition the phase transition is second order.

One of the first indications[4,5] that electron-phonon interactions are vital in understanding superconductivity arose in 1950 with the discovery of the isotope effect. It was discovered that the transition temperature depends on the mass of the atoms. In other words, samples made from different isotopes of the same element

will be characterized by different critical temperatures. The empirical law governing the relationship between T_c and the mass of the isotope is $T_c \propto M^{-1/2}$, where M is the mass of the isotope.

1.2 Theoretical Explanation of Superconductivity

The efforts to explain superconductivity can be separated into three main categories: 1) the phenomenological theories, 2) the mixed quantum mechanics-phenomenological theory and 3) the microscopic theory.

The first to explain the Meissner effect was the London theory[6], which was based on phenomenological arguments. Circulating supercurrents at the surface of the superconductor were the key used to explain the expulsion of the external magnetic field. But the exclusion of the field is not absolute. The field penetrates a thin surface layer of the sample, over a distance called the London penetration depth, λ. The London equations are a combination of Maxwell's equations and a postulated proportionality between the density of supercurrents and the vector potential. They describe both perfect conductivity (1.1) and perfect diamagnetism (1.2):

$$\mathbf{E} = \frac{\partial}{\partial t}(\Lambda \mathbf{J}) \tag{1.1}$$

$$\nabla \times \mathbf{J} = -\frac{1}{\Lambda} \cdot \mathbf{B}, \tag{1.2}$$

where **E** is the electric field, **J** the supercurrent density, **B** the magnetic induction and $\Lambda = \mu_0 \lambda^2$. The London penetration depth λ is the length scale over which the magnetic field exponentially decays as it penetrates the interior of the superconductor (see Figure 2). The expression for the decay of the magnetic field below the sample's

surface can be easily derived from the London Equations:

$$B(x) = B(0) \exp(-\frac{x}{\lambda}) \qquad (1.3)$$

As evidenced in equation 1.2, the magnetic field intensity and the current density at the surface of a superconductor are directly related. This relationship can also be extended for the case of critical values: a magnetic field with magnitude H_c at the surface of the sample will generate a critical current density J_c and vice versa. The concept of a critical current is very important because of its implications for the technological applications of superconductors.

The London theory is a weak field theory because λ depends on the magnitude of the magnetic field (which is not predicted by London's equations). It is also a classical theory, treating the electric charge carriers without taking in account the quantum effects.

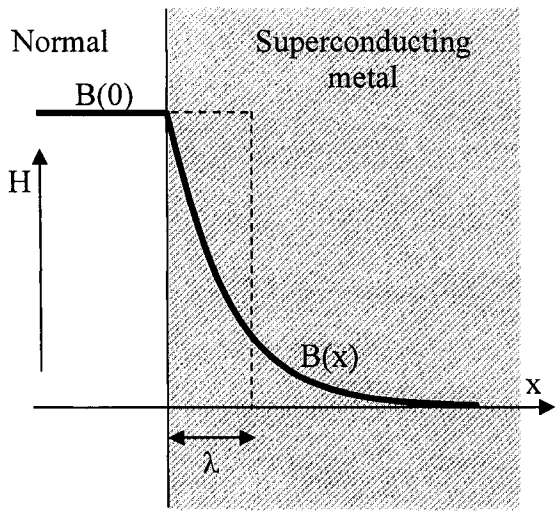

Figure 2 Profile of the magnetic flux penetrating inside a superconducting sample.

The first theory to successfully address quantum effects was the Ginzburg-Landau (GL) theory. The main innovation was the introduction of the order parameter, included as a pseudo-wave function $\psi(\mathbf{r}) = |\psi(\mathbf{r})|e^{i\varphi(r)}$. The order parameter relates to the symmetry difference between the superconducting and normal states. The low temperature phase has a reduced symmetry, and is therefore more ordered. Furthermore, the transition at T_c is discontinuous and is considered to be a second order phase transition[7] in the absence of an applied magnetic field.

GL theory argued that superconductivity can be explained only if the electric charge carriers are somehow different from normal electrons, referring to them as superelectrons. Also, the theory predicts that close to the transition temperature the free energy can be expanded in terms of superelectron density, or $|\psi(\mathbf{r})|^2$:

$$g_s = g_n + \alpha|\psi(\mathbf{r})|^2 + \frac{\beta}{2}|\psi(\mathbf{r})|^4 \qquad (1.4)$$

where g_s and g_n are the Gibbs free energies (per unit volume) for the superconducting and normal states, and α and β are expansion coefficients.

Showing that the superconducting state is more stable than the normal state leads to minimizing the g_s value. The solution of (1.4) is given by the GL equations: the first equation is a non-linear Schrodinger type equation while the second gives the expression for the supercurrent. Each equation has a corresponding characteristic length scale. The scale of the decay of the magnetic field is the GL penetration depth $\lambda(T)$, closely related to London's λ. The scale of the order parameter is the coherence length $\xi(T)$, which is the spatial variation of the order parameter (see Figure 3).

The reaction of a superconductor exposed to an external magnetic field is to produce superconducting shielding currents that generate a negative magnetization to

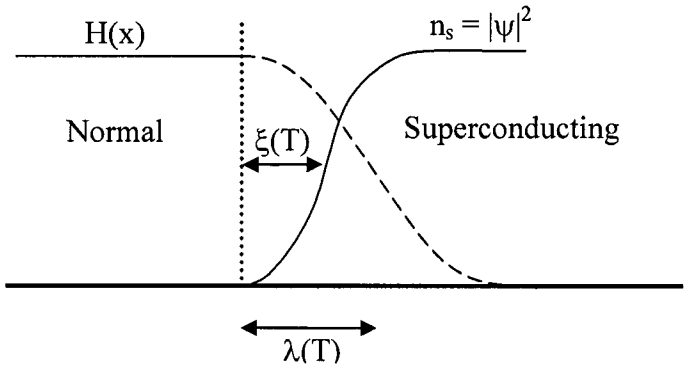

Figure 3 Normal to superconducting state interface. The concepts of the two characteristic length, penetration depth and coherence length are shown.

cancel out the field inside the sample, $M = - H_{ext}$. As Figure 4 shows, the free energy of a superconductor increases due to its response to applied magnetic fields. The thermodynamic critical field is associated[7] with the free energy difference between the normal and superconducting states:

$$g_n(T) - g_s(T) = \frac{1}{2}\mu_0 H_c^2(T), \qquad (1.5)$$

while the GL result relates the critical field with the two length scale: $H_c(T) \propto \phi_0/\lambda\xi$. The temperature dependence of the critical field is given by an empirical expression:

$$H_c(T) = H_c(0)[1-(T/T_c)^2] \qquad (1.6)$$

The validity of the GL theory is also limited: the solutions are only true near the critical temperature T_c because the free energy describing the superconducting state is given by the series expansion of the order parameter around T_c.

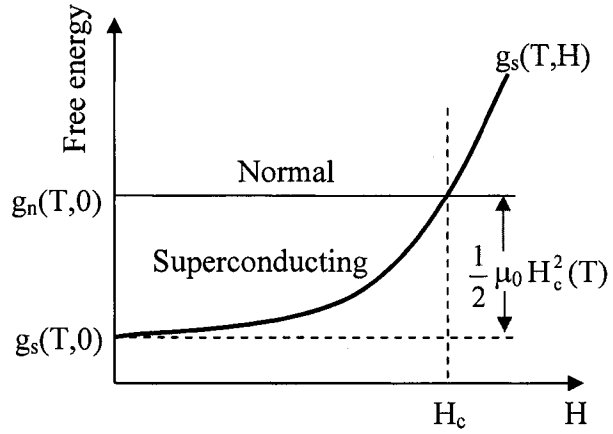

Figure 4 Free energy for the normal and superconducting states as a function of the external applied magnetic field.

A clear explanation of the physical mechanism of superconductivity came in 1957 with the microscopic theory of superconductivity[8] developed by Bardeen, Cooper and Schrieffer (BCS theory). The most important contribution of BCS model deals with the superconducting charge carriers. They showed that an attractive interaction can lead the electrons to form bound pairs, known as Cooper pairs. The Cooper pairs are characterized by a lower free energy than the normal, unpaired electrons. As a consequence, a gap in the electronic density of states will open at the Fermi surface. Similar to the band gap in semiconductors, electrons are forbidden to have energies within 2Δ around E_F, where $\Delta \propto \psi$ (order parameter in the GL theory) and E_F is the Fermi energy. The BCS theory predicts that the energy of the gap at 0K is $E_g(0) = 3.5k_BT_c$.

In terms of the BCS model, the electrons are correlated in Cooper pairs for an average time τ_s (phase-breaking time) and over a correlation length, ξ. The cause for the attractive potential, as was suggested by the isotope effect, is the electron-phonon interaction. A schematic illustration of the pairing mechanism is offered in Figure 5.

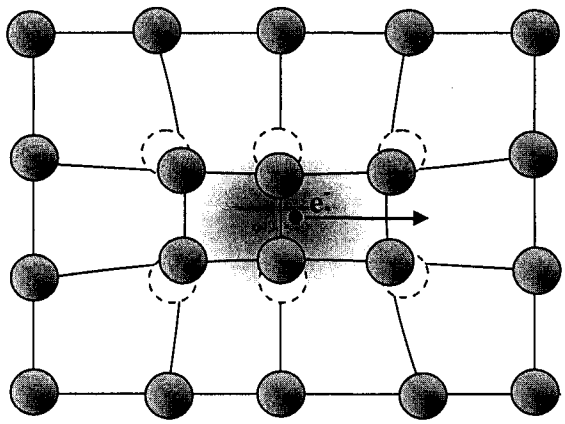

Figure 5 Cooper pair formation. If an electron is moving through a lattice of positive ions, its wake will create a distortion of the lattice manifested in a series of displaced ions. A second electron will be attracted by the region of higher positive charge (ions) density which will lead to pairing with the first electron.

1.3 Type I and Type II Superconductors

A useful number is the Ginzburg-Landau parameter which is the ratio of the two relevant length scales:

$$\kappa = \frac{\lambda}{\xi} \tag{1.7}$$

The temperature dependence of the penetration depth is depicted in Figure 6. The value of the ratio given by equation (1.7) is used to classify superconductors. In 1957, the same year as the BCS theory, Abrikosov[9] argued that $\kappa > 1/\sqrt{2}$ designated a novel class of superconductors (type II) that can respond to external magnetic fields in a new way. In contrast with type I superconductors ($\kappa < 1/\sqrt{2}$), which are perfect diamagnets up to the thermodynamic critical field H_c, type II superconductors can

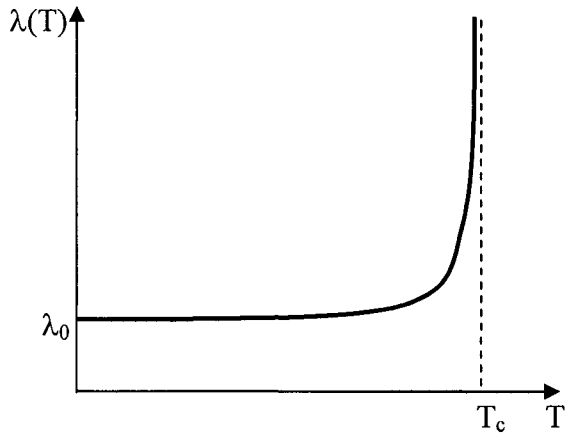

Figure 6 Variation with temperature of penetration depth. The dependence is observed to follow an expression close to: $\lambda(T) \cong \lambda(0)[1 - (T/T_c)^4]^{-1/2}$. The coherence length follows the temperature dependence in the same way as λ.

allow the applied magnetic field to pass through. From the energetic point of view, for a type II superconductor it is more favorable to split into a mixture of normal and superconducting regions. Superconducting elements are typically type I superconductors and superconducting alloys are typically type II.

The explanation of this different reaction of superconductors to applied magnetic fields lies in the understanding of the energy implications that arise from the formation of superconductor to normal interface. The formation of the boundary involves the appearance of an extra energy, called surface energy, in analogy with the surface tension between a liquid and its vapors. If this additional contribution to the Gibbs free energy is positive, overall, the energy will decrease proportional with the area of interphase boundary. Consequently, energy will be minimized by sample's exclusion of the field which corresponds to a minimum interphase area. On the other hand, if the surface energy is negative, formation of split, normal-superconducting domains will decrease the total free energy. Further explanation regarding the significance of G-L parameter will be given in the next chapter.

The way magnetic field enters a type II superconductor is not continuous, but rather in the form of vortices, discrete bundles of flux, also called flux quantum. The unit of flux is:

$$\phi_0 = \frac{h}{2e} \cong 2 \times 10^{-15} \text{ Vs} \qquad (1.8)$$

The presence of a charge q = 2e in the flux quantum expression represents strong evidence for the Cooper pair as the charge carrier in a superconductor.

The appearance of the normal cores generates two effects: a local increase of the free energy as energy is spent to break up the Cooper pairs inside the core, and a local decrease of the free energy as the core ceases to exhibit diamagnetism. In terms of free energy per unit length of flux line (vortex), the term $\pi\xi^2 \cdot 1/2\mu_0 H_c^2$ represents the energy increase resulting from the loss in electron order, while $\pi\lambda^2 \cdot 1/2\mu_0 H_c^2$ is the energy drop due to the penetration of the core by the magnetic field. Comparison of the two competing energy effects reduces more or less to a comparison of the coherence length, ξ with the penetration depth, λ. The overall contribution to the Gibbs free energy, identified as surface energy, is negative if $\xi < \lambda$. This explains why the G-L parameter, which is the ratio between the two characteristic lengths (equation 1.7), is used as a classification criterion for the superconductors.

Type I superconductors will become normal above H_c and the magnetic field will penetrate the entire sample. In contrast, type II superconductors will enter into a mixed state above a lower critical field, H_{c1}, where the magnetic field starts penetrating the sample in quantized bundles, known as vortices. The core of the vortex is in the normal state, while the rest of the sample remains in the superconducting state. The vortex system arranges itself into a triangular lattice,

characterized by a state of lower energy. The inter-vortex spacing is given by $a_0 \cong (\Phi_0/B)^{1/2}$.

As the applied field is increased, the distances between adjacent vortices decreases until the cores overlap at the upper critical field H_{c2}, where the entire sample is in the normal state. Thus, a type II superconductor is described by two critical fields: the lower critical field H_{c1} separating Meissner state from the mixed state and the upper critical field H_{c2} which defines the border between the mixed and normal states.

A good way to compare the properties of the two types of superconductors is through the magnetic phase diagram. The type I superconducting phase is bounded by three parameters: the critical temperature T_c, critical field H_c and critical current density J_c, and can be destroyed by raising either the temperature , the magnetic field, or the current above these critical values. The most commonly used phase diagram is magnetic field vs temperature or H-T diagram –as shown in Figure 7 a) and b) for a type I and type II superconductor, respectively.

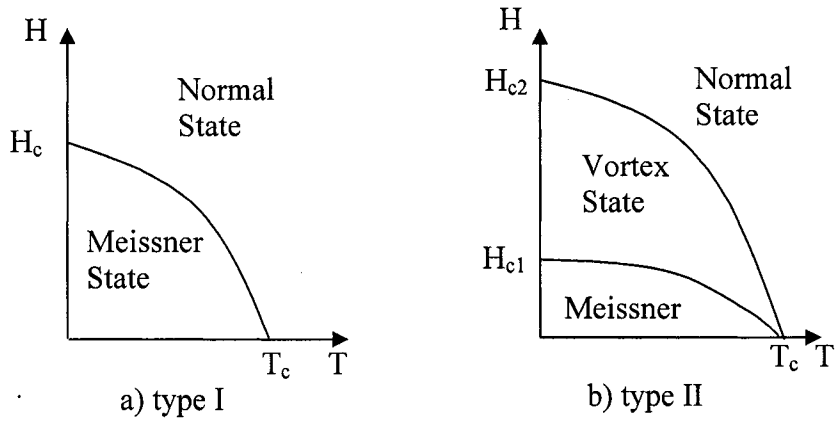

Figure 7 Magnetic phase diagrams. a) a type I superconductor will completely exclude the magnetic field if $H < H_c$; b) for the type II superconductor vortex state exists between the lower and upper critical field.

1.4 High-T_c Superconductors

In 1986 the field of superconductivity was shaken by a remarkable discovery: the breaking of what was thought to be an upper limit for the superconducting critical temperature. Bednorz and Muller were able to create a ceramic compound with $T_c \cong$ 30K, the highest critical temperature up to that time[10]. The discovery produced a chain-reaction in the scientific community and soon new materials were found with T_c > 90K[11]. The new superconducting materials, also called copper-oxides or cuprates, were considered remarkable not just for their high critical temperature, but because they are ceramics, which are normally insulators. With some noticeable exceptions (such as the surprising MgB_2)[12], the common feature of high-T_c superconductors (HTS) is the existence of the CuO_2 planes, generally regarded as the place where superconducting conduction occurs. The work in this dissertation is focused on the $YBa_2Cu_3O_{7-\delta}$ system. The layered systems are constructed of alternating conduction and binding slabs. In the case of $YBa_2Cu_3O_{7-\delta}$ (YBCO) single crystal the binding slabs, seen as charge reservoirs, are the two BaO bridging layers separated by CuO-chain layers (see Figure 8). The structure was determined through X-ray[13] and neutron diffraction[14,15].

The immediate consequence of the cuprate's layered structure is the high anisotropy, which translates into dissimilar properties (e.g. electric) along different crystal directions. For these HTS, or extreme type II superconductors, the typical value of GL parameter is $\kappa \sim 100$, in other words the magnetic field enters the sample almost without disturbance at high fields (large λ), while superconductivity may be confined only within the conduction layers at low temperatures (short ξ). This has a profound effect on the vortex matter properties and therefore on the magnetic phase diagram.

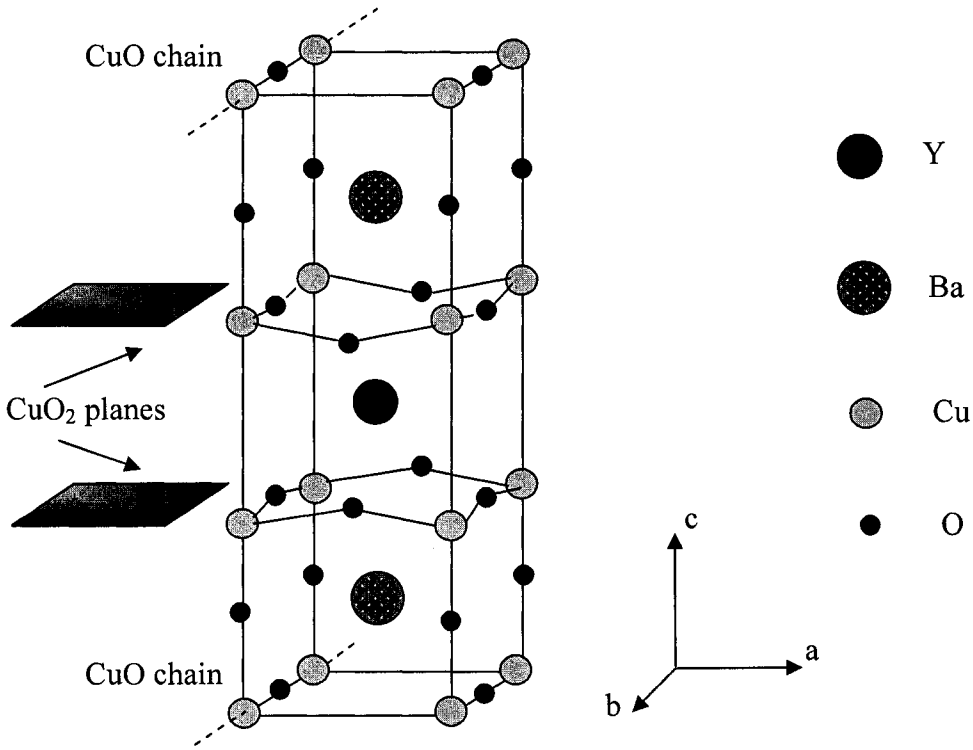

Figure 8 The crystal structure of $YBa_2Cu_3O_{7-\delta}$ (atoms size is not to scale). For $\delta < 0.65$ (oxygen deficiency mainly taken from CuO chains) the structure is orthorhombic. The size of the unit cell, for an optimally doped ($\delta \cong 0.09$) YBCO is a = 3.82Å, b = 3.89 Å and c = 11.68 Å.

As discussed further in the following chapters, the strong anisotropy, large GL parameter, together with relatively large thermal fluctuations add considerable complexity to the phase diagram. The strong thermal fluctuations are the consequence of high T_c, short coherence length and large anisotropy. The interplay between thermal fluctuations, pinning disorder and repulsive vortex-vortex interactions will have a decisive role in controlling the nature of the vortex system. HTS will distinguish themselves among the other type II superconductors by the appearance of a vortex lattice melting transition inside the vortex mixed state.

1.5 Applications

Practical applications of the superconductivity phenomenon were first guided by its basic definition: to carry electrical current without losses. Therefore, the initial projects were built mainly with the intention to save energy: motors, transmission lines and energy storage magnets. Two main obstacles prevented the quick development of superconductor materials capabilities: first one is obvious- the very low temperatures of operation require complex and costly refrigeration processes, while the second obstacle regards the property of a superconductor to self-destroy its state by creating powerful enough magnetic fields.

Type II superconductors, because of their ability to allow the flux lines to pass through, can be exposed to much higher magnetic fields, which makes them more suitable for practical applications[16]. Such conventional type II superconductors (typically NbTi or Nb_3Sn), or low temperature superconductors (LTS), are integrated into powerful magnets and electric resonators used in big particle accelerators such as CERN and Fermilab. Other uses for LTS include magnetic-levitated transport vehicles, electric generators, transformers and fault current limiters, but maybe the most impressive application, with a huge impact on human life is magnetic resonance imaging, or MRI. Powerful magnetic fields interact with atoms and molecules that exist in the human body and based on the energy exchanged in that process can produce high quality images of the inside of the human body[17,18,19].

After almost two decades from the moment high T_c superconductors (HTS) were discovered, promising new applications emerged in areas such as wireless communications[20], digital electronics[21] or magnetometry[22]. The successes achieved with HTS small-scale devices rely on the special properties associated with weak links, especially the Josephson quantum tunneling effects. This quantum

phenomenon, first predicted by Josephson[23] is described in terms of Cooper pairs tunneling through a thin insulating layer that separates two superconductors. A zero voltage supercurrent should flow through a thin insulating layer which separates two superconducting regions. Superconducting quantum Interference device (SQUID) consists of two parallel Josephson junctions able to detect and measure very weak magnetic fields. SQUID principle is based on recording small current variations caused by changes in the external magnetic field. With incredible sensitivity (able to detect magnetic fields 100 billion times smaller than the Earth's field), this small-scale device can observe the magnetic fields generated by human brain or heart or can be used to map magnetic anomalies in search for mineral deposits in Earth's crust.

The development of HTS technology can be compared, time wise, with implementation of similar complex new materials such as optical fibers and gallium arsenide semiconductors[24], but as R. Schrieffer reasoned decades ago, there are important applications of superconductors that were not yet considered.

References

[1] H. K. Onnes, 120b, 122b, 124c (1911)

[2] W. Meissner and R. Ochsenfeld, Naturwiss. **21**, 787 (1933)

[3] W. H. Keesom and J. A. Kok, Comm. Phys. Lab. Leiden **221**, 27 (1932)

[4] E. Maxwell, Phys. Rev. **78**, 477 (1950)

[5] C. A. Reynolds, B. Serin, W. H. Wright and L. B. Nesbitt, Phys. Rev. **78**, 487 (1950)

[6] F. London and H. London, Proc. Roy. Soc. (London) A **149**, 71 (1935)

[7] L. D. Landau, E. M. Lifshitz, Statistical Physics, 3rd edition., part **1**, English translation: Pergamon Press, Oxford (1980)

[8] J. Bardeen, L. N. Cooper, and J. R. Schrieffer, Phys. Rev. **106**, 162 (1957)

[9] A. A. Abrikosov, Zh. Éksp. Teor. Fiz. **32**, 1442 (1957); English translation: Sov. Phys. –JETP **5**, 1174 (1957)

[10] J. G. Bednorz and K. A. Müller, Z. Phys. B **64**, 189 (1986)

[11] M. K. Wu, J. R. Ashburn, C. J. Torng, P. H. Hor, R. L. Meng, L. Gao, Z. J. Huang, Y. Q. Wang and C. W. Chu, Phys. Rev. Lett. **58**, 908 (1987)

[12] J. Nagamatsu, N. Nakagawa, T. Muranaka, Y. Zenitani, J. Akimitsu, Nature **410** , 63-64 (2001)

[13] R. J. Cava, B. Batlogg, R. B. v Dover, D. W. Murphy, S. Sunshine, T. Siegrist, J. P. Remeika, E. A. Rietman, S. Zakurak, and G. P. Espinosa, Phys. Rev. Lett. **58**, 1676 (1987)

[14] M. A. Beno, L. Soderholm, D. W. Capone, D. G Hinks, J. D. Jorgensen, J. D. Grace, I. K. Schuller, C.U. Segre, and K. Zhang, Appl. Phys. Lett. **51**, 57 (1987)

[15] J. J. Capponi, C. Chaillout, A. W. Hewat, P. Lejay, N. Marezio, N. Nguyen, B. Raveau, J. L. Soubeyroux, J. L. Tholence and R. Tournier,

Europhys. Lett. **3**, 1301 (1987)

[16] J. E. Kunzler, E. Buehler, F. S. L. Hsu, and J. H. Wernick, Phys. Rev. Lett. **6**, 89–91 (1961)

[17] R.V. Damadian, Science **171**, 1151 (1971)

[18] P.C. Lauterbur, Nature **242,** 190-191 (1973)

[19] K. K Kwong, J. W. Belliveau, D. A. Chesler, I. E. Goldberg, R. M. Weisskoff, B. P. Poncelet, D. N. Kennedy, B. E. Hoppel, M. S. Cohen, R. Turner, H. -M Cheng, T. J. Brady, B. R. Rosen., Proc. Natl. Acad. Sci. **89,** 5675 (1992)

[20] E. R. Soares, K. F. Raihn, A. A. Davis, R. L. Alvarez, P. Marozick and G. L. Hey-Shipton, IEEE Trans. Appl. Supercond., **9** 4018-4021 (1999)

[21] D Winkler, Supercond. Sci. Technol. **16** 1583-1590 (2003)

[22] C. P. Foley; K. E. Leslie; R. Binks; C. Lewis; W. Murray; G. J. Sloggett; S. Lam; B. Sankrithyan; N. Savvides; A. Katzaros; K. -H. Muller; E. E. Mitchell; J. Pollock; J. Lee; D. L. Dart; R. R. Barrow; M. Asten; A. Maddever.; G. Panjkovic; M. Downey; C. Hoffman; R. Turner, Applied Superconductivity **9,** 3786 – 3792 (1999)

[23] B. D. Josephson, Phys. Lett. **1**, 251 (1962)

[24] A.P. Malezemoff, J. Mannhart, D. Scalapino, Physics Today **58**, 4 (2005).

CHAPTER 2

VORTEX PHYSICS

2.1 Introduction

A vortex is a filament of magnetic flux which is quantized with a unit of magnetic flux $\phi_0 = h/2e$ that penetrates the sample. It is generated by supercurrents circling the normal conducting core. The extent of the normal core, ξ, and the range the field extends into the surrounding superconductor, λ, are the defining parameters of a vortex (see Figure 9). As pointed out in Chapter 1, the superconducting order parameter decays from the edge of the core over a characteristic length, the coherence length, ξ, while the magnetic field is at its maximum in the center of the core and decays over the penetration depth, λ.

The mixed state, or vortex state, exists if the magnetic field is above H_{c1}. The field at which the flux starts to enter the material is H_{c1}, the lower critical field. This field can be deduced[1,2] from the condition that the free energy of the superconductor should be equal with or without the first penetrating flux line inside:

$$H_{c1} = \frac{\phi_0}{4\pi\mu_0\lambda^2}\ln\frac{\lambda}{\xi} \qquad (2.1)$$

As the externally applied magnetic field is increased, the vortex density increases proportional with the magnetic field strength and therefore so does the intensity of vortex-vortex interactions. For vortices with the same orientation the interaction is repulsive. This causes the vortex system to arrange itself into a

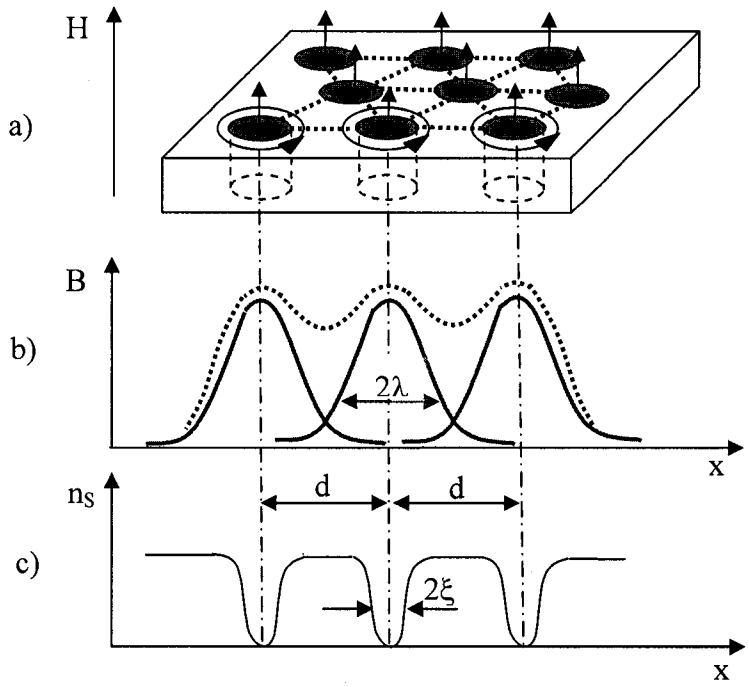

Figure 9 Neighboring vortices in a superconductor. a) Mixed state in applied magnetic field. The magnetic flux penetrating the sample is represented by the vertical arrows; the normal cores are encircled by supercurrents. b) Variation with position of flux density for individual vortices (solid curves) and total flux density (dashed curve). c) Variation with position of concentration of superelectrons n_S (n_S vanishes in the middle of the vortex cores).

triangular (hexagonal) lattice, also called the Abrikosov lattice[3], which minimizes the energy of the system. The field dependence of the inter-vortex distance is $a_0 \cong (\phi_0/B)^{1/2}$.

H_{c2}, or the upper critical field, is the field value for which the vortices overlap each other as the vortex lattice spacing becomes of the order of the coherence length. In analogy with (2.1) a connection between H_{c2} and ξ can be established:

$$H_{c2} = \frac{\phi_0}{2\pi\mu_0\xi^2} \qquad (2.2)$$

The two critical fields depend on temperature in the same manner as the thermodynamic critical field and are connected with H_c through the following relation:

$$H_{c2} \cong \kappa H_c \cong \kappa^2 H_{c1} \qquad (2.3)$$

In the case of HTS ($\kappa >> 1$) the vortex lattice can be easily deformed by thermal fluctuations so that it can melt into a vortex liquid (see Figure 10). While a superconductor is described by a state with the lowest energy, the existence of the thermal energy (~kT) will impose fluctuations of the energy. Other low energy states will become available and, even for currents less than J_c, a finite resistance will appear below T_c. The identification of $H_{c2}(T)$ becomes ambiguous for HTS as the resistivity transition broadens in magnetic field.

Furthermore, as we describe in more detail in the next section, vortex motion can be induced by the Lorentz force if an electrical current is passed through the

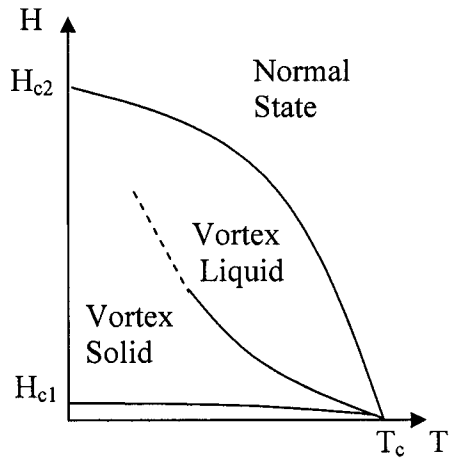

Figure 10 Simplified vortex phase diagram for HTS superconductors. In this extreme type II case ($\kappa >> 1$) the vortex phase is split between a solid and a liquid phase.

sample. On the other hand, vortex motion can be inhibited due to pinning exerted by crystal defects or disorder. Because vortex motion causes dissipation, stopping this flux flow becomes an objective of great importance. A very useful technique is to enhance pinning by inducing defects in the superconducting sample and one way to realize this is by irradiation.

Competition between vortex-vortex interactions, thermal fluctuations and pinning due to defects, added to the fact that vortices are elastic and can bend, gives rise to a very complicated system for the vortex matter. Consequently, the vortex phase diagram represents a fascinating research subject.

Several investigation techniques have been used in order to probe the structure of the vortex system. To locate individual vortices and image the Abrikosov lattice the following experimental methods were utilized:

- Bitter pattern decorations[4,5] small magnetic particles are evaporated in the proximity of the sample and preferentially stick to its surface in the regions where magnetic field is present. The technique is used at low fields (few Gauss) and appear to be relevant at very low temperatures (4.2K)[5]. Double sided Bitter decorations allow the observation of vortex correlations.
- scanning tunneling microscopy or STM[6,7]-electronic tunneling between the sample and a finely sharpened tip to create a two-dimensional map of electronic density variations at the surface of the sample (see Figure 11). This method can be exploited for the full range of magnetic fields, but is difficult to use for highly anisotropic superconductors (such as BSCCO), even at very low temperatures. STM was able to detect single vortices, but the method is not suitable for very large areas.
- magnetic force microscopy[8] - magnetic interaction exerted on a magnetic tip can

be translated into images of magnetic domains at the surface of the sample. This is a very sensitive and flexible technique, able to image single vortices under different conditions (temperature and magnetic field);

- scanning SQUID microscopy[9,10] uses an integrated SQUID magnetometer as a magnetic field sensor, with a flux sensitivity of 10^{-6} Φ_0 but capable of limited spatial resolutions (~10μm);
- small-angle neutron diffraction[11,12]. Due to the fact that neutrons have a magnetic moment they will be diffracted from a modulated magnetic structure, such as the flux line lattice. The method can be used for large samples; therefore will generate averaged values of physical quantities. In addition, the method is successful in detecting the melting transition of the vortex lattice;
- scanning Hall probe microscopy[13,14], Lorentz microscopy[15] and magneto-optical techniques[16,17] are among other techniques used to visualize the vortex system.

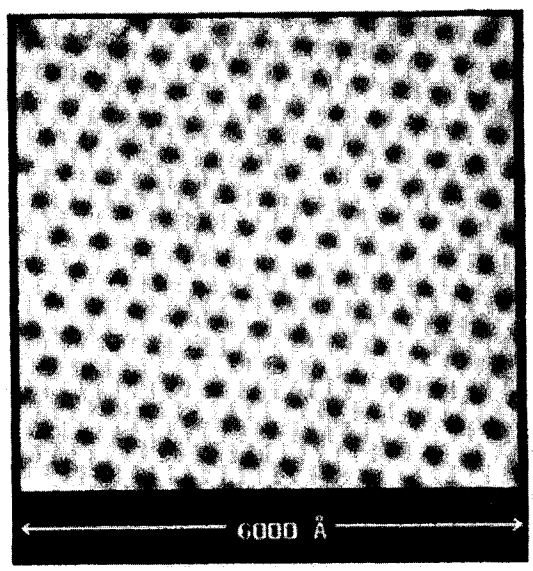

Figure 11 Scanning Tunneling Microscopy image of vortex lattice. The image was obtained[6] by H. F. Hess et al. in 1989 using a magnetic field of 1T in $NbSe_2$ at 1.8K.

2.2 Basic Vortex Dynamics

Consider a type II superconductor in the mixed state with an electrical current applied perpendicular to the direction of vortices. The vortices will experience a Lorentz force due to the interaction of the current and the magnetic field. The Lorentz force per unit length, acting on a single vortex, is given by:

$$\mathbf{F}_L = \mathbf{J} \times \phi_0, \tag{2.4}$$

where ϕ_0 represents a vector with a magnitude equal with the flux quantum ϕ_0 with its direction is along the vortex tube. Ideally, in the absence of defects, the vortex can move freely in response to the Lorentz force. As a reaction to vortex motion, an electric field is induced parallel to **J**:

$$\mathbf{E} = -\mathbf{v} \times \mathbf{B} \tag{2.5}$$

The appearance of this electric field causes dissipation[18]; the frictional force is proportional to the vortex velocity: $\mathbf{F}_f = -\eta\mathbf{v}$, where η is the friction coefficient. In order to reclaim the dissipation-free status, as well as the technological utility of type II superconductors, the vortices have to remain fixed in the presence of an electric current, i.e. for nonzero Lorentz forces.

Real materials incorporate defects and disorder, influencing the superconducting order parameter and giving rise to a pinning force which tends to suppress vortex motion. If the Lorentz force exceeds the pinning force a motion will be induced and vortices will reach a constant speed because of the friction force. From the equilibrium of the two forces acting on a vortex (Lorentz and friction) the

flux-flow (FF) resistivity can be deduced (below is presented the simple case when $\mathbf{B} \perp \mathbf{J}$):

$$\rho_{FF} = B\frac{\phi_0}{\eta} \tag{2.6}$$

Bardeen and Stephen[19] used the simplified model of a vortex with radius ξ and sharp boundaries in order to calculate the dissipation coefficient; their result was similar with the one obtained empirically[20] and it permitted the derivation of the flux flow at low temperatures as a function of the normal state resistivity, ρ_n:

$$\rho_{FF} = \rho_n \frac{H}{H_{c2}} \tag{2.7}$$

This linear dependence of flux flow resistivity on the external magnetic field (for $T << T_c$) represents the evidence of the dissipation mechanism that characterize the type II superconductors in the mixed state.

2.3 Vortex Pinning and Creep

Static vortices are the equivalent of a dissipation-free superconductor and this relates to pinning, or more precise, to the efficiency of pinning. In zero temperature, for a single vortex the pinning force can be expressed as:

$$\mathbf{F}_P = -\mathbf{J} \times \phi_0 \tag{2.8}$$

The maximum current density that can be sustained by the sample without vortex

motion is called the depinning critical current density J_c; this will be limited by the depairing current density which relates to the thermodynamic critical field ($J_0 \propto H_c/\lambda$)[18]. The ratio between the two critical currents J_c/J_0 represents a relevant criterion in assessing the strength of the pinning force (i.e. small value of the ratio is an indication of weak pinning).

The presence of disorder distorts the Abrikosov lattice as well as the dynamical conduct of vortices. Therefore, the problem of pinning has to be addressed by taking into consideration the interaction between vortices. Collective pinning theory[21], assumes that the total pinning force is the sum of individual pinning forces exerted by the active pinning centers. The pinning centers are assumed to be equally strong and randomly distributed over a volume V. The probability for a vortex to be in the proximity of a pinning center (within a range R) is the probability for that pinning center to influence a flux line. From the total number of pinning centers N_p, only a fraction n_vR^2 would manifest as active (n_v is the density of vortices). Thus, their sum fluctuations would be:

$$(N_p n_v R^2 \langle f_0^2 \rangle)^{1/2} = (V n_p n_v R^2 \langle f_0^2 \rangle)^{1/2} \qquad (2.9)$$

where $\langle f_0^2 \rangle$ represents the fluctuation of the individual pinning center-vortex interaction and n_p is the concentration of pinning centers, $n_p = N_p/V$. The pinning force per unit volume will then be:

$$F_p = (n_p n_v R^2 \langle f_0^2 \rangle / V)^{1/2} \qquad (2.10)$$

A good illustration of the pinning mechanism is given in Figure 12 by

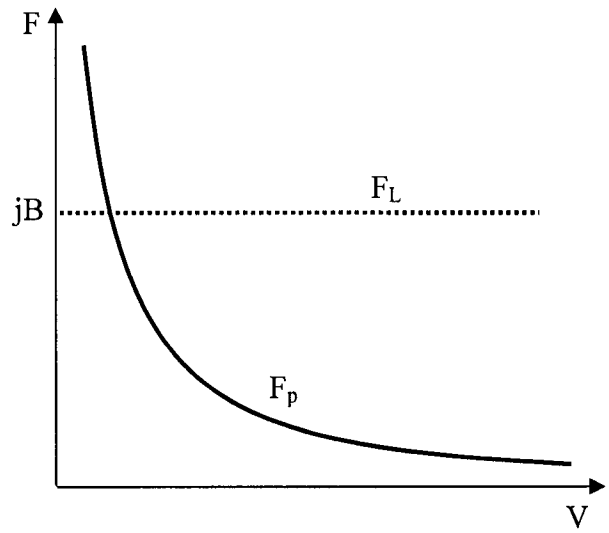

Figure 12 Comparative graph of Lorentz and pinning forces as function of volume. The driving Lorentz force is independent of V, while the total pinning force scales as $F_p \propto 1/\sqrt{V}$.

comparing the Lorentz force (equation 2.4), the force that drives the vortices, with the pinning force (equation 2.10). If the vortex system acts coherently, it can be inferred that only for small volumes the pinning will be effective, i.e. $F_P > F_L$. However, the total pinning can be enhanced if the large Abrikosov lattice is divided into smaller volumes, each one acting independently. This coherent volume is the result of the competition between the elastic strain energy involved in deforming the 3D vortex lattice and the resulting gain in pinning energy.

At higher temperatures the local distortion of the vortex lattice can become energetically unfavorable and vortices will be able to move. This motion, due to thermal fluctuations, takes place for bundles of flux lines and is called flux creep[22,23]. Thermal depinning is described[18] as a continuous crossover, a process in which vortex bundles jump from one pinning site to another through a small, finite motion, which generates dissipation. At a given temperature T, the probability P for this jump between pinning sites is proportional to the Boltzmann factor:

$$P \propto \exp(-U/k_BT), \tag{2.11}$$

where U is the activation energy. In the presence of a driving force, e.g. the Lorentz force $F_L = JBV_c$ the activation energy (in the direction of F_L) is less than the pinning energy U_0:

$$U = U_0 - JBV_c\delta = U_0(1-J/J_c), \tag{2.12}$$

where δ is the jumping distance and J_c the critical current in the absence of flux creep. The electrical field caused by the flux creep depends on the difference in jump probability along and against the driving force[24,25]:

$$E(J) \propto \exp(-U_0/k_BT)\,[\exp(+JU_0/J_ck_BT) - \exp(-JU_0/J_ck_BT)] \tag{2.13}$$

For $JU_0/J_ck_BT > 1$, or $J/J_c > k_BT/U_0$ the electric field reaction is strongly nonlinear, $E \propto \exp(J/J_c)$, accompanied by a logarithmic decay of screening currents with time. This result has been confirmed by experiments on low-T_c superconductors[26].

2.4 Thermally Assisted Flux Flow

High anisotropy, short coherence lengths and the range of working temperatures make thermal fluctuations more important in HTS. As a consequence, the HTS vortex system is soft compared with conventional type II superconductors.

In the presence of magnetic fields the resistive transition is strikingly broad[27,28]. As an example, in magnetic fields, HTS exhibit resistance well below T_c, even at low currents $J << J_c$. This phenomenon, called thermally assisted flux flow

(TAFF), is related to flux creep. The difference between the two exponentials in equation (2.13) can be expressed as sinh(x), with $x = JU_0/J_c k_B T$ and in the limit $J << J_c$ ($x << 1$), $\sinh(x) \cong x$, so that the resistivity can be expressed as[25,29]:

$$\rho_{TAFF} = \rho_0(B,T)\exp(-\frac{U_0}{k_B T}) \qquad (2.14)$$

The magnitude of the exponent in the above equation is large for low-T_c materials, making the TAFF regime irrelevant. In contrast, for HTS the exponent is considerably smaller which translates into a strong TAFF behavior.

2.5 Vortex Solid

The perfect vortex lattice represents the ideal case, where the vortex matter is not influenced by any disorder. In a real superconductor defects are inevitably present, distorting the vortex lattice and inducing glassy vortex phases instead[30]. The translational correlation function is a measure of the gradual decrease of translational order due to weak disorder:

$$C_{K_0}(r) = \overline{\left\langle e^{iK_0[u(r)-u(0)]} \right\rangle}, \qquad (2.15)$$

where [u(r)-u(0)] is the relative displacement (from the perfect lattice geometry) of two flux lines as function of their separation, r, while K_0 represents one of the first reciprocal lattice vectors. C(r) was calculated in a weak random forces model[31], and also by using the picture of collective pinning theory[21], leading to the same conclusion: long range crystalline order will be destroyed in the presence of any weak

disorder. Nevertheless, this contradicts with several experimental findings[11,31,32] reporting, at low magnetic fields, a almost perfect vortex lattice in clean BSCCO crystals.

The impasse was overcome by Giamarchi et al.[33,34] through a theoretical approach that neglected dislocations and considered the vortex system to be elastic at low fields and in the presence of weak disorder. The translational correlation function was found by applying the Gaussian variational method, and backed by computing the functional renormalization group. The result revealed the plausible existence of a special vortex state that manifests many metastable states, as a glass does, but exhibiting Bragg diffraction peaks[34,35,35], therefore demonstrating a fundamental characteristic of a crystal. This elastically distorted vortex lattice is called a Bragg glass (BrG), or quasi-lattice [see Figure 13 a)]. The lattice of a BrG is slightly distorted with a weak, power-law crystalline order decay, retaining its quasi-long range order at large scales.

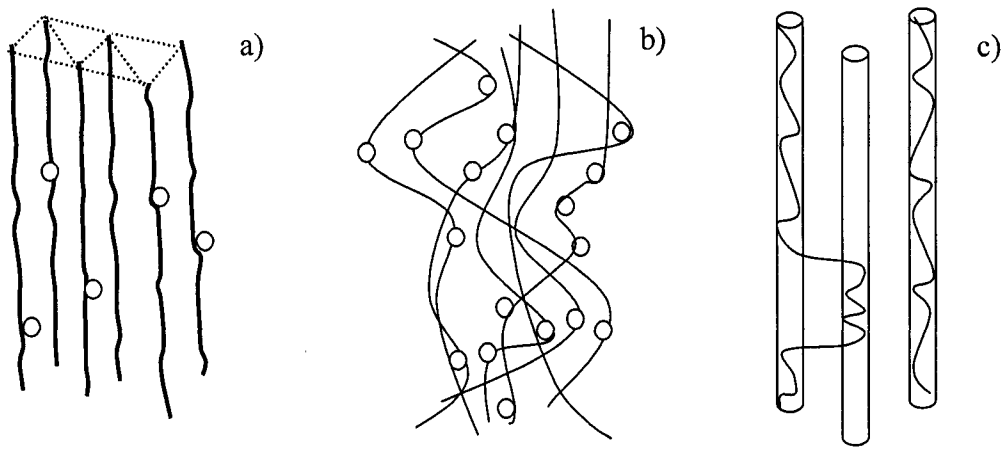

Figure 13 Vortex system for different disorder type and strength. a) the case of weak disorder; b) for stronger, uncorrelated point disorder an vortex entangled state will emerge; c) Bose glass will be the state of vortex system in the case of correlated defects- the drawing illustrates the example of columnar defects.

As the lattice accommodates itself to the pinning centers, it looses its long-range positional order. The type of the glassy state is dictated by the type and strength of the disorder. The interplay between thermal and elastic energy will regulate the properties of this solid vortex phase, but will also lead, at high temperatures, to a first-order melting transition[36,37,38].

Pinning and thermal fluctuations will dominate the physics of vortex systems in the presence of stronger disorder. Uncorrelated defects, such as impurities, intrinsic point defects, or defects generated by electron and proton irradiation can lead to the formation of a vortex glass[39,40]. This vortex state (VG) is a topologically disordered solid with frozen-in vortices, suggested to be entangled (see Figure 13 b) with a vanishing linear resistivity[41,42,43]:

$$\rho \propto \exp(-J_c/J)^{\mu}, \qquad (2.16)$$

where μ is a constant with a value between 0 and 1. This evidence argues for the status of a true superconducting phase for the vortex glass. The glassy transition to the vortex liquid state is predicted to be of second order.

In the case of a sufficiently high concentration of correlated disorder, such as twin planes or columnar defects[44,45,46], the predicted vortex state is a Bose glass[47,48,49]. Columnar tracks, obtained through heavy-ion irradiation, promote localization of the flux lines, confining vortex wandering (see Figure 13 c). The Bose glass phase (BG) is characterized by anisotropy and a strong angular dependence of the electrical resistivity. However, BG has an isotropic disorder structure, displaying characteristics similar to those of the vortex glass, but with an infinite correlation along the axis parallel to the columnar tracks.

Alternative vortex glass states that have been predicted include the class of window-like glasses. A defining characteristic of window glasses is the absence of a true thermodynamic equilibrium because the transition or crossover from the liquid to glass state is not accompanied by any detectable symmetry breaking[18]. There is no simple model describing the physics of window glasses, but relevant models include the polymer glass[50,51,52] and vortex molasses[52]. These models take into account a fast freezing of the dynamics which would mask any potential divergence of the spatial correlation length ξ (different from the coherence length).

2.6 Vortex Liquid

At sufficiently high temperatures or magnetic fields the shear modulus acting between vortices should vanish and the vortex system can thus transform into a vortex liquid[53]. This regime is characterized by the absence of the crystalline long-range order (with the exception of the hexatic phase) but with a locally maintained superconducting order parameter at magnetic fields much lower than the upper critical field[18], H_{c2}. In this field range a finite electrical resistivity was detected at low currents[54,55,56,57], indicating the possible existence of a phase transition in the mixed state, separating a solid from a liquid vortex state.

The vortex liquid can be analyzed through similar theoretical approaches which treat the vortex as a two-dimensional boson[58,59,60]. These models apply to thick samples or large enough magnetic fields and describe the flux liquid as being entangled due to thermal fluctuations (see Figure 14). This regime is dominated by flux line wandering, leading to a complex motion in which vortices commonly switch their positions. There is also evidence for the existence of a disentangled liquid intermediate regime[60,61], characterized by large excursions of the vortices.

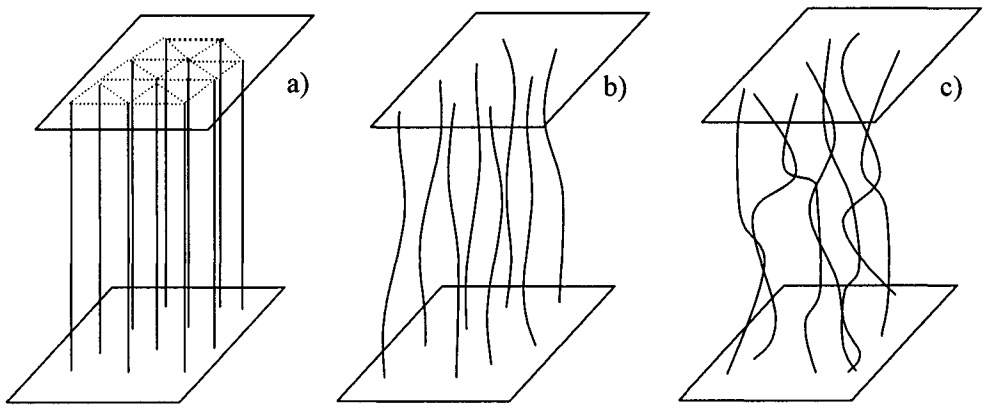

Figure 14 Schematic representations of flux line phases. a) Undistorted vortex lattice; b) disentangled flux line liquid; c) entangled vortex liquid.

The vortex liquid viscosity is greatly increased by entanglement, permitting some of the pins to become effective over larger distances, thereby limiting flux motion and decreasing the resistivity. A hydrodynamic model is proposed as a different theoretical description of the vortex liquid[62]; the liquid phase behavior is traced in terms of a set of friction and viscosity parameters.

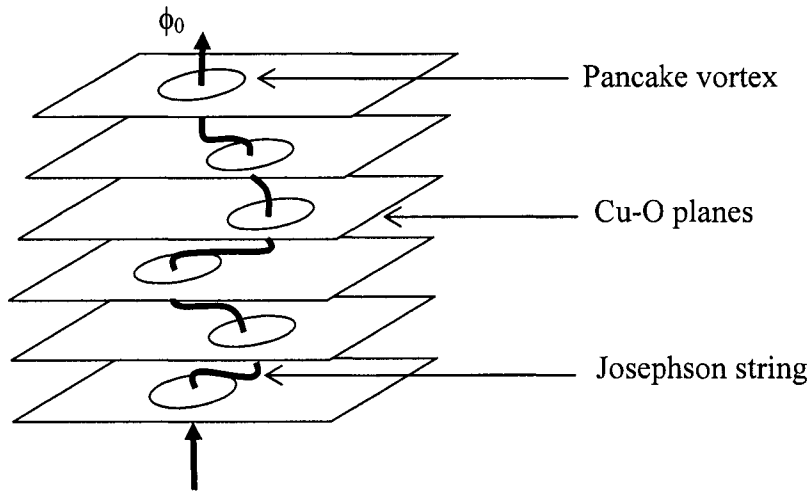

Figure 15 Pancake vortex in a strongly layered superconductor. The magnetic field is parallel to the c axis of the crystal.

The layered structure of many HTS causes the vortex line to have a discrete nature, as opposed to the continuous, elastic string that describes the flux line inside a less anisotropic superconductor. Vortex lines inside highly anisotropic BSCCO are not rectilinear, but stacks of 2D pancake vortices connected by Josephson coupling- for fields parallel with the c axis of the crystal (see Figure 15). In the framework of this vortex model, the observed broadening of the resistive transition was attributed to thermal fluctuations[63,64], which suggest a melting transition in two stages[65]: as the temperature is increased, the vortex lattice transforms first into a vortex-line liquid, followed by the formation of independently moving 2D vortices in different layers. BSCCO has many complicated vortex phases and is primarily ruled by the crossing lattice states[66].

2.7 Melting Transition

In clean or very weakly disordered samples there is consistent experimental evidence[67,68,69] for a first order melting transition. In strongly disordered samples the transition can be a second order transition.

A discontinuity in the first derivative of the free energy is the indication of a first order phase transition (FOPT). Since the entropy is defined as $S = -(\partial G/\partial T)$, there will be a entropy discontinuity at the transition, which is related to the latent heat of transition ($L = T\Delta S$) between the superconductor and normal states.

Empirically, melting of the vortex lattice occurs when the thermal and elastic pinning energies become equal as the displacement of the vortices reaches a fraction c_L of the vortex spacing. This rule is known as the Lindemann criterion:

$$\langle u^2 \rangle = c_L^2 \alpha^2, \qquad (2.17)$$

with the Lindemann number c_L typically in the range[70] 0.1 - 0.3.

Evidence for the existence of a FOPT was obtained from a variety of experimental methods. In YBCO calorimetric measurements revealed a narrow peak in the specific heat at the transition (T_m), confirming the melting as a first-order transition[71]. The change in entropy and the latent heat can be deduced[72,73] by integrating the peak area of $C/T = \partial S/\partial T$.

Magnetization measurements in YBCO showed discontinuities, which is also thermodynamic evidence of FOPT[37,74]; so is the jump in the local magnetic field observed in $Bi_2Sr_2CaCu_2O_8$ (BSCCO). These results indicate that the vortex liquid is denser than the solid, similar to the transition between ice and water.

Although transport measurements do not offer a direct thermodynamic investigation tool, the technique is very useful due to its high sensitivity to vortex motion. The kink in the resistivity (in clean YBCO samples) at T_m was for several years considered as a strong indication of the first-order character of the transition[67,68,75]. It was shown that there is a coincidence between the first-order transition signature in magnetization and the sharp step displayed at the onset of resistivity[39,76] signs of vortex melting transition; melting phase transition indicated by the onset of the resistivity kink coincide with the step in magnetization. Furthermore, in another comparative study[77] the position of the peak in the specific heat at the melting transition perfectly matched the onset of the step in magnetization.

Using a magneto-optical technique developed by Soibel et al.[78] it became possible to image the melting process in a disordered superconductor (BSCCO), uncovering complex vortex behavior regarding the solid-liquid interface, pinning and nucleation. They found a coexistence of vortex liquid droplets with the solid which indicates the first order character of the melting transition. In HTS, the combination

between disorder and anisotropy play an important role in controlling the phase separation.

2.8 Critical Points

The FOMT manifests only over a certain field range, being limited by critical points. In electrical transport measurements this is manifested by the disappearance of the sharp drop in resistivity as it is substituted by a continuous transition. At high magnetic fields the first-order signature of the transition vanishes at an upper critical point H_{ucp} as the transition changes into a second order one. This critical point is very sensitive to disorder: in very clean YBCO samples the first-order transition persisted up to[79] ~30T and around 9-10T in untwined, optimally doped YBCO[68,80,81], while it is much lower in BSCCO (around 50mT)[38].

In a typical YBCO crystal, the kink in $\rho(T)$ disappears at low fields, indicating the existence of a lower critical point, H_{lcp}. The reported value of H_{lcp} in the literature varies between 5T[82,83] and 0.5T[73], or even lower[84].

The end points of the first-order melting line show great sensitivity to sample quality, particularly to oxygen content[74,85], but also to intrinsic correlated defects, such as twin boundaries in YBCO, which seem to push the upper critical point to higher fields[73,82].

Point defects induced by irradiation (protons and electrons) lower the position of H_{ucp} on the FOMT[79,84], while columnar defects caused by heavy ion irradiation can have the opposite effect, raising H_{ucp}[80], if the irradiation dose is chosen within a limited range. The role of a few columnar tracks is to efficiently stabilize the lattice by straightening the vortices. On the other hand, random point defects encourage vortex-line wandering because of pinning. Vortex meandering and entanglement are

recognized[81] to be essential attributes of H_{ucp}. In general, at high fields the solid state of vortex matter becomes glassy and the density and type of disorder are decisive factors for the occurrence of this state.

The effect of proton irradiation on H_{lcp} is striking: it will increase about two orders of magnitude for a fluence[84] of 1.5×10^{15} p/cm^2, and even merge with the H_{ucp} for a high enough dose (2.0×10^{15} p/cm^2), so that the FOMT is completely suppressed. The electron irradiation hardly affects the lower critical point[84] and this is explained in the terms of pinning strength; the existence of H_{lcp} is related to the amount of defects in the sample and is even believed to be absent in a defect-free material. The lower critical point becomes detectable if the pinning strength near transition exceeds the strength of inter-vortex interaction[86].

In contrast to the effect on H_{ucp}, heavy ion irradiation, in moderate doses, raise the H_{lcp} and a Bose glass transition is observed below it, also indicating the existence of a new transition with increasing vortex density[81].

In summary, in the presence of weak disorder, the experiments reveal at least three distinct phases of the vortex system: a Bragg glass, representing a close to ordered vortex solid, a disordered solid or vortex glass and a vortex liquid, possibly transforming into a pancake gas. As studies show, additional vortex phases may appear as well, depending on type and density of the disorder present in the system[77,87].

The typical magnetic field- temperature phase diagram for high temperature superconductors (HTSC) has as a central feature the first order vortex melting line, which marks the transition between a vortex liquid and a Bragg glass. Below, Figure 16 presents the general phase diagram for YBCO single crystals.

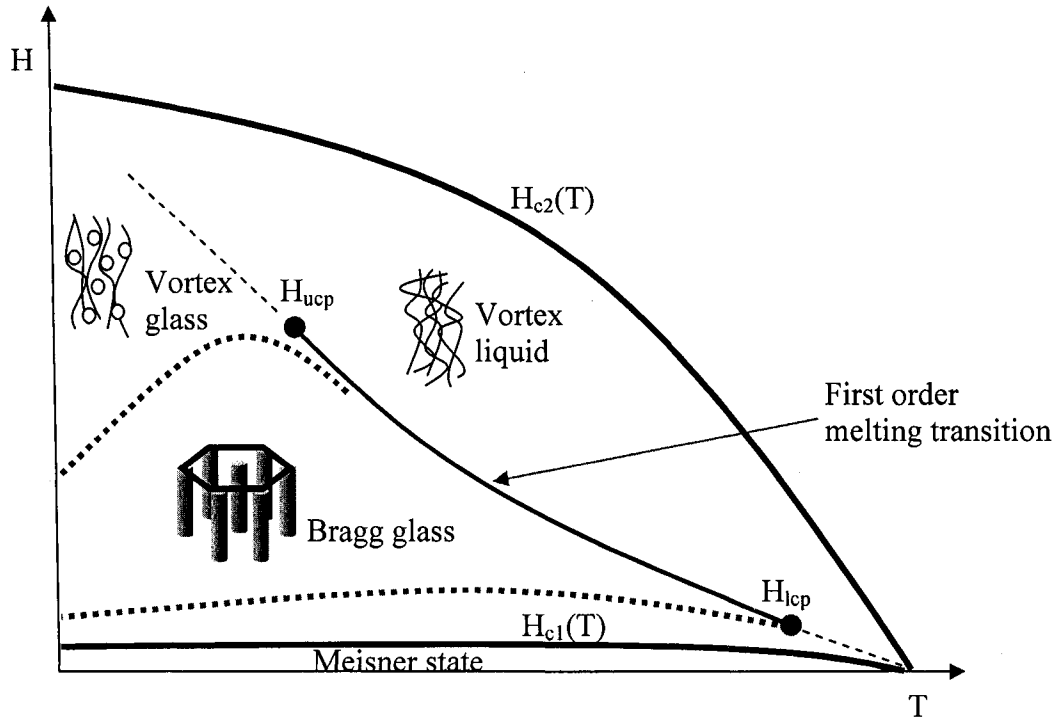

Figure 16 Proposed phase diagram for optimally doped YBCO. The first-order melting transition is limited by the two critical points, H_{ucp} and H_{lcp}. The dashed lines denotes second (or higher) order phase transitions. It is not clear what kind of transitions occurs below H_{lcp} and what is the vortex state at low magnetic fields.

References

[1] M. Tinkham, Introduction to Superconductivity (New York: McGraw-Hill) ch 5, (1975)

[2] V.V. Schmidt, The Physics of Superconductors, Nauka Publishers, Moskau, ch. 5, (1982)

[3] A. A. Abrikosov, Sov. Phys. JETP, **5**, 1174 (1957)

[4] H. Träuble and U. Essmann, J. Appl. Phys. **25**, 273 (1968)

[5] P. L. Gammel, D. J. Bishop, G. J. Dolan, J. R. Kwo, C. A. Murray, L. F. Schneemeyer, and J. V. Waszczak, Phys. Rev. Lett. **59**, 2592–2595 (1987)

[6] H. F. Hess, R. B. Robinson, R. C. Dynes, J. M. Valles, Jr., and J. V. Waszezak, Phys. Rev. Lett. **62**, 214 (1989)

[7] I. Maggio-Aprile, Ch. Renner, A. Erb, E. Walker, and O. Fischer, Phys. Rev. Lett. **75**, 2754–2757 (1995)

[8] A. Moser, H. J. Hug, I. Parashikov, B. Stiefel, O. Fritz, H. Thomas, A. Baratoff, H.-J. Güntherodt, and P. Chaudhari, Phys. Rev. Lett. **74**, 1847-1850 (1995)

[9] L. N. Vu, M. S. Wistrom and D. J. Van Harlingen, Physica B, **194**, 1791-1792 (1994)

[10] C. C. Tsuei, J. R. Kirtley, C. C. Chi, Lock See Yu-Jahnes, A. Gupta, T. Shaw, J. Z. Sun, and M. B. Ketchen, Phys. Rev. Lett. **73**, 593–596 (1994)

[11] R. Cubitt, E. M. Forgan, G. Yang, S. L. Lee, D. McK. Paul, H. A. Mook, M. Yethiraj, P. H. Kes, T. W. Li, A. A. Menovsky, Z. Tarnawski, and K. Mortensen, Nature (London) **365**, 407 (1993)

[12] S. T. Johnson, E. M. Forgan, S. H. Lloyd, C. M. Aegerter, S. L. Lee, R. Cubitt, P. G. Kealey, C. Ager, S. Tajima, A. Rykov, and D. McK. Paul, Phys. Rev. Lett. **82**, 2792 (1999)

[13] H. D. Hallen, R. Seshadri, A. M. Chang, R. Miller, L. N. Pfeiffer, K. West, C. A. Murray, H. F. Hess, Phys. Rev. Lett. **71**, 3007 (1993)

[14] A. M. Chang, H. D. Hallen, H. F. Hess, H. L. Kao, J. Kwo, R. Wolf,

J. van der Zeil and T. Y.Chang, Appl. Phys. Lett. **61**, 1974 (1992)

[15] K. Haralda, T. Matsuda, H. Kasai, J. E. Bonevich, T. Yoshida, U. Kawabe, and A. Tonomura, Phys. Rev. Lett. **71**, 3371 (1993)

[16] D. W. Pohl, W. Denk and M. Lanz, Applied Physics Letters **44**, 651 (1984)

[17] M. A. Paesler and P. J. Moyer, "Near-Field Optics: Theory, Instrumentation and Applications," John Wiley and Sons, Inc., New York (1996)

[18] G. Blatter, M. V. Feigel'man, V. B. Geshkenbein, A. I. Larkin, V. M. Vinokur, Rev. Mod. Phys. **66**, 1125 (1994)

[19] J. Bardeen, and M. J. Stephen, Phys. Rev. **140**, A1197 (1965)

[20] A. R. Strnad, C. F. Hempstead, and Y. B. Kim, Phys. Rev. Lett. **13**, 794-797 (1964)

[21] A. I. Larkin, and Yu. N. Ovchinnikov, J. Low Temp.Phys. **34**, 409–428 (1979)

[22] P. W. Anderson, Phys. Rev. Letters **9**, 309 (1962)

[23] P. W. Anderson, Y. B. Kim, Rev. Mod. Phys. **36**, 39–43 (1964)

[24] M. Tinkham, Introduction to Superconductivity, McGraw-Hill, Inc., Singapore, (1996)

[25] D. Dew-Hughes, Cryogenics **28**, 674 (1988)

[26] M. R. Beasley, R. Labusch, and W. W. Webb, Phys. Rev. **181**, 682–700 (1969)

[27] Y. Iye, T. Tamegai, H. Takeya and H. Takei, Jpn. J. Appl. Phys. **26**, 1057 (1987)

[28] T. T. M. Palstra, B. Batlogg, R. B. van Dover, L. F. Schneemeyer and J. V. Waszczak, Appl. Phys. Lett. **54**, 763 (1989)

[29] P. H. Kes, J. Aarts, J. van den Berg, C. J. van der Beek, and J. A. Mydosh, Supercond. Sci. Technol. **1**(5), 242–248 (1989)

[30] A. I. Larkin, Sov. Phys. JETP **31**, 784-786 (1970)

[31] R. N. Kleiman, P. L. Gammel, L. F. Schneemeyer, J. V. Waszczak, and D. J. Bishop, Phys. Rev. Lett. **62**, 2331 (1989)

[32] K. Harada, T. Matsuda, H. Kasai, J. E. Bonevich, T. Yoshida, U. Kawabe, and A. Tonomura, Phys. Rev. Lett. **71**, 3371-3374 (1993)

[33] T. Giamarchi, and P. Le Doussal, Phys. Rev. B **52**, 1242 (1995)

[34] T. Giamarchi, and P. Le Doussal, Phys. Rev. B **55**, 6577 (1997)

[35] T. Klein, I. Joumard, S. Blanchard, J. Marcus, R. Cubitt, T. Giamarchi, P. Le Doussal, Nature **413**, 404 (2001)

[36] H. Pastoriza, M. F. Goffman, A. Arribére, and F. de la Cruz., Phys. Rev. Lett. **72**, 2951 (1994)

[37] E. Zeldov, D. Majer, M. Konczykowski, V. B. Geshkenbein, V. M. Vinokur, H. Shtrikman, Nature (London) **375**, 373 (1995)

[38] U. Welp, J. A. Fendrich, W. K. Kwok, G. W. Crabtree, and B. W. Veal., Phys. Rev. Lett. **76**, 4809 (1996)

[39] M. P. A. Fisher, Phys. Rev. Lett. **62**, 1415 (1989)

[40] D. S. Fisher, M. P. A. Fisher, and D. A. Huse, Phys. Rev. B **43**, 130-159 (1991)

[41] D. Ertas and D. R. Nelson, Physica (Amsterdam) **272C**, 79 (1996)

[42] D. López, E. F. Righi, G. Nieva, and F. de la Cruz, Phys. Rev. Lett. **76**, 4034–4037 (1996)

[43] D. López, L. Krusin-Elbaum, H. Safar, E. Righi, F. de la Cruz, S. Grigera, C. Feild, W. K. Kwok, L. Paulius, and G. W. Crabtree, Phys. Rev. Lett. **80**, 1070–1073 (1998)

[44] J. R. Thompson, Y. R. Sun, H. R. Kerchner, D. K. Christen, B. C. Sales, B. C. Chakoumakos, A. D. Marwick, L. Civale, and J. O. Thomson, Appl. Phys. Lett. **60** (18), 2306 (1992)

[45] C. J. van der Beek, M. Konczykowski, V. M. Vinokur, T. W. Li, P. H. Kes, G. W. Crabtree, Phys. Rev. Lett. **74**, 1214 (1995)

[46] R. A. Doyle, W. S. Seow, Y. Yan, A. M. Campbell, T. Mochiku, K. Kadowaki, G. Wirth, Phys. Rev. Lett. **77**, 1155 (1996)

[47] D. R. Nelson and V. M. Vinokur, Phys. Rev. Lett. **68**, 2398 (1992)

[48] D. R. Nelson and V. M. Vinokur , Phys. Rev. B **48**, 13060 (1993)

[49] A. I. Larkin and V. M. Vinokur, Phys. Rev. Lett. **75**, 4666 (1995)

[50] D. R. Nelson, "Phase Transitions and Relaxation in Systems with Competing Energy Scales", edited by T. Risk and D. Sherrington, Kluwer, Dordrecht, pp. 95–117 (1993)

[51] C. Carraro and D. S. Fisher, Phys. Rev. B **51**, 534-538 (1995)

[52] C. Reichhardt, A. van Otterlo, and G. T. Zimányi, Phys. Rev. Lett. **84**, 1994-1997 (2000)

[53] R. Labusch, Phys. Status Solidi **32**, 439 (1969)

[54] T. T. M. Palstra, B. Batlogg, L. F. Schneemeyer, and J. V.Waszczak, Phys. Rev. Lett. **61**, 1662 (1988)

[55] T. T. M Palstra, B. Batlogg, R. B. van Dover, L. F. Schneemeyer, and J. V. Waszczak, Phys. Rev. B **41**, 6621 (1990)

[56] M. Tinkham, Phys. Rev. Lett. **61**, 1658 (1988)

[57] R. H. Koch, , V. Foglietti, W. J. Gallagher, G. Koren, A. Gupta, and M. P. A. Fisher, Phys. Rev. Lett. **63**, 1511 (1989)

[58] D. R. Nelson, Phys. Rev. Lett. **60**, 1973-1976 (1988)

[59] D. R. Nelson and H. S. Seung, Phys. Rev. B **39**, 9153-9174 (1989)

[60] M. P. A. Fisher and D. H. Lee, Phys. Rev. B **39**, 2756 (1989)

[61] M. V. Feigel'man, Physics A **168**, 319 (1990)

[62] M. C. Marchetti and D. R. Nelson, Phys. Rev. B **42**, 9938-9943 (1990)

[63] D. H. Kim, K. E. Gray, R. T. Kampwirth, and D. M. McKay, Phys.Rev. B **42**, 6249 (1990)

[64] H. A. Blackstead and G. A. Kapustin, Physica (Amsterdam) **219C**, 109 (1994)

[65] L. I. Glazman and A. E. Koshelev, Phys. Rev. B **43**, 2835-2843

(1991)

[66] A. Grigorenko, S. Bending, T. Tamegai, S. Ooi, M. Henini, Nature **414**, 728-731 (2001)

[67] H. Safar, P. L. Gammel, D. A. Huse, D. J. Bishop, W. C. Lee, J. Giapintzakis, and D. M. Ginsberg, Phys. Rev. Lett. **70**, 3800-3803 (1993)

[68] M. Charalambous, J. Chaussy, and P. Lejay, Phys. Rev. B **45**, 5091-5094 (1992)

[69] W. K. Kwok, J. Fendrich, S. Fleshler, U. Welp, J. Downey, and G. W. Crabtree, Phys. Rev. Lett. **72**, 1092-1095 (1994)

[70] S. Ryu, S. Doniach, G. Deutscher, and A. Kapitulnik, Phys. Rev. Lett. **68**, 710-713 (1992)

[71] A. Schilling, R. A. Fisher, N. E. Phillips, U. Welp, D. Dasgupta, W. K. Kwok, and G. W. Crabtree, Nature (London) **382**, 791 (1996)

[72] A. Schilling, R. A. Fisher, N. E. Phillips, U. Welp, W. K. Kwok, and G. W. Crabtree, Phys.Rev. Lett. **78**, 4833 (1997)

[73] A. Junod, M. Roulin, J.-Y. Genoud, B. Revaz, A. Erb, and E. Walker, Physica (Amsterdam) **275C**, 245 (1997)

[74] R. Liang, D. A. Bonn and W. N. Hardy, Phys. Rev. Lett. **76**, 835 (1996)

[75] M. Charalambous, J. Chaussy, P. Lejay, and V. Vinokur, Phys. Rev. Lett. **71**, 436-439 (1993)

[76] D. T. Fuchs, E. Zeldov, D. Majer, R. A. Doyle, T. Tamegai, S. Ooi, and M. Konczykowski, Phys. Rev. B **54**, R796-R799 (1996)

[77] F. Bouquet, C. Marcenat, E. Steep, R. Calemczuk, W. K. Kwok, U. Welp, G. W. Crabtree, R. A. Fisher, N. E. Phillips, and A. Schilling, Nature (London) **411**, 448 (2001)

[78] A. Soibel, E. Zeldov, M. Rappaport, Y. Myasoedov, T. Tamegai, S. Ooi, M. Konczykowski, V. B. Geshkenbein, Nature **406**, 282-287 (2000)

[79] K. Shibata, T. Nishizaki, T. Sasaki and N. Kobayashi, Phys. Rev. B **66**, 214518 (2002)

[80] T. Nishizaki, T. Naito, S. Okayasu, A. Iwase and N. Kobayashi, Phys. Rev. B **61**, 3649-3654 (2000)

[81] W. K. Kwok, R. J. Olsson, G. Karapetrov, L. M. Paulius, W. G. Moulton, D. J. Hofman and G. W. Crabtree, Phys. Rev. Lett. **84**, 3706-3709 (2000)

[82] M. Roulin, A. Junod, A. Erb and E. Walker, Phys. Rev. Lett. **80**, 1722 (1998)

[83] F. Bouquet, C. Marcenat, Physics and Materials Science of Vortex States, Flux Pinning and Dynamics. Kluwer Academic Publishers, Dordrecht, p. 743.(1998)

[84] L. M. Paulius, W.-K. Kwok, R. J. Olsson, A. M. Petrean, V. Tobos, J. A. Fendrich, G. W. Crabtree, C. A. Burns, and S. Ferguson, Phys. Rev. B **61**, R11910-R11913 (2000)

[85] T. Nishizaki, Y. Onodera, N. Kobayashi, H. Asaoka, and H. Takei, Phys. Rev. B **53**, 82 (1996)

[86] G. W. Crabtree, W. K. Kwok, L. M. Paulius, A. M. Petrean, R. J. Olsson, G. Karapetrov, V. Tobos and W. G. Moulton, Physica C **332**, 71-79 (2000)

[87] D. T. Fuchs, E. Zeldov, T. Tamegai, S. Ooi, M. Rappaport, and H. Shtrikman, Phys. Rev. Lett. **80**, 4971 (1998)

CHAPTER 3

EXPERIMENTAL TECHNIQUES

3.1 $YBa_2Cu_3O_{7-\delta}$ Single Crystal Growth

The work presented here is based on electrical transport and specific heat measurements on $YBa_2Cu_3O_{7-\delta}$ single crystals. Sample preparation starts with crystal growth, using a self-flux method[1]. The quest for a high purity, defect-free crystals represents the motivation for using this method.

High purity (99.99%) powders of Y_2O_3, $BaCO_2$ and CuO are carefully mixed with a Y:Ba:Cu molar ratio of 5:27:68. A uniform powder of this mixture is obtained after grinding for ~30 minutes with an agate mortar and pestle. The powder is then shaped into a pellet by pressing it into a mold with a hydraulic press at a pressure of about 1.7×10^7 N/m^2, for 1 minute. A typical pellet is 3/4" in diameter and 1/4" in height.

The pellet is then placed on the raised center of a rectangular gold crucible. This geometry is designed to help the melting flux to disperse easily from the waste material that will remain in the center of the crucible. The procedure to grow crystals takes about seven days, during which time in which the pellet follows a controlled heating (up to 983°C) and a slow cooling, in stages, as shown in Figure 17.

During the initial stages of crystal growth, the initial $YBa_2Cu_3O_{7-\delta}$ unit cell is tetragonal, with no CuO chains, only Cu atoms in the top and bottom planes. The oxygen is absorbed afterwards, in the cooling stage of the growing process and the crystal goes through a transition from the tetragonal to the orthorhombic structure (see

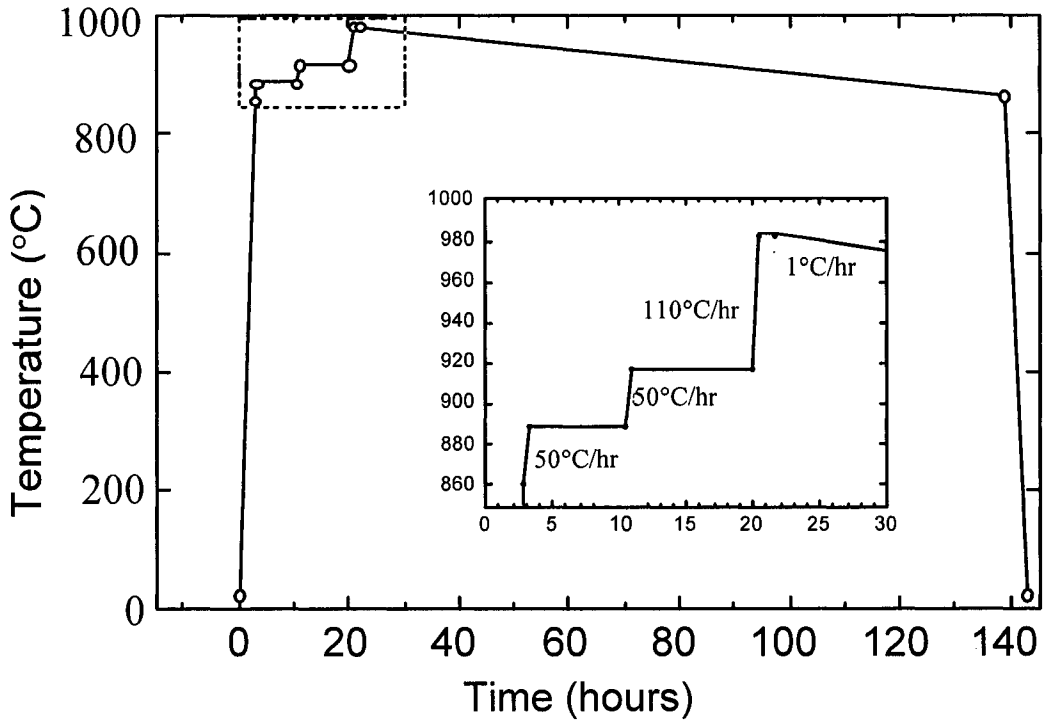

Figure 17 Temperature dependence on time for crystal growing using gold crucible.

Figure 8); the latter configuration is superconducting but it is stable only at temperatures below ~500°C. Superconductivity will not occur if the oxygen deficiency δ exceeds 0.6.

As the temperature decreases, the flux recedes towards the cooler walls of the crucible, leaving behind black and shiny, irregularly-shaped crystals. If the growth procedure is successful, up to ~100 crystals can be extracted from the crucible. Typical crystal dimensions are ~ 0.8 × 0.8 × 0.08 mm^3, with the c axis along the shortest distance. Crystals are removed by gently tapping the bottom of the crucible, while the crucible is held in an upside down position. The crystals are then individually cleaned, using a razor and ethyl alcohol to remove any remaining flux.

3.2 Oxygenation

Oxygen content is of great importance as many properties of $YBa_2Cu_3O_{7-\delta}$ depend on it. As-grown crystals are not just oxygen deficient, but the distribution of oxygen atoms is not homogeneous. These factors considerably lower the critical temperature (60 to 80K) and broaden the transition (over ~30K)[2].

In order to achieve optimal superconducting properties (such as $T_c \cong 93K$ and a narrow transition of about 0.3K) the crystals have to be annealed in an oxygen atmosphere. The annealing temperature and oxygen pressure are the key factors that influence the oxygen concentration.[3,4,5]

The diffusion process is rather slow and requires fairly long anneals (between one week and 10 days). In the case of thick crystals, the period of time needed for annealing has to be adjusted as the diffusion rate along the c axis is substantially lower than within the ab plane[6]. To anneal, the crystals are placed in small quartz crucibles which sit in the center of a quartz tube, inside a tube furnace. The highest T_c (~93K for an oxygen deficiency $\delta \cong 0.09$[7]), corresponding to the optimal oxygenation, is obtained at ambient pressure at a temperature of ~420Kwith an oxygen gas flow at a rate of ~2 cm^3/min. At the end of the annealing procedure the temperature is slowly decreased at a rate of ~4°C/min, until it reaches room temperature.

3.3 Untwinned $YBa_2Cu_3O_{7-\delta}$ Crystals

For an oxygen deficiency of $\delta \cong 0.5$ the population of oxygen vacancies along both, the a and b axis become equal, resulting in a tetragonal unit cell – the a and b dimensions are equal. As the number of the oxygen atoms in the unit cell increases (in the CuO chains) the system makes the transition from tetragonal to orthorhombic

structure. Because the a and b dimensions are so similar, the a and b axis spontaneously alternates during oxygenation in response to slight strains or imperfections. This creates twin boundaries along the ⟨110⟩ directions and an associated strain field of about 30Å in width (see Figure 18).

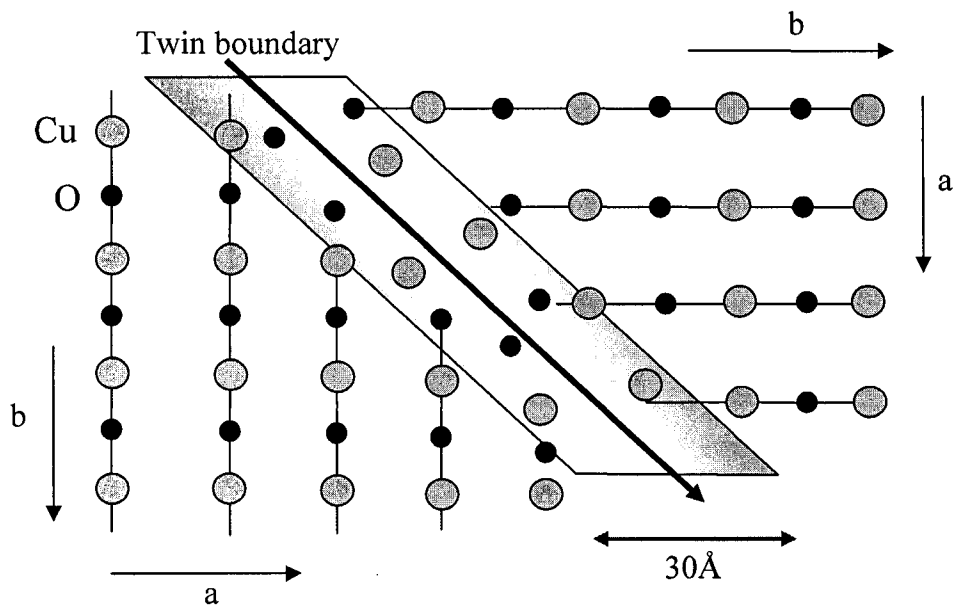

Figure 18 Twin boundaries and the accompanying strain field.

Different twin domains reflect polarized light differently and the twins can be easily detected under a polarized light microscope as dark, diagonal lines. The twins represent planar defects that influence vortex motion. In order to study the influence of defects on vortex motion, crystals free of pre-existing defects such as twin boundaries are required. A great deal of our work is focused on the effects of irradiation induced defects on vortex behavior and, unless twin defects are removed, it is hard to separate the influence of the irradiation damage.

Twins can be removed through a thermo-mechanical method.[8,9,10] A detwinning device, illustrated below, in Figure 19, is used to apply pressure of the

order of ~10^7 N/m^2 in one direction. We modified the design of the detwinning device, replacing the original Brass holder with a high temperature ceramic. This was done in order to minimize the sample contamination during the detwinning procedure and to eliminate the expansion of the metal holder during heating, as the metal expands more than the glass plates and the ceramic. The pressure is applied through a quartz rod and a glass slide, using a micrometer, so that the pressure can be fine tuned. A second glass plate is slid above the crystal. The sample is placed above a cartridge heater and between two gold foils which act as a buffer. The temperature is controlled so that the sample temperature will be maintained at a constant 420°C for 7-8 hours. An oxygen line creates a flow of oxygen over the sample, preventing a change in the oxygen concentration during the detwinning process.

The success of the procedure depends on how rectangular the geometry of the crystal is. If the crystal is a rectangle, the applied pressure can be transmitted uniformly throughout the crystal. Some of the crystals must be cleaved and frequently the detwinning has to be repeated several times.

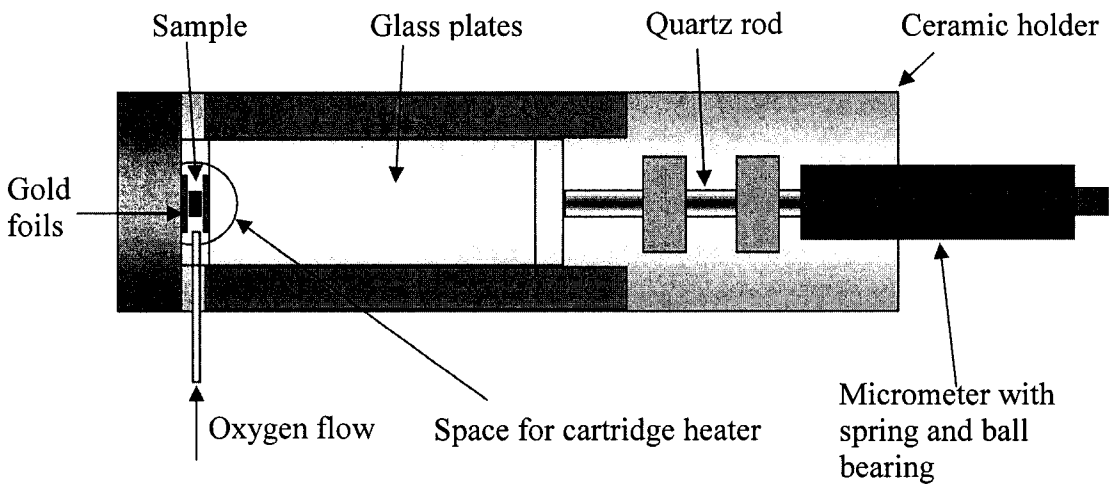

Figure 19 Detwinning device.

3.4 Electrical Transport Measurements

Because the sample itself has a small resistivity, the four-wire measurement method is the appropriate technique. As seen in Figure 20, the outer two leads supply current to the sample, the inner two leads to sense the voltage drop across the sample due to the resistance of the material.

The first step in preparing the samples for resistivity measurements is attaching the electrical contacts, which must have low resistances in order to avoid heating and noise, preferably around 1Ω. The effectiveness of electrical contacts is greatly influenced by the quality of the faces where contacts are applied, i.e. ab top and bottom planes. Rough surfaces or existence of a thin oxide layer at the surface are factors that impose a light polishing procedure.

Furthermore, the best way to achieve a low contact resistance is through a combination of two techniques. First gold pads are evaporated on the surface of the sample. The role of the gold pads is to lower the surface resistance of the crystal. To ensure the diffusion of gold into the top layers of the material, the sample is annealed at 420°C in flowing oxygen for six hours after the evaporation procedure. The second

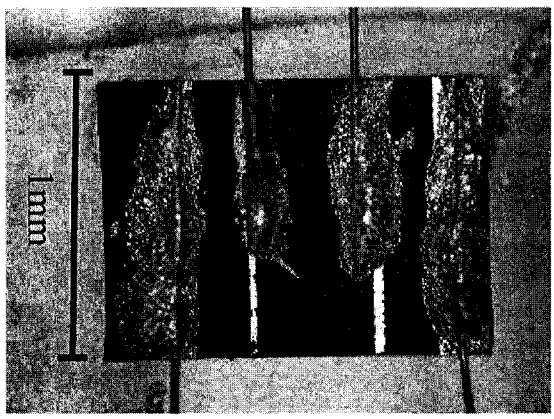

Figure 20 Detail of the crystal with four gold wires attached to it.

step is to attach gold or platinum lead wires using silver epoxy (EPO-TEK H20E). At this stage the crystal has to be affixed to an insulating base, large enough to maintain crystal's stability while attaching the wires. A small piece of sapphire glass is used as a substrate and a microscope glass slide is utilized as temporary base. The crystal and the two pieces of glass are glued together by using GE varnish, a common adhesive and insulator.

Given the dimensions of a typical crystal, as well as the diameter of the gold wires (25μm), the work is continued under a microscope. A thin wire is used as a brush to paint narrow stripes of silver epoxy on the gold pads. The gold wires that will be used to supply the current and measure the voltage are carefully placed on the painted stripes and then embedded in silver epoxy. In order to cure the epoxy, the crystal is placed on a hot plate at a temperature of ~150°C for few minutes. In this way, a low contact resistance (1-2Ω) can be achieved (see Figure 20).

The sample is now ready to be placed on the sample holder, a G-10 insulating puck with a copper core, as illustrated in Figure 21. The sample thermometer is mounted in contact with the copper core, on the opposite face from where the sample sits.

The ac-resistivity of the sample is measured at a low frequency of 23Hz, using a current in the range 0.1mA to 3mA. The low-signal measurement technique reduces noise; however, to prevent induction from magnetic fields and noise from thermal power, the conduction wires should be twisted pairs. Measurements are performed at a constant electrical current by including a large resistance (600Ω) in the circuit. Because the current is supplied by a constant voltage output from the lock-in amplifier, the large resistor is placed into the circuit with the purpose of maintaining a constant current. A very accurate lock-in amplifier (SR 830) is utilized to monitor the

voltage signal coming from the sample after being preamplified by a low-noise passive transformer (SR 554).

All instruments are connected to a computer through a GPIB interface. Data acquisition and instrument control is realized in a LabVIEW environment.

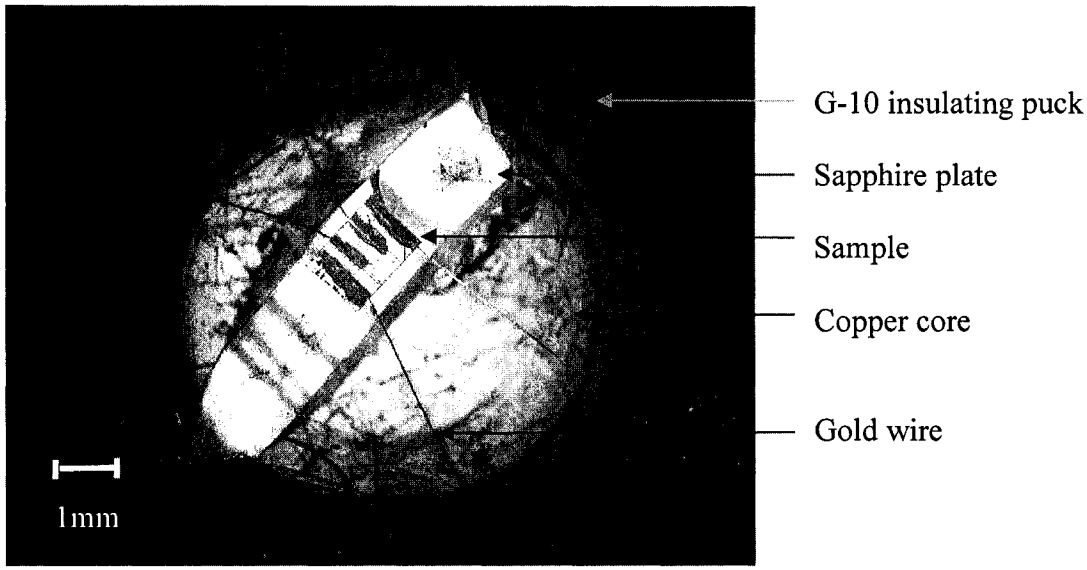

Figure 21 Sample mounted for electrical transport measurements.

3.5 Proton Irradiation

The proton irradiation procedures were performed at WMU's Van deGraaff accelerator. A 9MeV proton beam was directed parallel with the c axis of the crystal. To insure a uniform beam, a 1.2μm thick gold foil is mounted in the path of the beam. The beam is tuned to ensure that it is centered on the sample and is uniform over the ~1cm^2 area of the target holder. The uniformity of the beam is determined with Gafchromic radiographic film.

The irradiation is performed at room temperature and a low flux of 6.25×10^{10} p/cm^{2}sec is used in order to reduce heating. This resulted in sample temperatures less

than 20°C above room temperature due to heating from the beam. TRIM calculations[11] give a range of ~280μm for 9MeV protons in $YBa_2Cu_3O_{7-\delta}$. This is larger than the thickness of the crystals used in this investigation. The defects created by the irradiation are primarily vacancy- displacement pairs, with the rough values: 8% - Y, 15% - Ba, 23% - Cu, 54% - O. Some of the defects cluster, resulting in larger defects.

The results of more detailed TRIM calculations for the case of a 40μm thick crystal used in our investigation (YBA285) can be found in Table 1, below. A threshold energy displacement of 20eV was used in the calculation. The computation of the defect densities and spacings was performed by taking in account that ~30% of defects anneal out at room temperature[12,13]. Combined Transmission Electron Microscopy (TEM) and critical current measurements indicate that the defects are uncorrelated and that 70% of defects are point like, while 30% of defects are clusters of atoms with an average size of ~30Å[14].

Table 1 9MeV Proton Irradiation Effects on Crystal YBA285

Irradiation dose (10^{15} p/cm^2)	0.5	1.0	1.5	2.0
Vacancies/ion (for a 40μm path)	5.3			
Defect density (cm^{-3})	$4.64x10^{17}$	$9.28x10^{17}$	$13.9x10^{17}$	$18.6x10^{17}$
Defect spacing (Å)	129	103	89.6	81.3

3.6 AC Specific Heat Measurements

Specific heat measurements are a valuable investigation technique, as they reveal thermodynamic properties of the superconducting sample[15]. In the ac method used here, heat is transferred periodically to the sample from a heater wire in contact with the sample. The alternating power, $P = P_0(1 + \cos\omega t)$, is provided by the lock-in amplifier at a carefully chosen frequency (typically around 1Hz). The corresponding period should considerably exceed the thermal diffusion time, but be a lot shorter than the relaxation time of the sample-bath system.[15,16] If these conditions are met, the response of the sample will be oscillatory, with the temperature of the oscillations inversely proportional to both the input frequency and the heat capacity of the material:

$$T_{sample} = T_{bath} + T_{dc} + T_{ac}\cos(\omega t + \varphi), \qquad (3.1)$$

where $T_{dc} = P_0/K$ and $T_{ac} = P_0/\omega C$, with K as the thermal conduction coefficient of the thermocouple.

Using a very small amount of GE varnish, the sample is attached at the cross of two 10 μm diameter Chromel and Constantan wires. With the crystal situated at this junction of two thermocouples, the dc and ac temperature of the sample can be measured simultaneously (see Figure 22). A thin layer of GE varnish electrically insulates the crystal from the heater wire, mounted on the top of the crystal. With the heater in direct contact with the sample, the heat transfer between heater and crystal is very good and does not require the presence of a gas atmosphere in the sample chamber.

The technique is proven to be sensitive not just for very small samples with

masses of the order of tens of μg) but also for larger samples, at lower signal frequencies (below 1Hz).

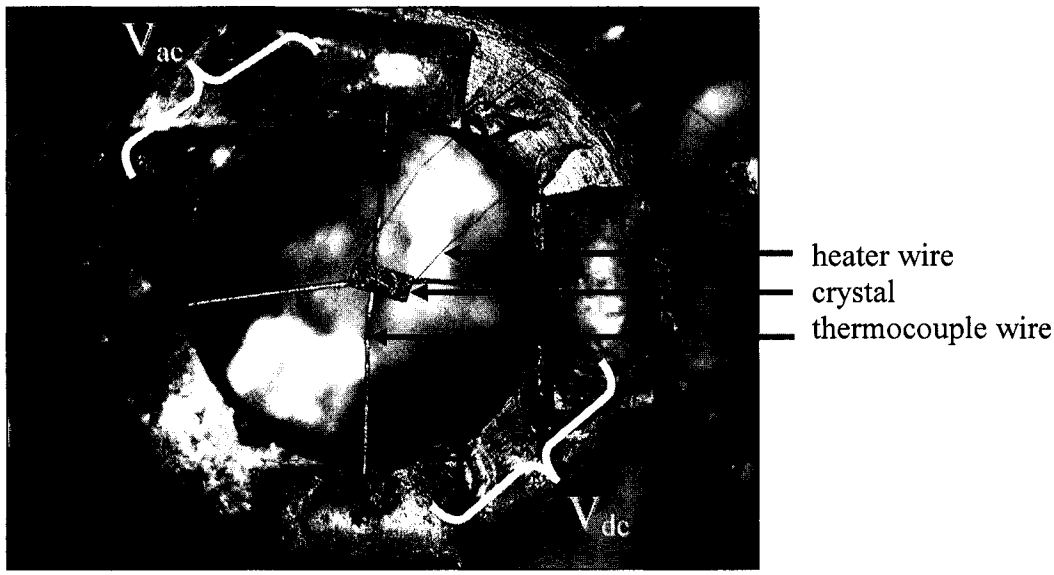

Figure 22 Specific heat measurements setup.

3.7 Temperature and Magnetic Field Control

The sample temperature is monitored by a Cernox thermometer, suitable for low-temperature measurements as this type of sensor offers high sensitivity at low temperatures and over a fairly broad range, with reduced errors due to external magnetic fields. The temperature is regulated by a LakeShore 340 temperature controller through a proportional-integral-derivative (PID) control loop. The way PID control algorithm works is by controlling the output based on temperature setpoint and feedback from the control sensor. Using a Cernox CX-1050-SD-HT the temperature accuracy at 77K is ±84mK, with a stability of 2.6mK. To limit the temperature gradients in the sample chamber, we use low cooling rates (typical value

of 0.1K/min).

The investigation of superconducting properties is conducted with the assistance of a cryostat equipped with a 7T split-coil superconducting magnet. The magnet, consisting of an Nb-Ti wire solenoid, is built to create a constant horizontal magnetic field inside a space with the diameter of 1cm, with homogeneity of ±0.1%. Because the magnet is cooled with liquid helium, ^{4}He, a persistent switch is employed to optimize Helium consumption. The persistent switch can alternate its state between a superconductor and a normal metal, isolating the magnet from the power supply, or allowing charging/discharging of the magnet, respectively. The sample is placed in the space of constant magnetic field, inside a steel chamber enclosed in a vacuum jacket. Heat transfer between the outside helium reservoir and the sample is made possible by thermal radiation, or much quicker, through a needle valve, a direct line that can be opened between sample space and helium dewar.

References

[1] D. L. Kaiser, F. Holtzberg, B. A. Scott, T. R. and McGuire, Appl. Phys. Lett., **51**, 1040 (1987)

[2] J. J. Capponi, C. Chaillout, A. W. Hewat, P. Lejay, N. Marezio, N. Nguyen, B. Raveau, J. L. Soubeyroux, J. L. Tholence, and R. Tournier, Europhys. Lett. **3**, 1301 (1987)

[3] T. B. Lindemer, J. F. Hunley, J. E. Gates, A. L. Sutton, Jr., J. Brynestad, C. R. Hubbard, P. K. Gallagher, J. Am. Ceram. Soc. **72**(10), 1775 (1989)

[4] P. Meuffels, R. Naeven, and H. Wenzl, Physica (Amsterdam) **161C**, 539 (1989)

[5] J. D. Jorgensen, B. W. Veal, A. P. Paulikas, L. J. Nowicki, G. W. Crabtree, H. Claus, and W. K. Kwok, Phys. Rev. B **41**, 1863 (1990)

[6] S. J. Rothman, J. L. Routbort, U. Welp, and J. E. Baker, Phys. Rev. B **44**, 2326 (1991)

[7] A. I. Rykov, S. Tajima, F. V. Kusmartsev, E. M. Forgan, and C. Simon, Phys. Rev. B **60**, 7601 (1999)

[8] U. Welp, M. Grimsditch, H. You, W. -K. Kwok, M. M. Fang, G. W. Crabtree, and J. Z. Liu, Physica C **161**, 1 (1989)

[9] H. Schmid, E. Burkhardt, B. N. Sun, and J. P. Rivera, **157**, 555 (1989)

[10] D. L. Kaiser, F. W. Gayle, R. S. Roth, L. S. Schwartzendruber, J. Mater. Res. **4**, 745 (1989)

[11] J. F. Zeigler, J. P. Biersack, U. Littmark, The Stopping and Range of Ions in Solids vol.1, Pergamon Press (1986)

[12] M. Konczykowski, Physica A **168**, 291 (1990)

[13] G. C. Xiong, H. C. Li, G. Linker, and O. Meyer, Phys. Rev. B **38**, 240-243 (1988)

[14] L. Civale, A. D. Marwick, M. W. Elfresh, T. K. Worthington, A. P. Malozemoff, and F. H. Holtzberg, Phys. Rev. Lett. **65**, 1164 (1990)

[15] P. F. Sullivan and G. Seidel, Phys. Rev. **173**, 679 (1968)

[16] S. E. Inderhees, M. B. Salamon, T. A. Friedmann, D. M. Ginsberg, Phys. Rev. B **36**, 2401 (1987).

CHAPTER 4

INVESTIGATION OF YBCO UNIVERSALITY RESPONSE TO PROTON IRRADIATION

4.1 Motivation of Investigation -Comparative Review Regarding Results Obtained in the Case of Different Induced Defects

There is an essential relationship between the behavior of flux lines and the value of the critical current density, J_c, with direct repercussions for technological applications of superconductors. Especially in the case of the HTS, the presence of controlled disorder can boost J_c and enhance the overall superconducting properties of the material. The ability to pin the vortices strongly depends on the type and density of disorder. The pinning strength can also depend on the orientation of the vortices relative to defects. The static and dynamic distribution of vortices is influenced by how they interact with the disorder present in the system. The free energy of flux lines can increase or decrease. A decrease of the free energy will result in the case where it is energetically favorable for the vortices to stick to the defects.

It is assumed[1,2] that defects pin because in this way they avoid superconducting condensation at their location. The elementary pining energy, describing the interaction between an individual flux line and one defect, is on the order of the product between the condensation energy density ($1/2\mu_0 H_c^2$) and the intersection volume between the flux line and the defect. Therefore, point defects will be able to pin only a small part of the flux line that penetrates the material, even in the case of dense disorder, when the same vortex is interacting with several defects.

Using reasonable assumptions, Civale et al.[3,4] found very strong flux pinning

due to defects created by heavy-ion irradiation when compared with those created by proton irradiation. This can be easily explained by relating the strength of the pinning with the length of the flux line able to be confined by the defect. In the case of the columnar tracks induced by heavy-ion irradiation, the maximum pinning force is obtained when the vortex is pinned over its entire volume, in other words when the magnetic field is parallel with the tracks and the diameter of the columnar defects is on the order of the coherence length, ξ. Columnar tracks are linear microstructures containing damaged material (in the amorphous state), where the superconductivity is weakened.

In general, columnar defects induced by heavy ion irradiation are stronger pinners than the uncorrelated defects created by proton irradiation. However, in certain cases[5] a comparable increase of J_c as a result of proton and heavy-ions irradiation can be found. But there are many variables that can influence the outcome of this type of investigation. On one hand is the type, energy and dose of the ions used, while on the other hand are the initial properties of the samples that will be utilized in the irradiation.

Our work is focused on the consequences of proton irradiation on the behavior of the vortex matter in YBCO. The literature is abundant on the subject[6,7,8,9,10,11], but reporting slightly different modifications of sample's properties upon irradiation. In this context, we found very useful to investigate how universal the response of the samples to proton irradiation is, how strong the influence of preexisting defects is, and how our results compare with those obtained in similar inquires. There are few facts that make our study unique. First of all, the work focuses on the effects on the first order melting in a systematic way, looking at how the melting temperature shifts and how the width of the melting transition changes upon proton irradiation.

Furthermore, the investigation concentrates on finding the dose needed to suppress the 1st order melting and stressing the effects on the lower critical point. Therefore, our work is very important in the context of the present understanding of vortex physics as it tries to elucidate fundamental problems regarding vortex dynamics.

4.2 Presentation of the Samples

Four optimally doped, detwinned YBCO single crystals were considered in this study. To ensure that the crystals are twin-free, the angular dependence of the electrical resistivity was measured, where the direction of magnetic field with respect with the crystallographic c axis was varied from 0° to 90° while keeping the current perpendicular to the applied magnetic field (Figure 23). The curve depicting this dependence was proved to be smooth, with no dip at 0 degrees, establishing that the crystals we used were clean. The angular dependence is due to the anisotropy of the crystal structure.

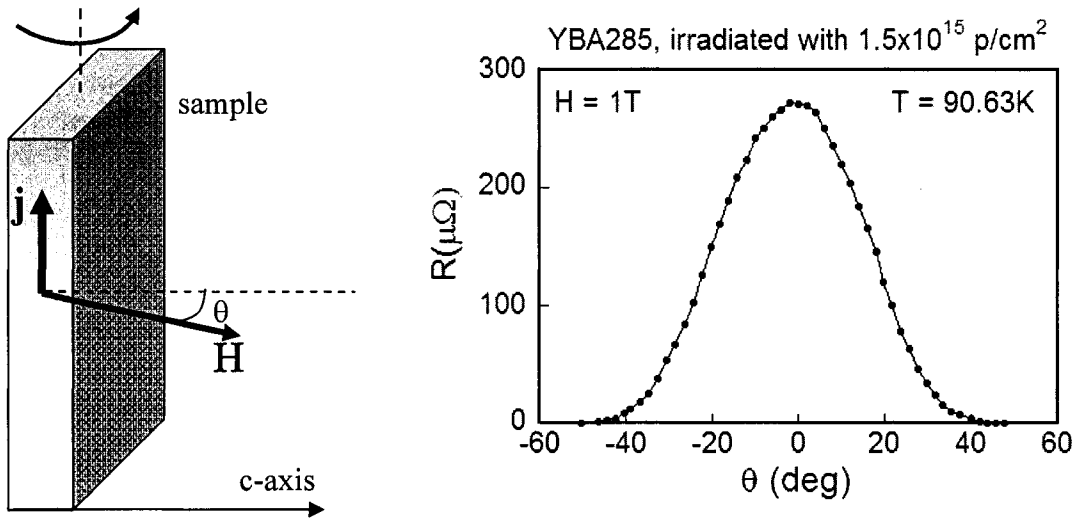

Figure 23 Angle dependence of the electrical resistance. Orientation of the magnetic field relative to the crystal c-axis is illustrated at left, while the variation of resistance with the angle is exemplified at right, for the case of YBA285, after irradiation.

The samples were successively irradiated with 9MeV protons, with fluences ranging from 0.25 to 2.0×10^{15} p/cm^2. The superconducting properties were probed using a combination of electrical transport and ac specific heat measurements.

Properties of the crystals are summarized in Table 2, which lists irradiation doses, zero field superconducting transition temperatures T_c (determined from the peak of resistivity's derivative), transition widths (T_c to zero resistivity) as well as the relative resistivity [$\rho_{relative}$= ρ(95K, irradiation dose)/ρ(95K, unirradiated)] and the corresponding height of the peak in the specific heat($|C_{transition} - C_{95K}|/ C_{95K}$). The increase of normal state resistivity ρ(95K) after the proton irradiation was less than 6% even at the highest dose and is comparable with other published results. There is also a general agreement about the degradation of the superconducting properties following irradiation. We found that within the scatter of the measurements, there was no detectable change in T_c to within ~0.6 K. The previous reports of the response of the critical temperature to irradiation vary. Several studies using 3MeV proton irradiation found that the critical temperature drop is ~1K[12] for 1×10^{16} p/cm^2 and up to 1.5K[13] and 2K[3] for a double dose. For example, in the case of YBA285, if the change in T_c were linear with dose, this would correspond to a maximum change of ~ 0.2K for the highest dose used in our study, which is within the scatter of the measurements. The width of superconducting transition remains roughly unaffected.

4.3 Transport Measurements Results

The left panel of Figure 24 a) presents the normalized resistivity $\rho_n(T) = \rho(T)/\rho(95K)$ as a function of normalized temperature for the sample YBA285 before irradiation in applied magnetic fields ranging from 0 to 8T, in 1T increments. The field was applied parallel to the crystallographic c axis. In the zero field case the

Table 2 Summary of properties of samples employed in this study

CRYSTAL	YBA285					YBA256				WYB005		ULM1001	
Dimensions (μm)	880x440x40					680x630x150				750x660x80		1340x1150x200	
Dose (10^{15} p/cm^2)	0.00	0.50	1.00	1.50	2.00	0.00	0.50	1.50	2.00	0.00	1.00	0.00	1.00
T_{c0} (K)	92.80	92.85	92.81	92.83	92.90	92.99	93.20	93.15	93.30	93.43	93.35	92.27	91.60
δT_c (K)	0.43	0.44	0.36	0.39	0.33	0.28	0.18	0.18	0.18	0.79	0.75		
Resistance measurements-$\rho_{relative}$	-	1.035	1.051	1.049	1.063	-	1.095	1.219	0.992	-	1.010	N/A	N/A
Specific Heat measurements-Peak's height (%)	N/A					N/A				N/A	2.68	3.80	3.75

resistivity drops sharply at the superconducting transition, with a transition width of only 300 mK and zero resistivity occurring at 92.8 K. As the field is increased, the transition broadens and moves toward lower temperatures. At 8T, the transition width has increased to 5K and the zero resistivity temperature has shifted down to 77.8K.

Besides the broadening of the superconducting transition, another significant feature can be seen in the resistivity curves. The electrical resistivity exhibits a discontinuous drop to zero over the full range of nonzero magnetic fields used in this investigation. This sudden decrease of resistivity is associated with a first order phase transition as the high temperature vortex liquid freezes into a vortex solid. For this crystal, the kink occurs at roughly $\rho_n \approx 10\%$ for the 1T transition and the height of the kink increases with increasing field, reaching a maximum of $\rho_n \approx 14\%$ of the signal for 2T, after which it decreases with increasing field.

The first order phase transition can be seen more clearly in the derivative of $\rho(T)$, shown in the right panel of Figure 24 a), where the discontinuity in $\rho(T)$ appears as a sharp peak. It has been shown that the onset of the sharp, narrow peak in $d\rho/dT$ coincides with the onset of the step in magnetization measurements[14,15]. Thus we define the first order melting temperature T_m as being the onset of the peak in $d\rho/dT$. In a typical crystal, the kink in $\rho(T)$ disappears at low fields, indicating the existence of a lower critical point (H_{lcp}), where the first order melting transition (FOMT) line is replaced by a continuous transition. The reported H_{lcp} in the literature varies between 5T[16,17] and 0.5T[18]. For YBA285, the value is unusually low, lower than the magnetic fields values applied in the investigation (>0.05T). At higher fields the FOMT terminates at an upper critical point (H_{ucp}), but this is not observable in the case of YBA285 due to the limitations of the experiment: the maximum value of the applied magnetic field of our system is 8T. The melting transition broadens as it

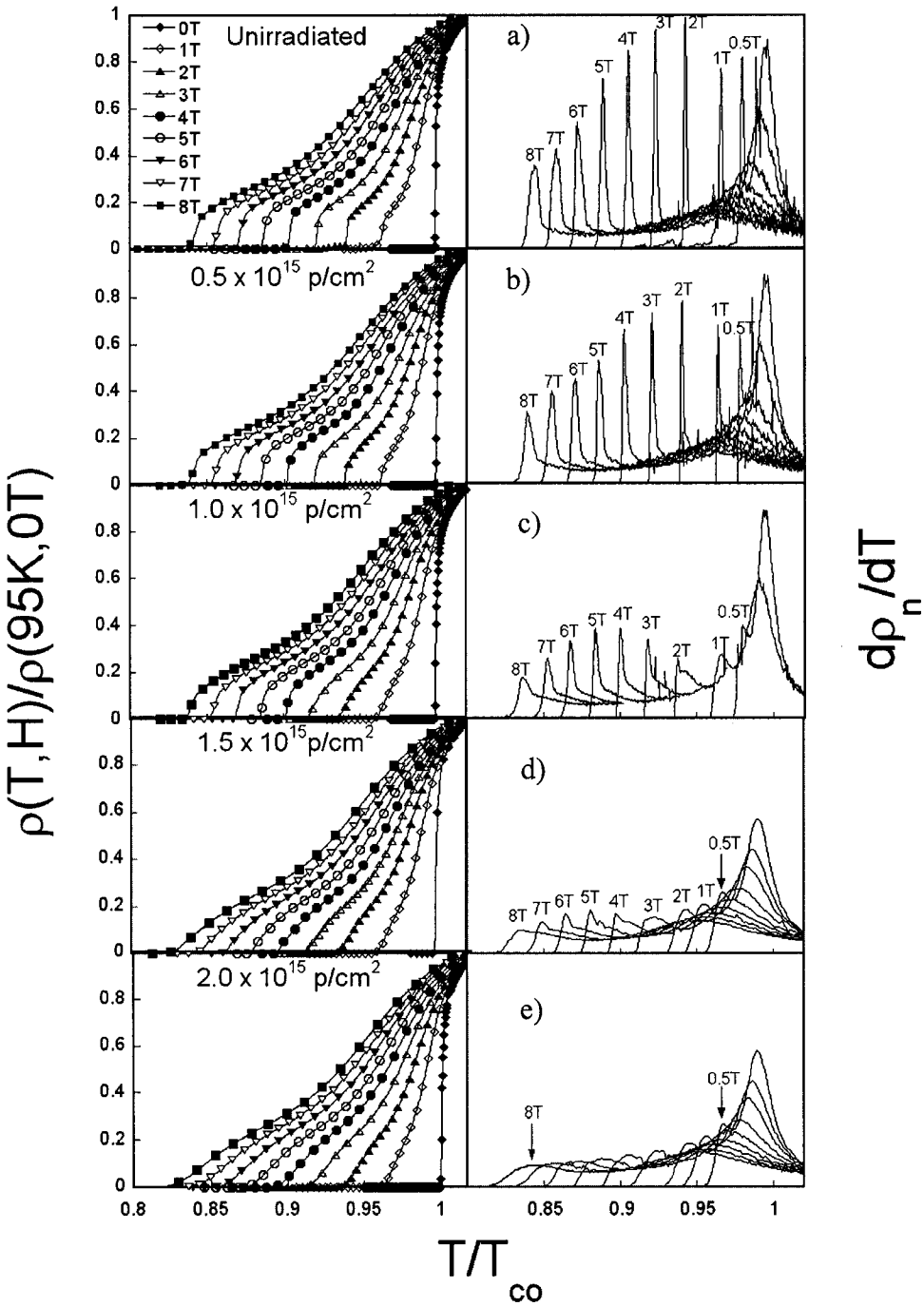

Figure 24 Field dependence of the normalized resistivity (left panel) and its derivative (right panel) for YBA285. The data are presented for different irradiation doses and for magnetic field values ranging from 0T to 8T, in 1T steps (with the exception of the lowest field shown, 0.5T).

draws near an upper critical point, starting from 0.1K at the lowest field considered in the study (0.05T), reaches roughly 0.5K at low fields to become more than 1K for the highest field used, 8T. Compared with the broadening of T_c transition this is several times lower: ~7 times lower at 0.05T and ~5 times lower at 8T.

The sample was then successively irradiated and then measured after each irradiation. The results indicate that the size of the kink in the resistivity [left panel of Figure 24 b) to e)] and the height of the peak in its derivative [right panel of Figure 24 b) to e)] decrease progressively with the irradiation dose. We did not include here the results for the 0.25×10^{15} p/cm^2 because the changes imposed by this low dose are insignificant.

Further understanding of the response to proton irradiation can be found in the behavior of the lower critical point. Figure 25 illustrates how we find H_{lcp}; the graph depicts the specific case of sample YBA285 after an irradiation with a dose of 1.0×10^{15} p/cm^2. The peak in the temperature derivative of resistivity marks the

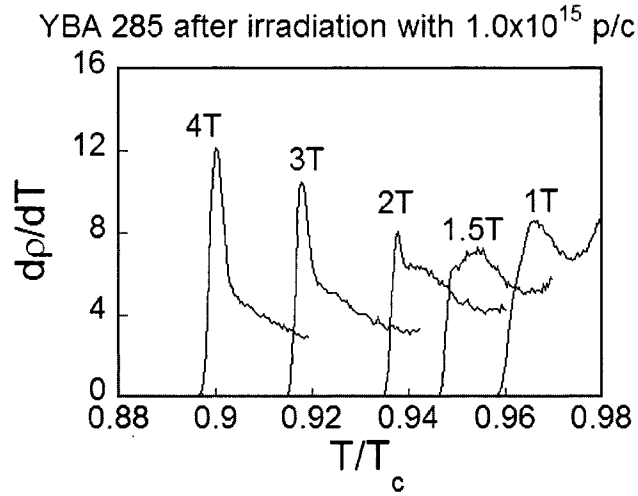

Figure 25 Focus on how the peak in the resistivity derivative disappears in a decreasing magnetic field. The series of fields were chosen above and below the lower critical point.

presence of the first order transition for fields equal with and larger than 2T. The peak is not visible at 1.5T or lower, so the probable value of H_{lcp} in this case is 1.75T, with an uncertainty of ±0.25T.

In the quest for a bigger picture, is interesting to follow how the position of the lower critical point depends on the increasing point disorder. While an irradiation dose of 0.5×10^{15} p/cm^2 shifts H_{lcp} to 0.1T, higher doses have a more impressive impact upon the position of the lower critical point: for 1.0×10^{15} p/cm^2 H_{lcp} is 1.75T, while for 1.5×10^{15} p/cm^2 it reaches 4T. For a 1.5×10^{15} p/cm^2 irradiation dose H_{ucp} drops into our measured field range and can be observed at 7T. Increasing the irradiation dose (2.0×10^{15} p/cm^2) leads to the disappearance of the kink in $\rho(t)$ and the associated peak in $d\rho/dT$ at all fields, suggesting the suppression of the FOMT (Figure 24 e). These results suggest that the FOMT is suppressed as the two critical points move toward each other on the melting line and finally merge.

To determine how universal this response to proton irradiation is, we compared these results with those obtained on two other detwinned crystals: YBA256 and WYB005. The outcomes for the normalized resistivity and its derivative with respect to the normalized temperature for all three crystals are compared in Figures 26 and 27, respectively. The graphs are arranged so that the columns indicate the data for a given crystal and the rows correspond to a given irradiation dose. T_{c0} ranged from 92.80K for YBA285 to 93.43K for WYB005 and showed very little change upon irradiation.

The first evident feature is the presence of the FOMT for all the three crystals. However, the size and the sharpness of the resistivity kink associated with the FOMT differ from one sample to another and this is mirrored by the height and the width of derivative's peak. Before irradiation the kink in the normalized resistivity reaches its

maximum at ~2T for YBA285 while it appears at ~4T for both YBA256 and WYB005. The maximum height of the kink, mirrored by the corresponding peak in the derivative, varies among the three crystals; the largest occurs for YBA285, at 13.3% from the normal resistivity value (at 95K) and drops to 9.6% for WYB005 and 4.2% for YBA256. Thus the initial states of the three crystals vary before irradiation, most likely due to slight variations in the purity, oxygen content and size of the sample.

Despite the differences in the initial conditions, the qualitatively shape of the ρ and dρ/dT curves is very similar and responds similarly to irradiation. All three show a gradually decrease in the ρ(t) kink height and in the melting temperature. The precise response of the melting transition will be discussed in more detail after the presentation of the ac specific heat results.

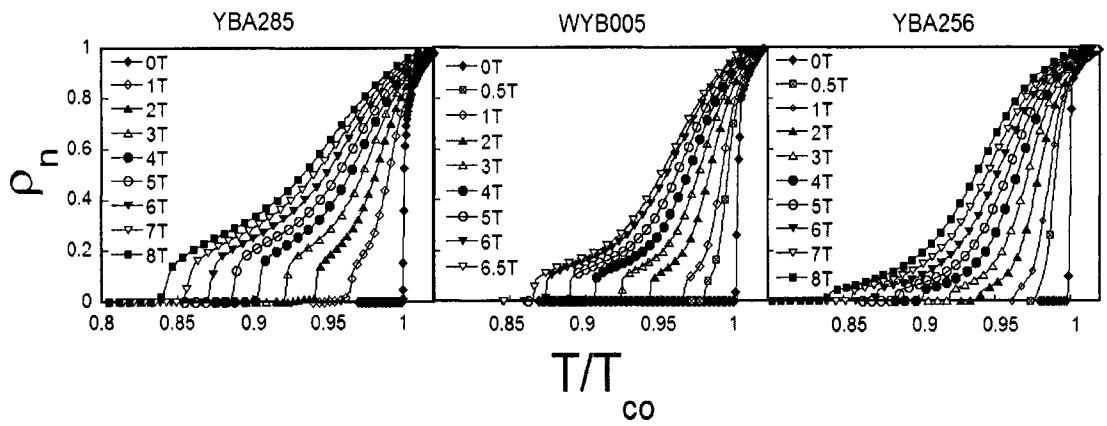

Figure 26 Transport measurements results before irradiation. The results are presented for fields between 0 and 8T for two of the samples (YBA285 and YBA256). The maximum field available in the case of WYB005 is 6.5T. The kink in the resistivity, that indicates the melting transition, is visibly different: the sharpest appear to be for the sample WYB005, while is much more reduced for sample YBA256.

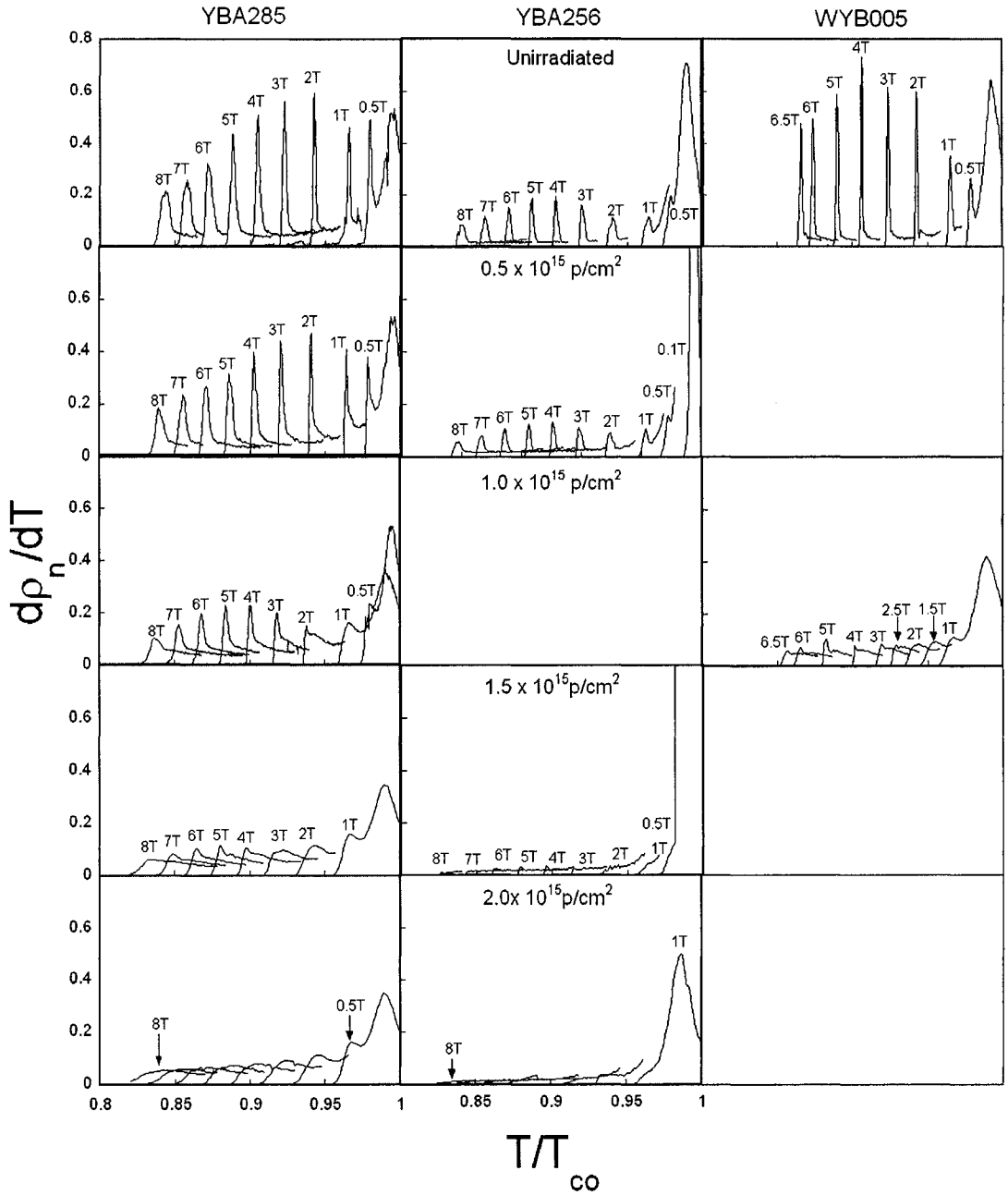

Figure 27 Evolution of temperature derivative of electrical resistivity with irradiation. Rows show the results corresponding to the same irradiation dose. While the magnitude of the peaks differs from one crystal to another, the trend upon irradiation is the same: a decrease of the peaks sizes and a downward shift in temperature.

4.4 AC Specific Heat Measurements Results

We extended our investigation by probing the vortex matter through the ac specific heat technique. The specific heat data for ULM1001 are displayed in Figure 28. Measurements were taken before and after irradiation with 9Mev protons to a dose of 1.0×10^{15} p/cm^2. The magnetic field ranged from 0 to 14T and was applied parallel to the crystallographic c axis. To picture the details more clearly, we have subtracted the background of the zero field specific heat $C_0(T)$ from the data taken in the presence of the magnetic field. The results present the temperature dependence of the relative change in specific heat.

The superconducting transition appears as a clear increase in the specific heat of the sample. This ΔC variation at the transition is 3.88% of the zero field specific heat signal and remains unaffected by the proton irradiation. This jump in the specific heat looses its sharpness in the presence of magnetic field, becoming more flat and shifting downward in temperature as the field increases. The gradual crossover from the normal state to the superconducting state manifests itself through the appearance of a plateau in the $\Delta C/C$ data, and is similar for different fields.

The distinct thermal signature of the FOMT is indicated by the sharp peak in the specific heat data, as shown in Figure 28 by the arrow for H = 4T. Before irradiation, the specific heat peak indicating the FOMT represents 0.41% from the signal at its maximum, which occurs at 4T, while after irradiation the height of the peak drops to just 0.16% from the signal, at the same field. The attenuation of the melting transition signature is visible at all field values and confirms the results obtained through electrical transport measurements. Moreover, the peak shifts to lower temperatures after irradiation, an effect also present in the resistivity results.

At the melting transition, the specific heats displays not just a peak but also a

step-like increment, present even when the peaks disappear, consistent with similar reports[18,19]. Before irradiation the peaks associated with the FOMT are visible for the whole range of magnetic fields presented in Figure 28, while after irradiation the signature of the first order transition is limited to a narrow field range, 2 to 5T. The

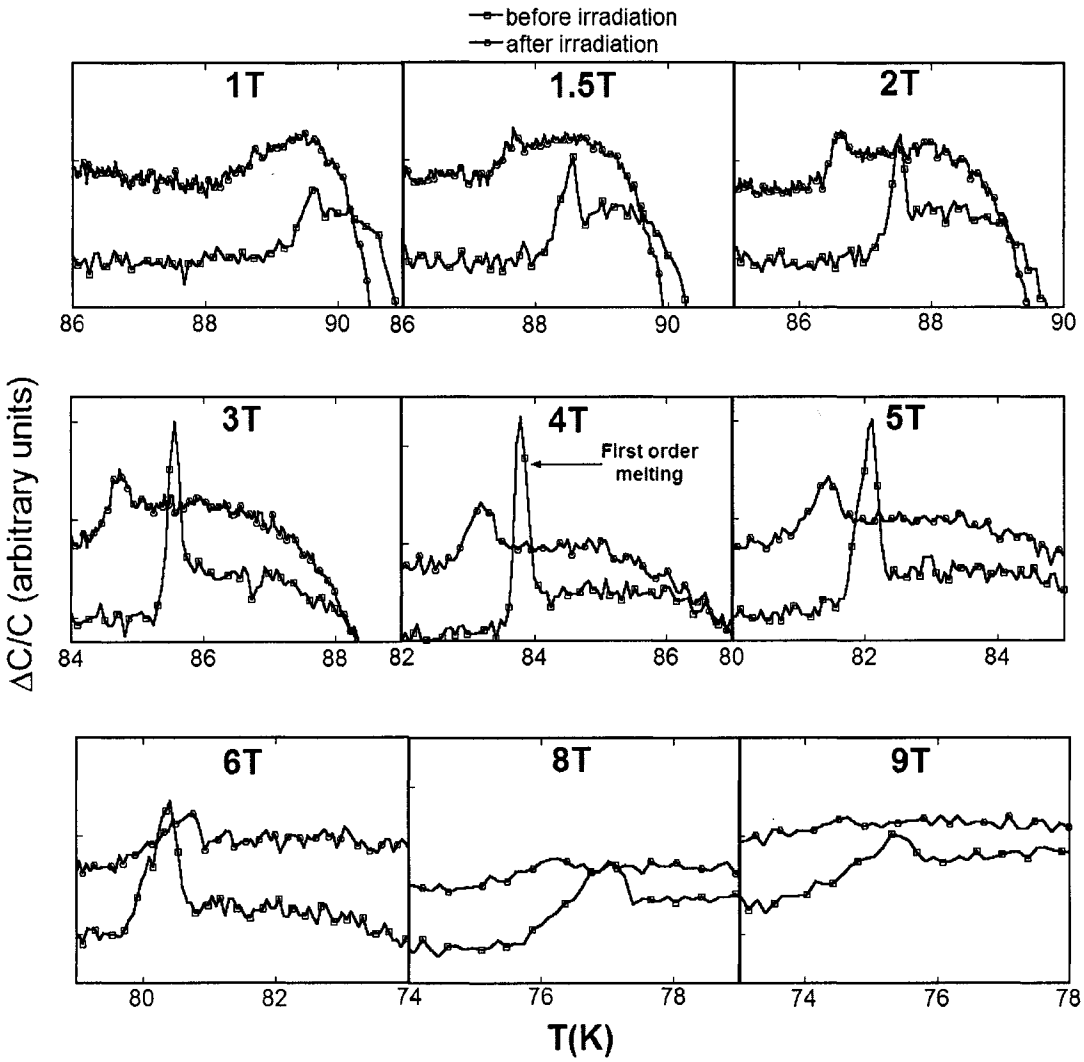

Figure 28 Specific heat measurements results. The impact of proton irradiation is visible by comparing data obtained at the same fields, before and after irradiation. Results are presented for fields between 1 and 8T. (In order to preserve the proportions, the x-y window has the same size).

presence of the steps in the specific heat data is associated with a second order phase transition. As described by specific heat measurements results, the evolution of the melting transition upon irradiation is marked by correspondence with the results obtained from resistivity measurements. In order to elaborate the parallelism between the two type of measurements and to confirm the findings for all crystals, in the second part of this chapter we will survey the evolution of defining superconducting properties with irradiation, such as the melting temperature, the width of the transition, the critical current and the resistivity angular dependence.

4.5 Melting Transition Evolution upon Irradiation

The general trend upon irradiation is verified by the fairly good grouping of melting temperature values for different doses and magnetic field values, as shown in Figure 29: T_m drops fairly linearly for all four crystals and the slope of the line is alike. For clarity, the top graph presents the linear fit of the melting temperature evolution with irradiation.

As seen from the electrical transport measurements, the qualitatively shape of ρ and $d\rho$ curves is the same, indicating the same response upon irradiation: a gradually lessening of FOMT indicators as the melting temperature is decreasing. T_m drops 0.54K for YBA285, 0.46K for YBA256 and 0.7K for WYB005 after a 1.0×10^{15} p/cm^2 irradiation dose and for a magnetic field of 6T. A similar shift is recorded from the specific heat measurements: at 5T, T_m drops 0.35K after a 1.0×10^{15} p/cm^2 irradiation. The average T_m shift of ~0.51K/10^{15} p/cm^2 compares very well with other published results[11]. The maximum irradiation dose for which the melting can be observed is 1.5×10^{15} p/cm^2. At higher doses the melting transition is completely suppressed.

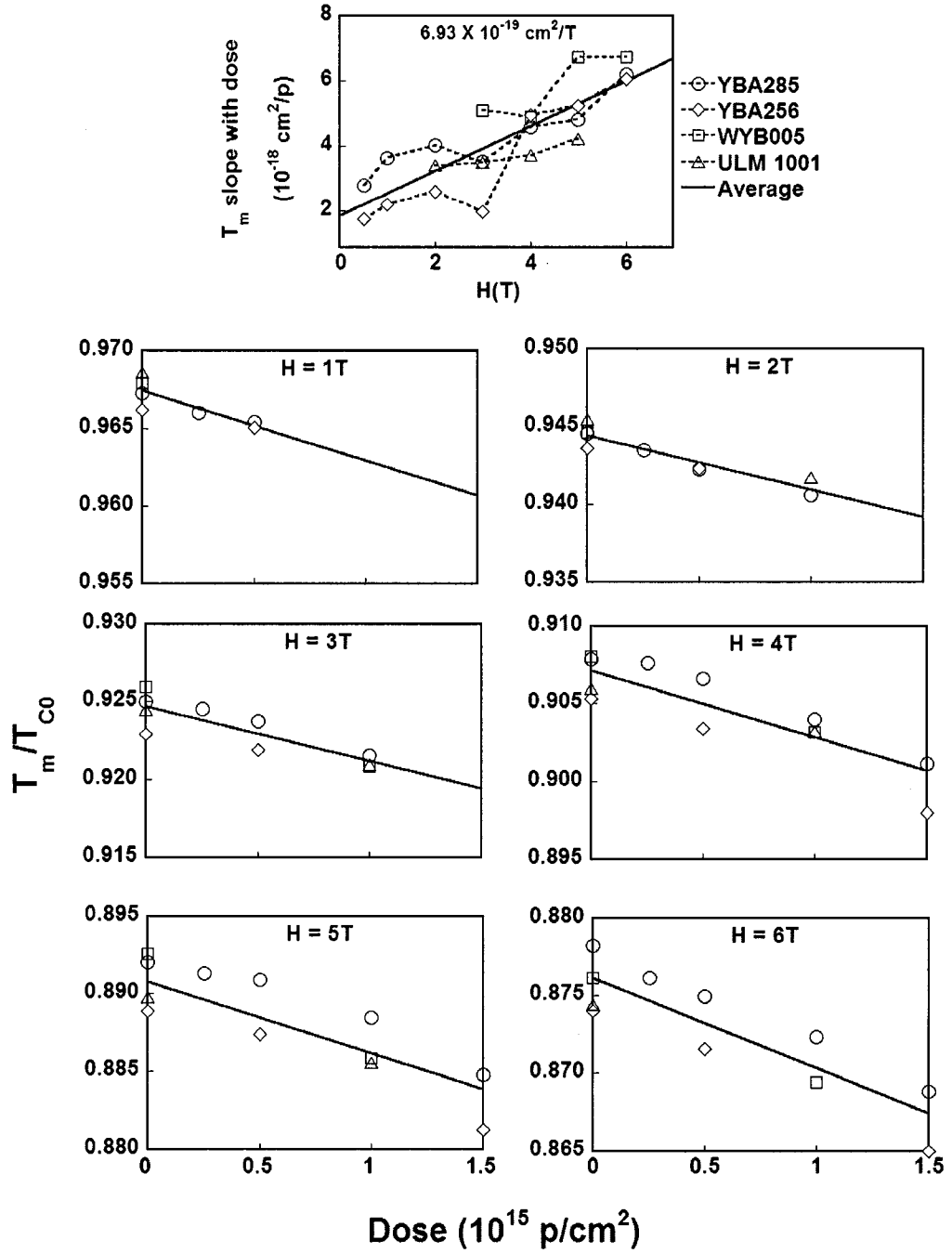

Figure 29 Melting temperature evolution with irradiation. The shift of T_m is observed here for different magnetic fields, from 1 to 6T, showing consistency among the different crystals measured and independent of the type of measurement. The top graph summarizes the response of T_m/T_{c0}, displaying a similar slope that increases with the field.

In agreement with our previous affirmation, increasing the defect density pushes the melting transition toward lower temperatures. The shift of the melting temperature with proton irradiation is indicating an increased vortex entanglement favored by point disorder[20,21].

4.6 Effect of Proton Irradiation on the Melting Transition Width

Figure 30 displays the comparative evolution of the transition width upon

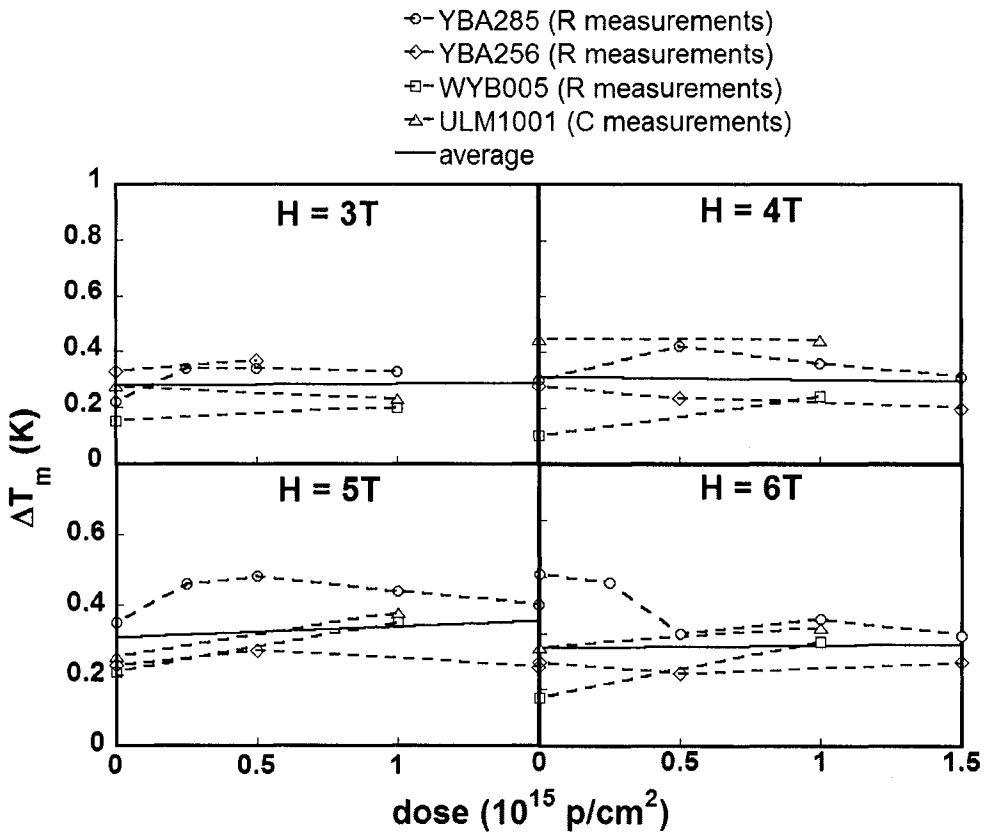

Figure 30 Melting transition width evolution with irradiation for magnetic fields ranging from 3 to 6T. All four crystals considered for this study preserve the width of the melting transition. The results of the linear fits are as follows: $y = 0.2794 + 0.00875x$ for 3T; $y = 0.3120 - 0.01344x$ for 4T; $y = 0.3080 + 0.03405x$ for 5T and $y = 0.3494 + 0.01128x$ for 6T.

irradiation. To incorporate both specific heat and resistivity measurements, the transition width was calculated from the difference between the temperatures corresponding to the peak in dρ/dT or C and the peak's onset temperature (T_m).

As Figure 31 summarizes, within reasonable limits, the transition remains narrow for all four samples considered in this study and there is a similar reaction to the magnetic field. FOMT does not broaden with increasing density of point disorder, signaling a high liquid to solid interface energy[11].

Despite the downward shift of T_m, the irradiation does not affect the melting transition width, as is exemplified in Figure 32 for the resistivity measurements on sample YBA285. We define the melting transition width as the difference between the onset temperature and the temperature corresponding to the same value of resistivity derivative. In energy terms, the response of the transition width is determined by the balance between the energy spent in creation of a surface between the two phases and the energy acquired for a coherence volume to change its phase relative to the surrounding material[22,23].

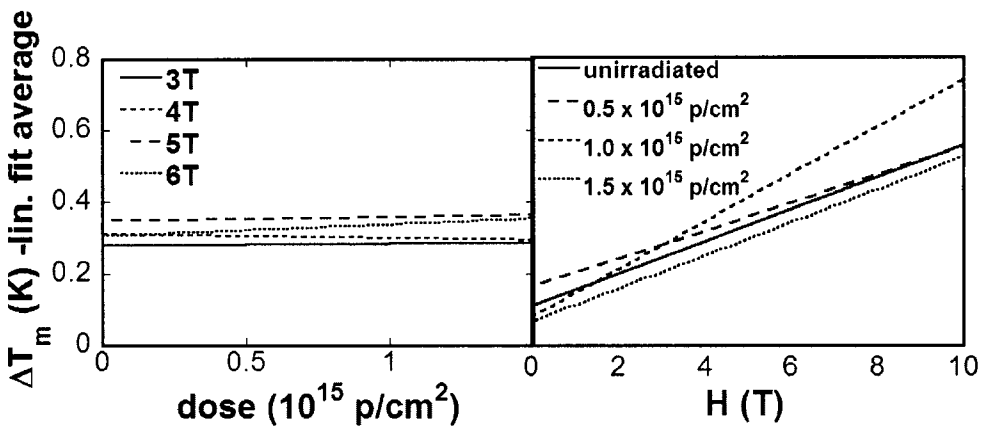

Figure 31 Irradiation dose and field dependence of melting transition width. The two graphs compare the ΔT_m averages: increasing defect density does not change the width of the melting transition, while increasing fields provoke similar increases of ΔT_m for all samples.

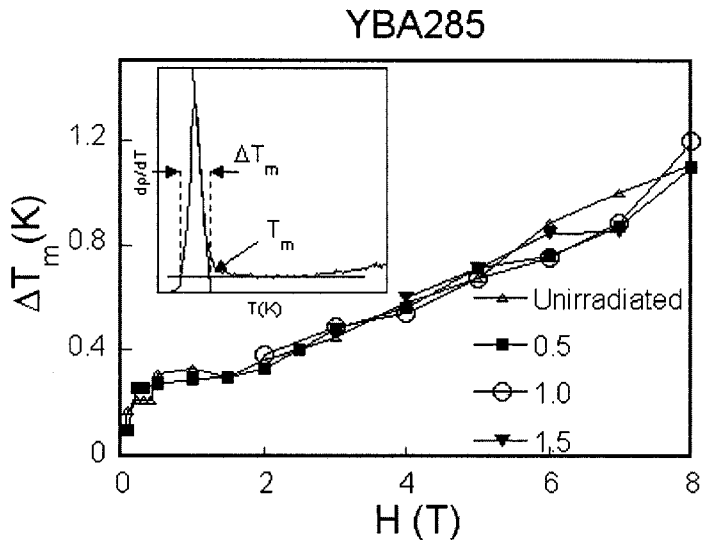

Figure 32 Melting transition width for different irradiation doses (in units of 10^{15} p/cm^2).Transition width is defined as the distance, measured in Kelvin, between the onset temperature of dρ/dT and the temperature corresponding to the same dρ/dT value, close to the point where resistivity becomes zero- as shown in the inset.

4.7 Current-Voltage Characteristics and Critical Current

The behavior of the vortex matter is extremely sensitive to the presence of defects in the sample, and so is the critical current density. Therefore, a relevant exploration of vortex matter phase transitions can be made by measuring the I-V characteristics in the critical regions. The log-log graphs successfully show the reaction of the vortex system upon crossing the demarcation line between the liquid and solid state. In the vortex liquid phase, the E vs J dependence exhibits a linear relationship, as an indication of an ohmic dissipation presence in this regime, while below the melting temperature the relationship becomes profoundly nonlinear (Figure 33 unirradiated, left side). As we follow the manner in which the proton irradiation influences the shape of I-V dependence (Figure 33, 0.25 to 2.0×10^{15} p/cm^2), we discover an altered

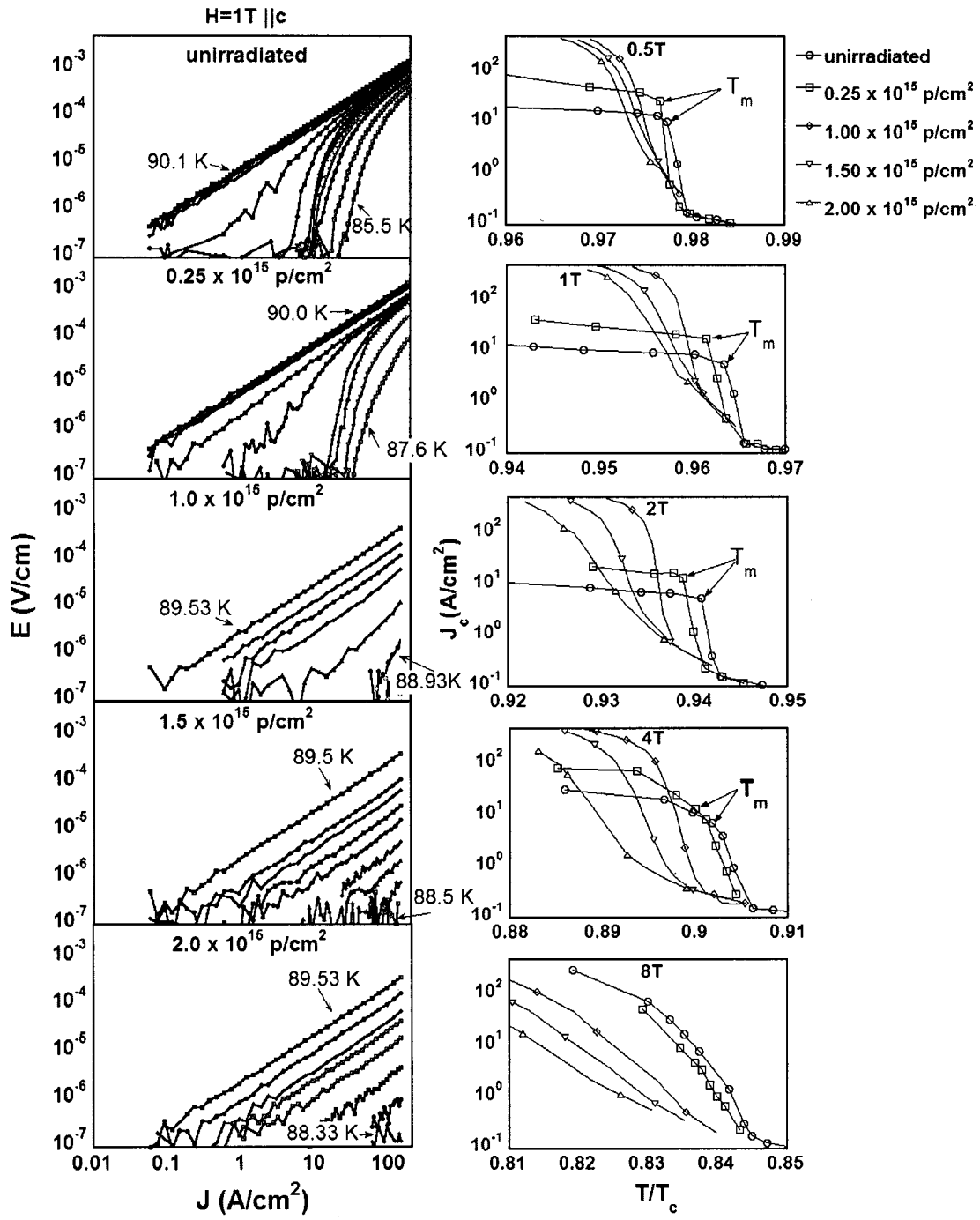

Figure 33 Evolution with irradiation of the I-V curves (left side) and critical current density (right side) for crystal YBA285. T_m was determined as the intersection between the linear fit of the quickly decreasing portion of the J_c function and its upper part, situated at lower temperatures.

contour of the curves. They become more linear with increasing irradiation dose.

To find the critical currents corresponding to different temperatures we used a criterion of 10^{-6} V/m to define J_c. There is a good correlation between the values of the melting transition temperature extracted from the J_c graphs (Figure 33, right side) and T_m established using the derivative of resistivity as reference. As reported previously[24,25], J_c decreases with increasing temperature following a quasi-exponential dependence and drops sharply when the melting temperature is reached. The shape of the J_c curves changes dramatically with irradiation: the sudden dip at T_m gradually disappears as the curves flatten out. Besides the altered shape, the onset of J_c changes, too. The melting temperature, as well as the onset of J_c moves down in temperature with irradiation.

The increase of the critical current with irradiation is temperature dependent: for example, at 1T and 88K, J_c is enhanced by a factor of approximately 50 after a 1×10^{15} p/cm^2 irradiation dose, but just by an order of magnitude if the dose is 2×10^{15} p/cm^2, consistent with many earlier reports[5,26,27,28]. In other words, for particular temperature and magnetic field values there is an optimal enhancement of the critical current in the terms of the irradiation dose[29]. This is because T_m is shifting down to lower temperatures with increasing dose.

4.8 Angular Dependence of Resistivity

The angular behavior of the resistivity for sample YBA285 is shown in Figure 34 as a function of the angle of the applied field with respect to the c axis of the crystal for H=2T. The magnetic field is rotated in a plane perpendicular to the current density, such that the Lorentz force is always at its maximum value. The magnetic field was tilted from the 90° (H || b-axis) to 0° (H || c-axis) at different fixed

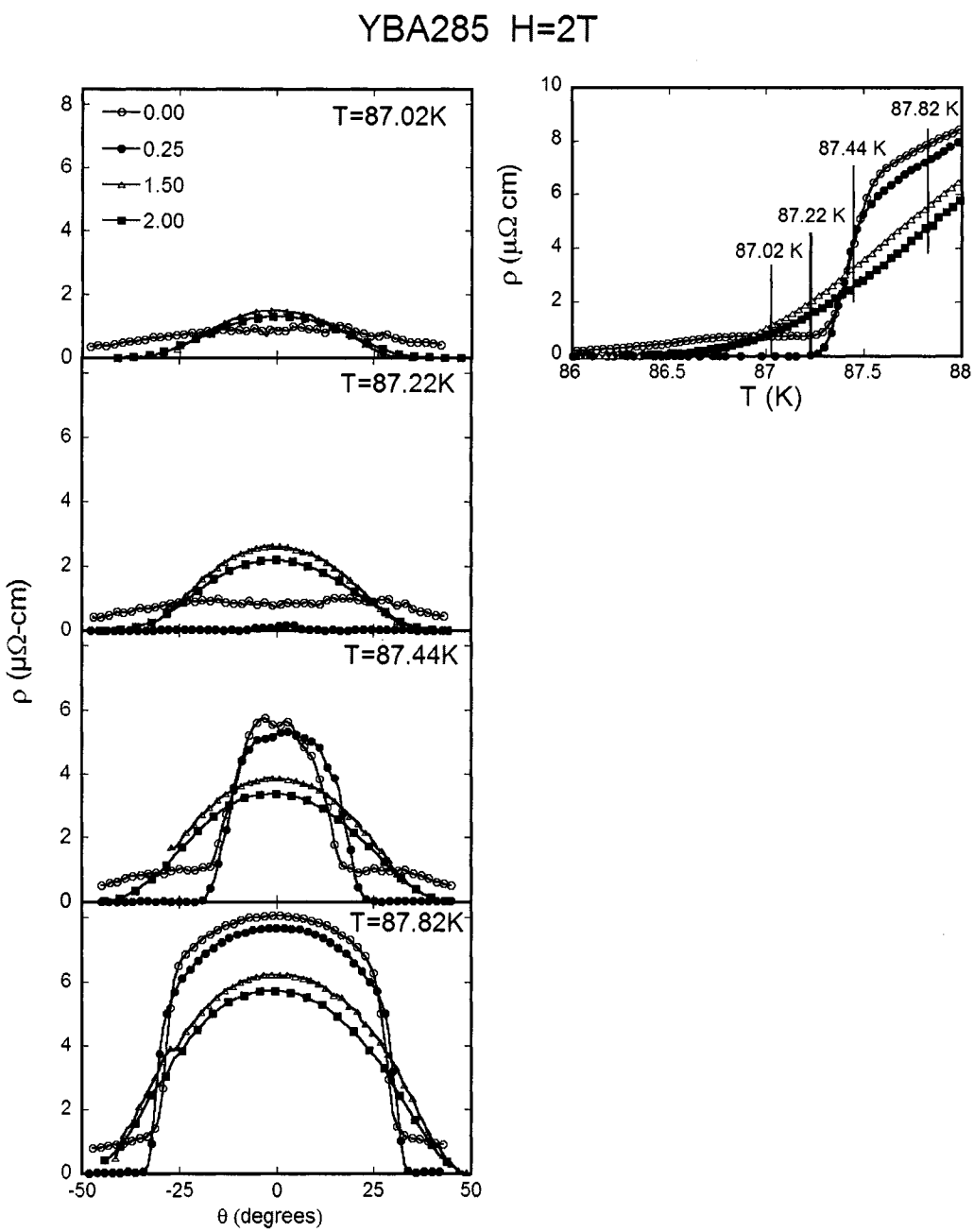

Figure 34 The change in the angular dependence of resistivity upon irradiation. Results are shown for sample YBA285. The right hand graph depicts the temperature at which the four ρ vs θ curves were taken. The irradiation dose is presented in units of 10^{15} p/cm^2.

temperatures, in an applied field H = 2T. The resistivity is a smooth function of the angle with a maximum value for the case when the field is aligned parallel to the c-axis and a minimum when the field is parallel to the b-axis. This angular dependence of the resistivity arises from the anisotropy of the material. The shape and size of the resistivity peak depend also on the chosen constant temperature for which the angular sweep was done: the peak becomes evident at higher temperatures and is loosing its sharpness with increasing irradiation dose. The fact that the curves are smooth in the proximity of 0 degrees proves the fact that defects induced by proton irradiation are uncorrelated. In the case of correlated defects, such as columnar tracks caused by heavy-ion irradiation, a sharp, downward cusp is reported in the angular dependence of resistivity. The resistivity decreases abruptly when the vortices and the columnar defects are aligned.

4.9 Comparative Phase Diagrams

The vortex phase diagram of high temperature superconductors represents an extensive field of research. Competition between vortex-vortex interactions, thermal fluctuations and pinning due to defects present in the sample is the key factor in understanding the variety of vortex matter states and the transitions that separate them. As discussed in chapter 2, the prominent aspect of HTS magnetic field-temperature phase diagram is the first order vortex melting line, the fingerprint of the transition between a vortex liquid and a Bragg glass[30,31,32,33].

The proton irradiation influence is summarized in the comparative phase diagram, Figure 35. The initial position of the melting line is almost the same for all four samples, with slightly different ending points at low fields- but this will be the topic of next chapter. The upper critical point is visible only in the case of ULM1001,

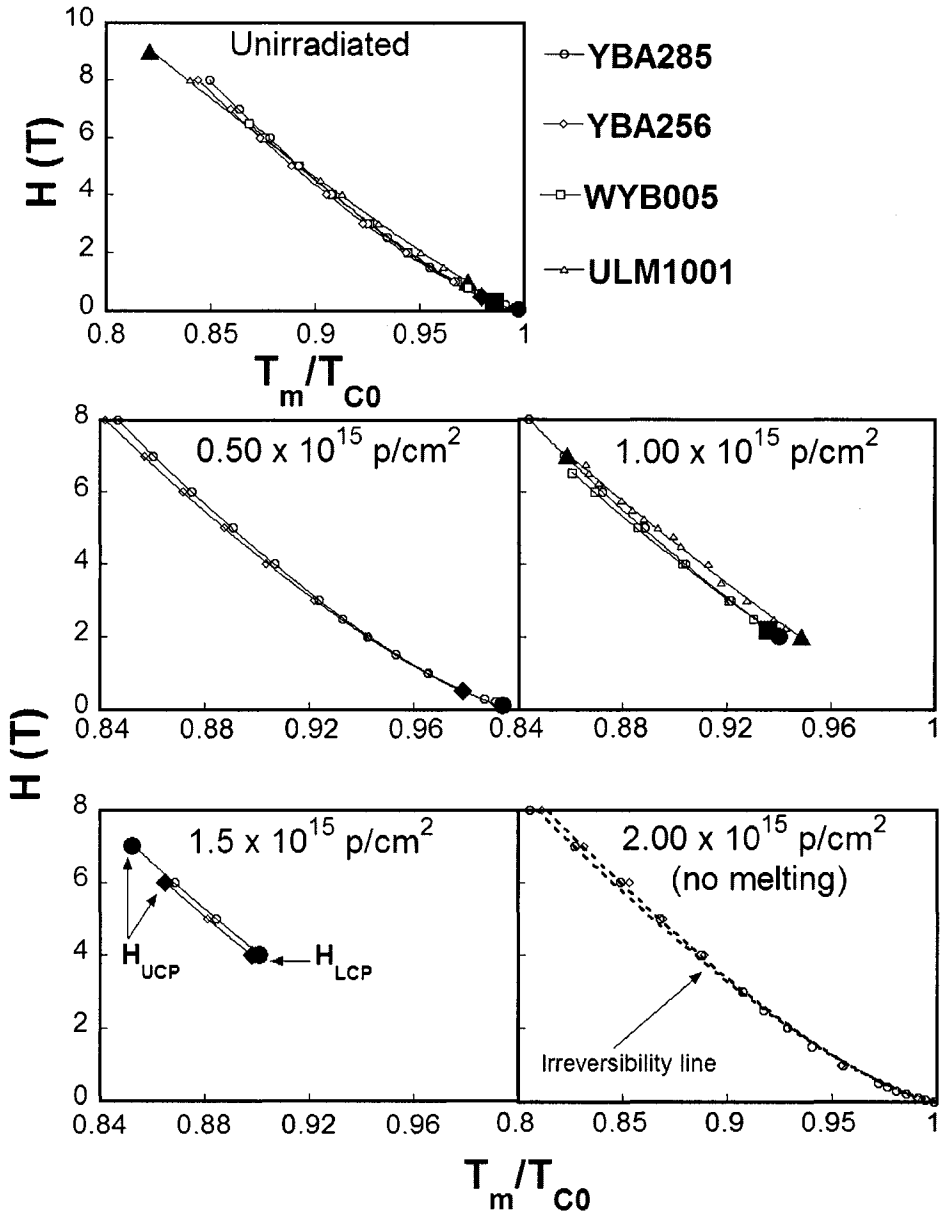

Figure 35 Comparative phase diagrams. Evolution with proton irradiation is presented for all four samples considered in this study. The solid, larger symbols denote the critical points of the FOMT. The transition was fitted through a power law: $H = H_0(1 - T/T_{c0})^n$, with H_0 around 100T and n~1.3. The data used in these phase diagrams were obtained through electrical transport measurements, with the exception of ULM1001, for which specific heat results were used.

at 9T. For the other crystals the upper critical point is above the magnetic field values used in the investigation.

The power fits applied before irradiation led to the following values for H_0: 97.22T for YBA285, 66.23T for YBA256, 110.96T for WYB005 and 104.35T for ULM1001.The values determined for the exponent n (same order of the samples) are: 1.34, 1.16, 1.39 and 1.38.

There is a good correlation of the results regarding the evolution of the melting transition line. Established through both type of measurements, resistivity and specific heat, proton irradiation pushes the melting transition downward in temperature. Among all four crystals, there is a solid consistency in the location of FOMT at different irradiation doses. The melting lines vary from one sample to another by less than 1% of T_m before irradiation. Moreover, we discovered that the response of the critical points is very similar for all samples, visible in the way that H_{lcp} shifts up in field and H_{ucp} shifts down in field as the point defect density increases. We were also being able to verify the validity of a threshold in the irradiation dose that will produce a confluence of the upper and lower critical points, suppressing the first order melting transition. This happens at a dose of 2×10^{15} p/cm^2, where the transition between vortex liquid and solid states becomes continuous, i.e. a second order phase transition.

In conclusion, we investigated the vortex phase diagram by the means of electrical transport and specific heat measurements. Four YBCO single crystals were used in the investigation with the purpose of establishing how universal the response of the vortex matter to proton irradiation is. While the initial conditions for the four crystals were different, we were able to obtain a consistent, unified picture of the evolution of the properties describing the vortex matter behavior.

References

[1] A. M. Campbell and J. E. Evetts, Adv. Phys. **21**, 199 (1972)

[2] E. V. Thuneberg, J. Kurkijärvi, and D. Rainer, Phys. Rev. B **29**, 3913-3923 (1984)

[3] L. Civale, A. D. Marwick, M. W. McElfresh, T. K. Worthington, A. P. Malozemoff, F. H. Holtzberg, J. R. Thompson, M. A. Kirk, Phys. Rev. Lett. **65**, 1164–1167 (1990)

[4] L. Civale, A. D. Marwick, T. K. Worthington, M. A. Kirk, J. R. Thompson, L. Krusin–Elbaum, Y. Sun, J. R. Clem, and F. Holtzberg Phys. Rev. Lett. **67**, 648-651 (1991)

[5] T. J. Shaw, J. Clarke, R. B. van Dover, L. F. Schneemeyer, and A. E. White, Phys. Rev. B **54**, 15411-15416 (1996)

[6] R. B. van Dover, E. M. Gyorgy, A. E. White, L. F. Schneemeyer, R. J. Felder, and J. V. Waszczak, Phys. Rev. Lett. **56**, 26 (1990)

[7] G. C. Xiong, H. C. Li, G. Linker, and O. Meyer, Phys. Rev. B **38**, 240-243 (1988)

[8] K. Yokota, T. Kura, S. Katayama, M. Ochi, M. Murakami, A. Chayahara, and M. Satho, Phys. Rev. B **45**, 3098-3102 (1992)

[9] E. Mezzetti, S. Colombo, R. Gerbaldo, G. Ghigo, L. Gozzelino, B. Minetti, and R. Cherubini, Phys. Rev. B **54**, 3633-3639 (1996)

[10] A. M. Petrean, L. M. Paulius, W.-K. Kwok, J. A. Fendrich, and G. W. Crabtree, Phys. Rev. Lett. **84**, 5852-5855 (2000)

[11] L. M. Paulius, W.-K. Kwok, R. J. Olsson, A. M. Petrean, V. Tobos, J. A. Fendrich, G. W. Crabtree, C. A. Burns, and S. Ferguson, Phys. Rev. B **61**, R11910-R11913 (2000)

[12] T. K. Worthington, M. P. A. Fisher, D. A. Huse, Phys. Rev. B **46**, (1992)

[13] J. R. Thompson, Yang Ren Sun, F. Holtzberg, Phys. Rev. B **44**, 1 (1991)

[14] D. T. Fuchs, E. Zeldov, D. Majer, R. A. Doyle, T. Tamegai, S. Ooi, and M. Konczykowski, Phys. Rev. B **54**, R796-R799 (1996)

[15] J. A. Fendrich, U. Welp, W. K. Kwok, A. E. Koshelev, G. W. Crabtree, and B. W. Veal, Phys. Rev. Lett. **77**, 2073-2076 (1996)

[16] M. Roulin, A. Junod, A. Erb, and E. Walker, Phys. Rev. Lett. **80**, 1722 (1998)

[17] F. Bouquet, C. Marcenat, Physics and Materials Science of Vortex States, Flux Pinning and Dynamics. Kluwer Academic Publishers, Dordrecht, p. 743.(1998)

[18] A. Schilling, R. A. Fisher, N. E. Phillips, U. Welp, W. K. Kwok, and G. W. Crabtree, Phys.Rev. Lett. **78**, 4833 (1997)

[19] A. Junod, M. Roulin, J. -Y. Genoud, B. Revaz, E. Walker, A. Erb, C. Marcenat, R. Calemczuk and F. Bouquet, Physica C: Superconductivity, **282-287**, Pages 1425-1426 (1997)

[20] D. López, L. Krusin-Elbaum, H. Safar, E. Righi, F. de la Cruz, S. Grigera, C. Feild, W. K. Kwok, L. Paulius, and G. W. Crabtree Phys. Rev. Lett. **80**, 1070-1073 (1998)

[21] D. López, E. F. Righi, G. Nieva, and F. de la Cruz, Phys. Rev. Lett. **76**, 4034 (1996)

[22] Y. Imry and M. Wortis, Phys. Rev. B **19**, 3580-3585 (1979)

[23] J. Frenkel, Kinetic Theory of Liquids, p. 382 (Dover, New York, 1955)

[24] A. P. Malozemoff, Mater. Res. Bull. **15**, 50 (1990)

[25] J. R. Thompson, Y. R. Sun, L. Civale, A. P. Malozemoff, M. W. McElfresh, A. D. Marwick, and F. Holtzberg, Phys. Rev. B **47**, 14440-14447 (1993)

[26] P. D. Panetta, J. E. Ostenson, D. K. Finnemore, and C. L. Snead, Jr., Phys. Rev. B **52**, 15570-15574 (1995)

[27] G. C. Xiong, H. C. Li, G. Linker, and O. Meyer, Phys. Rev. B **38**, 240 (1988)

[28] C. Reichhardt, A. van Otterlo, and G. T. Zimányi, Phys. Rev. Lett. **84**, 1994-1997 (2000)

[29] G. Blatter, M. V. Feigel'man, V. B. Geskenbein, A. I. Larkin, and V. M. Vinokur, Rev. Mod. Phys. **66**, 1125 (1994)

[30] U. Welp, J. A. Fendrich, W. K. Kwok, G. W. Crabtree, and B. W. Veal, Phys. Rev. Lett. **76**, 4809-4812 (1996)

[31] H. Pastoriza, M. F. Goffman, A. Arribére, and F. de la Cruz, Phys. Rev. Lett. **72**, 2951-2954 (1994)

[32] R. Liang, D. A. Bonn, and W. N. Hardy, Phys. Rev. Lett. **76**, 835-838 (1996)

[33] T. Klein, I. Joumard, S. Blanchard, J. Marcus, R. Cubitt, T. Giamarchi, P. Le Doussal., Nature **413**, 404 (2001).

CHAPTER 5

INVESTIGATION OF THE YBCO PHASE TRANSITION BELOW THE LOWER CRITICAL POINT

5.1 Evolution with Irradiation of the Lower Critical Point

The last part of the previous chapter has followed the evolution of the melting transition line upon proton irradiation. Implicitly, these changes are reflected in the response to irradiation of the low field terminal point from the FOMT, the lower critical point. H_{lcp} is interesting from various perspectives: First, its existence has not been reported in other HTS materials and seems to be specific to YBCO crystals[1,2,3,4]. Furthermore, the evolution of the lower critical point upon irradiation opens up an uncharted portion of the phase diagram, raising intriguing questions regarding the natures of the vortex matter states located in that region.

In chapter 4 we presented experimental proof that H_{lcp} can be relatively easily influenced by induced uncorrelated disorder, confirming similar findings[4,5,6]. The response of the lower critical point is dependent on the strength and density of the defects. Following the universality trend, in all four crystals investigated, the lower critical point reacts very similarly to induced point defects. While obvious in the comparative phase diagrams (Figure 35), a better perspective of how the lower critical point reacts to proton irradiation is displayed in Figure 36. In small doses, the irradiation leaves H_{lcp} appears to be unaffected. While more data is needed to conclusively confirm this, we have tentatively identified a threshold value (0.5×10^{15} p/cm^2), beyond which the pinning strength is powerful enough to disorder the vortex lattice, forcing FOMT to terminate at higher fields as the irradiation dose is increased.

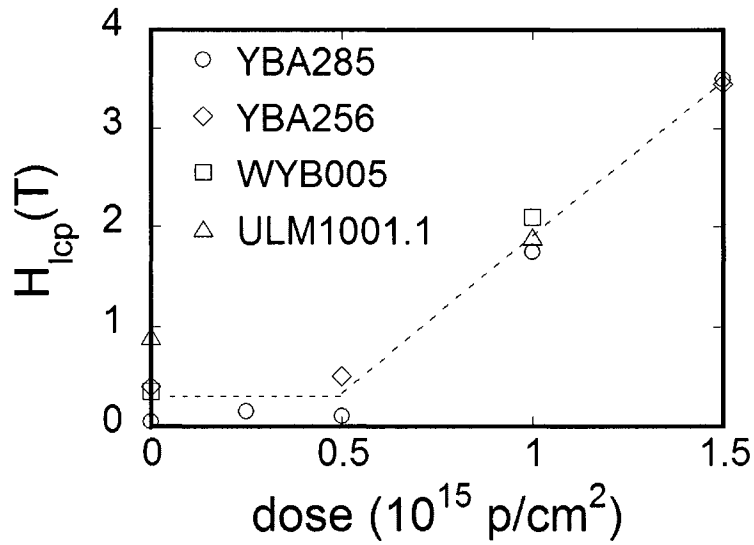

Figure 36 Response of the lower critical point to proton irradiation. The dashed line is just to guide the eye.

In the range where the position of H_{lcp} is influenced by proton irradiation, H_{lcp} appear to increase linearly with the dose. Within the limits given by the irradiation doses utilized, the linear upward shift of H_{lcp} is registered for all samples considered in the investigation. As an example, the value of the lower critical point is roughly the same, 2T for 1.0×10^{15} p/cm^2, 3.5T for 1.5 x 10^{15}p/cm^2, while vanishing for 2.0×10^{15} p/cm^2 as the melting transition is suppressed. In this range, where H_{lcp} is sensitive to irradiation, the approximate shift of the lower critical point with dose is 3.2T/10^{15} p/cm^2. The similar behavior upon irradiation of H_{lcp} for all four crystals validates the universality attribute conferred to proton irradiated YBCO crystals in the previous chapter.

The angular dependence of the lower critical point of the first-order melting line for crystal WYB005 is depicted in Figure 37. Before irradiation the angular dependence of H_{lcp} is smooth around 0 degrees, increasing from 0.3T at 0° to 1.6T at

90°. The higher value of $H_{lcp}(90°)$ relative to $H_{lcp}(0°)$ is typical of the anisotropy of the material. After irradiation the curvature of the line changes. Due to the scarcity of measurements, the experimental uncertainty leaves the exact shape of this curve uncertain. It is interesting to note that after irradiation, the anisotropy of H_{lcp} is reversed, with H_{lcp} (90°) being less than H_{lcp} (0°). It is not clear why this should occur.

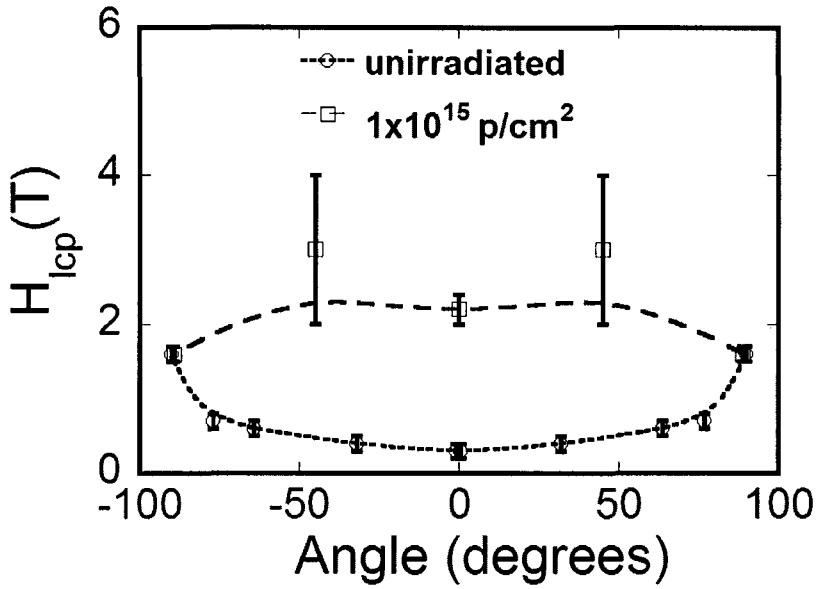

Figure 37 Angular dependence of the lower critical point. The results are presented for the sample WYB005. The error bars denote the precision of the measurements and are related to the availability of data at a specific field.

5.2 Nature of the Lower Critical Point

The vortex phase diagram of high temperature superconductors represents a large field of research. Theoretically predicted and experimentally confirmed in most of the reports, the solid state of vortex matter becomes glassy at high fields and the density and type of disorder are decisive factors for the occurrence of this

state[7,8,9,10,11]. Consequently, the first order melting transition line (FOMT) terminates at higher fields at an upper critical point, which appears to be present in both YBCO[12,13,14,15] and BSCCO[16,17]. The position of this upper critical point (UCP) is related to the type of defects present in the sample[6,11,15,18]. However, in some samples, H_{ucp} can be absent or above the highest magnetic fields (~30T) that are used in a typical study.

As explained in the first section of this chapter, the lower critical point is particularly interesting because is connected with the possible existence of new, unexplored vortex states and transitions, as emphasized in Figure 38. The diagram concentrates the attention on the H-T region surrounding H_{lcp}.

In our work we tried to address some fundamental questions: is there a phase transition below the H_{lcp} and if so, what is the order of this phase transition?

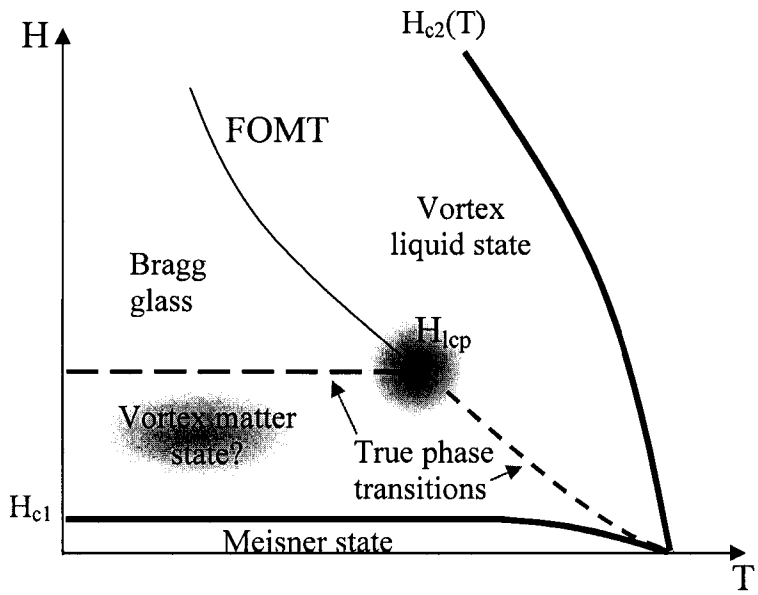

Figure 38 Proposed YBCO vortex phase diagram in the region of lower critical point.

Furthermore, what is the nature of the vortex matter that occurs below H_{lcp} in the low temperature region? There are two possible theoretically proposed vortex states that might occur below H_{lcp}, the vortex glass and the vortex molasses states. In the work that follows, we check for the signatures of both phases.

The manner we conceive to examine the low-field vortex matter is by trying to connect it with the existence of the LCP and the presumed transition that meets FOMT at this critical point. From our specific heat measurements (see Figure 28) we can affirm that a second order phase transition is present below the lower critical point, a fact sustained by the step present in the specific heat data.

A more detailed analysis can be performed for the case of sample WYB005, which was measured after irradiation using both techniques: specific heat and electrical resistivity. Results are presented in Figure 39. In the upper part, the two graphs showing the analyzed data are in very good agreement as for the position of H_{lcp} after irradiation. The peak of resistivity derivative is present at 2.5T and above this field value, signaling the melting transition, while at 2T and below the peak is absent. The cross over between a peak and a step in the specific heat data is visible in the upper, right graph; going down in field, the last distinguishable peak is at 2.25T, while becoming a step at 2T and below this value. The lower graph summarizes the irradiation effect on the FOMT and implicitly on the lower critical point. The magnetic phase diagram confirms the accord between the two types of measurements, especially regarding the response of the lower critical point to irradiation. Below 2.25T, representing the approximate value of H_{lcp}, the presence of the step in the specific heat data proves that there should be a second order transition.

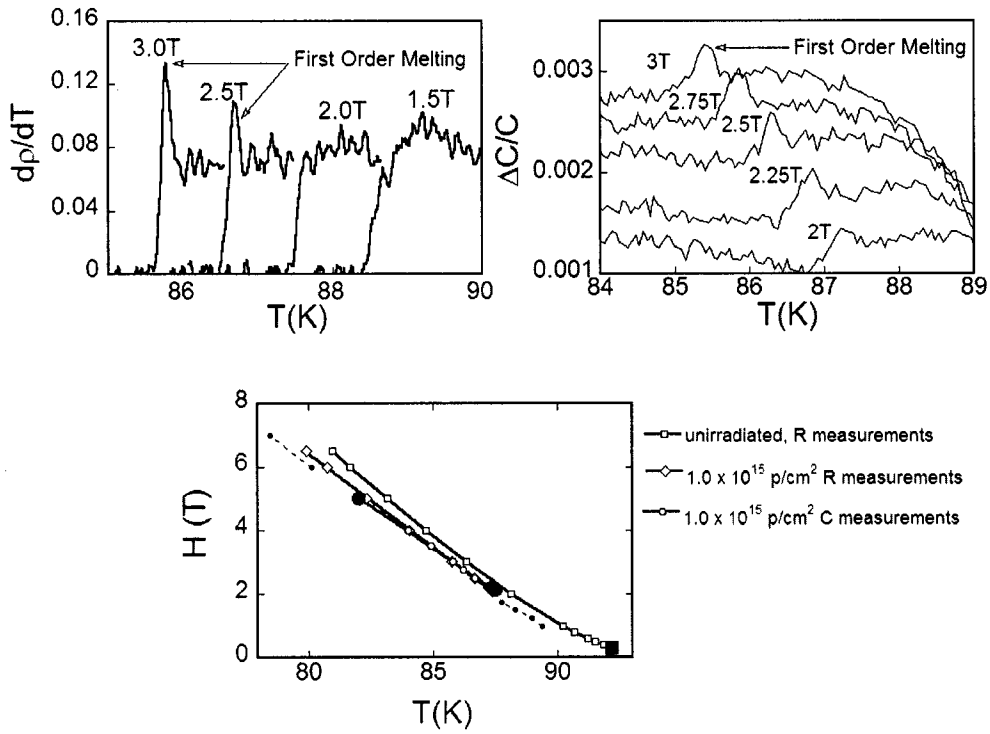

Figure 39 Comparative graphs concentrating on the response of the lower critical point to proton irradiation in the case of WYB005 (dose = 1.0×10^{15} p/cm^2). The upper, left graph depicts the electrical transport results, and the left one is showing the specific heat measurements results. The field values are chosen in such a way that the attention is concentrated on the H_{lcp}. The magnetic phase diagram (lower graph), is revealing the evolution of the melting transition upon irradiation. The dashed line represents the position of the step in the specific heat data.

5.3 Vortex Glass - Overview

The vortex glass state (VG) is described by vortices fixed in a random pattern with no long-range positional order. Appearing in disordered systems[19], the vortex glass state is predicted to be a thermodynamic phase with no dissipation in the limit of low current densities. In other words, it should have a true critical current. Furthermore, the VG is accompanied by a sharp thermodynamic second-order phase

transition.

As FOMT is replaced by a second order phase transition, critical scaling behavior is expected in the vicinity of transition for a VG state. Therefore, macroscopic quantities describing the system can be conveyed in terms of the characteristic length and time scale: the vortex glass correlation length ξ_{VG} and the vortex glass relaxation time τ_{VG}. Both are divergent at the transition:

$$\xi_{VG} \propto |T-T_g|^{-\nu}, \tag{5.1}$$

$$\tau_{VG} \propto |T-T_g|^{-\nu z} \tag{5.2}$$

where ν and z are the static and the dynamic critical exponents, respectively ($\nu > 0$, $z > 0$).

The dynamic response of vortex system is summarized in Figure 40 (Blatter[20]

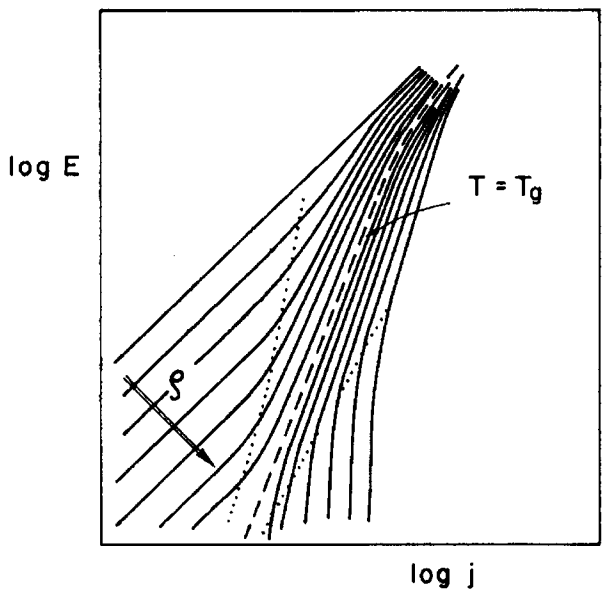

Figure 40 Current-voltage characteristic for a superconductor in the region of a glassy transition. This represents the theoretically predicted curves at the vortex glass transition (from Blatter[20] *et al.*).

et al.). In the Ohmic region, the resistivity just above the transition where the system is still liquid is given by $\rho = \rho_0(T-T_g)^s$, where the critical exponent $s = \nu(z-1)$ is field-independent with a predicted value[20] ranging between ~ 2.7 and ~ 8.5. Furthermore, at the glass transition (T_g) the current density and the electric field can be expressed as powers of these exponents: $J \propto \xi^{1-d}$ and $E \propto \xi^{1+z}$, with $d = 3$, the dimensionality of the system, while below T_g the system is glassy over large distances.

5.4 Experimental Observation of Vortex Glass Matter

First experimental evidence of a vortex glass was reported[30] in epitaxial YBCO films, where values of the critical exponents are $z \cong 4.8$ and $\nu \cong 1.5$ were reported, leading to a value of $s \cong 6.5$ for the combined critical exponent. Indications of the VG were found in YBCO[21] and BSCCO[22] single crystals, but also in low-T_c materials[23,24,25]. Several comparative studies[26,27,28,29] had found critical exponents describing the VG in single crystals which were more scattered and with values below those of films. While there is a remarkable experimental effort to investigate the existence of the vortex glass (VG) state in the magnetic phase diagram[7,11,27,28,30,31,32,33], there is still a great deal of controversy over the conclusiveness of the evidence. While some results seem to contradict the vortex glass theory [29], there are also papers that claim those who found scaling did not do it correctly. Others[34,35] advocate the universality of vortex glass scaling. The procedure of determining T_g and the temperature range of scaling can influence the final exponents values, which might partially account for differences between different studies[35].

Most of the published articles focus on probing the presence of the vortex glass at high magnetic field values, while few articles[33,36] identify modifications in the

universal character of phase transition at low fields. This low field vortex phase is recognized to be distinct from the VG phase, but is not clearly defined. The vortex slush, an intermediate state at low magnetic fields, is reported[12,37,38] to appear as a consequence of a glassy transition that follows the first order transition.

Two good examples of how systematically induced defects can influence the position of the critical points on FOMT, as well as the nature of vortex states, are offered by the work of Paulius et al[4] and Kwok et al[10]. In an other investigation[15], for a YBCO crystal with a high density of point disorder induced by 9MeV proton irradiation, the melting transition was completely suppressed. The results presented evidence for the VG over a large region of the phase diagram.

5.5 Vortex Glass - Scaling Approach

In order to search for the presence of the VG state, we attempted to scale the resistivity data. The noise is not significant in the resistivity data, but it can be obstructive in the derivative, therefore the first step in the analysis procedure is to perform data smoothing, in order to eliminate the experimental noise. We notice that best results in finding an average data point are obtained when using a fixed temperature interval rather than a window of fixed number of points. Choosing the right size of temperature interval window is crucial, as the power-law behavior is present over a small temperature range. While the scientific data were analyzed in KaleidaGraph, we used the LabVIEW environment to write a routine with the purpose of smoothing the raw data. Instead of choosing a window with a fixed number of points, we obtained better results by averaging the data from a temperature interval of typically 100mK.

The second step of the scaling procedure is determining the correct range of

temperatures over which the data can be fit, meaning the limits within which the resistivity displays the power law dependence predicted by the vortex glass theory. While this is difficult to determine directly from the resistivity or its temperature derivative alone, the ratio of the two should be a straight line in the anticipated range:

$$\frac{\rho}{(d\rho/dT)} = \frac{T}{s} - \frac{T_g}{s} = (\frac{1}{s})T - \frac{T_g}{s}, \qquad (5.3)$$

where 1/s as slope and T_g/s (T_g is the second order glass transition temperature) is x-intercept of the linear fit. A linear fit is then used to determine T_g, while the power fit on the original, raw data will lead to finding the values for s and ρ_0.

Results of a successful scaling analysis[5] are presented in Figure 41 and Figure 42. These results are from a YBCO single crystal irradiated with 9MeV protons to a much higher dose (3×10^{16} p/cm^2) than used here. The linear portion of the ratio of resistivity with its derivative is fairly large, about 2K, and the value obtained for the critical exponent s (5.3 ±0.7) is consistent with the vortex glass theory and field independent.

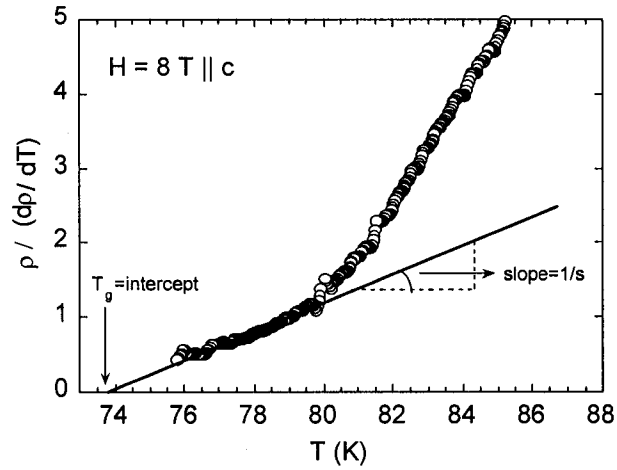

Figure 41 Approximation of the range where resistivity exhibits a power low dependence by using the linear portion of ρ/(dρ/dT). The results belong to the work of Petrean *et al*[5].

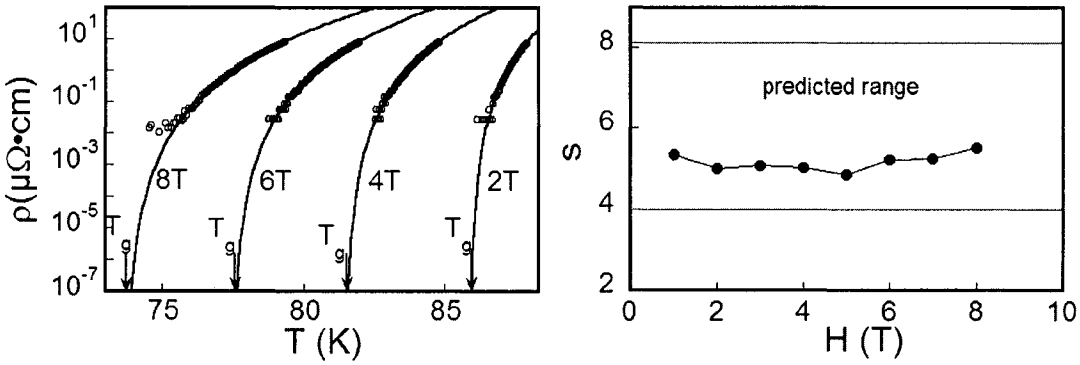

Figure 42 Results of successful VG scaling[5]. The left side graph shows the range of temperatures where the resistivity can be fit to a power law. The right side graph demonstrate the validity of the results: the critical exponent s is field-independent and has values in the theoretically predicted range.

5.6 Vortex Glass Scaling Attempt

One of the purposes of this study is to reveal the nature of the vortex matter below H_{lcp}, and one way to do that is to search for vortex glass signature around transition. While we considered the VG scaling for several magnetic field values and irradiation doses, in Figure 43 we exemplify our scaling attempt for two samples (WYB005 and YBA285) at their maximum irradiation dose. We were able to obtain the linear fit for $\rho/(d\rho/dT)$ over a fairly short range of temperatures (less than 1K), range for which a good power fit was obtained for ρ, but the s value obtained is field dependent (the case of YBA285 crystal) or is out of the accepted range (the case of WYB005 crystal). The vertical line is the s vs H graph for WYB005 corresponds to the H_{lcp} after irradiation and therefore imposes an upper limitation to the region where the considerations regarding critical exponent are relevant. A similar line for the case of YBA285 is missing because at that dose (2.0×10^{15} p/cm^2) the FOMT is completely suppressed and there are no critical points.

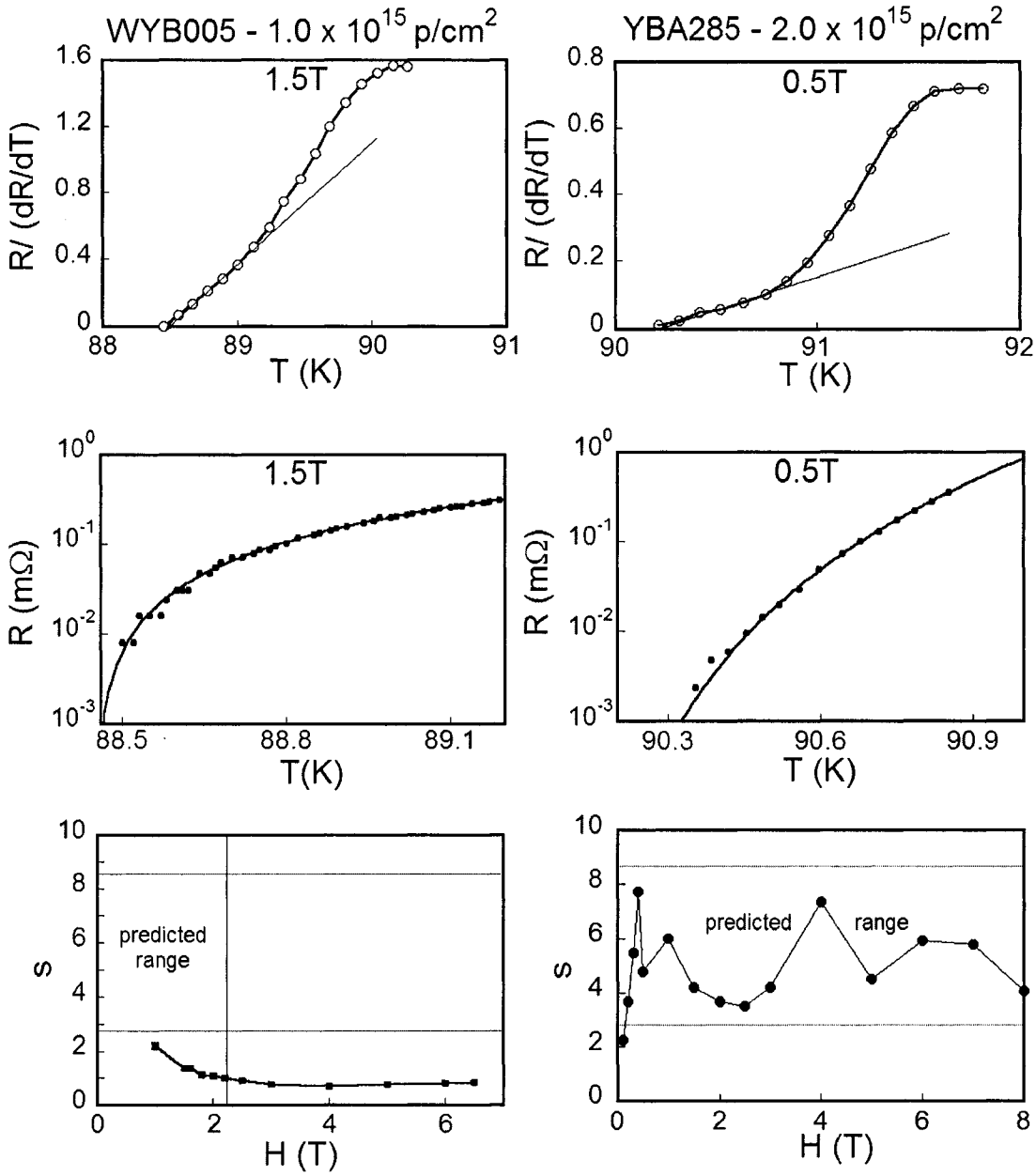

Figure 43 Results of vortex glass scaling attempt for two of our samples: WYB005 and YBA256. Comparing with a good scaling, the range of resistivity power fit is considerably shorter (from 2-3K, as in the case depicted in Figure 41, to less than 1K in this case). The value obtained for critical exponent s is out of the predicted range (WYB005) or is field dependent (YBA256).

In conclusion, the results attempting to show evidence of vortex glass state below H_{lcp} are indecisive. Furthermore, as we pointed out in the previous chapter, the current-voltage characteristics available for one of our sample (YBA285) did not matched the predicted critical behavior corresponding to a vortex glass ($T < T_g$). The inconsistency with the VG picture is evident as the I-V curves become more linear upon irradiation (see Figure 33). Below T_g the electrical field dependence on current density should be power-law like, manifesting in a downward curvature for all currents. Therefore, a discussion regarding a scaling of I-V curves was excluded as being irrelevant.

5.7 Vortex Molasses Scaling Attempt

Vortex molasses (VM) scenario[39] is inspired by the window-glass-like characteristics of a melting transition or crossover without an apparent breaking of any symmetry. In other words, from the point of view of describing the vortex melting, VM is a VG that will not experience a real phase transition, but rather a history dependent crossover. In conformity with VM model, the system approaching the transition will undergo a very rapid freezing of the dynamics and any potential divergence of the special correlation length ξ would be masked by quick freezing. This behavior is considered to be consistent with the Vogel-Fulcher law of temperature dependence of the resistivity:

$$\rho = \rho_0 \exp[-1/(T-T_g)] \qquad (5.4)$$

However, our attempt to fit our resistivity data to this exponential dependence on temperature was unsuccessful. As exemplified in Figure 44 for the sample

WYB005, at low temperatures, closer to the presumptive transition, the exponential fit given by the equation 5.4 does not match our data. While the figure illustrates the mismatch for just two field values, we repeated the procedure for several magnetic fields (below H_{lcp}), for different samples, but ended up with the same negative result.

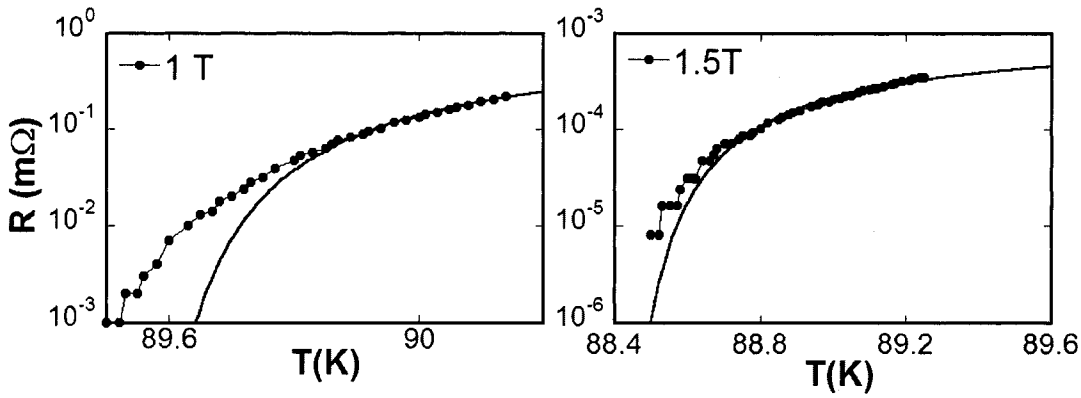

Figure 44 Vortex molasses scaling attempt exemplified for the case of WYB005, for 1 and 1.5T.

5.8 Conclusion

In conclusion, we have probed the vortex phase diagram by using electrical transport and specific heat measurement techniques. In the first part of our work we have focused on grounding the universality of vortex matter response to proton irradiation. The inquiry was conducted by choosing four YBCO single crystals that were systematically irradiated and measured subsequently. Our findings lead to a reproducible, unified picture of the evolution of the properties describing the vortex matter behavior. The fact that the initial conditions for the four crystals were different, did not constitute a factor of instability and did not affected the universality behavior of the vortex system.

In the second part of our investigation (Chapter 5) we have concentrated on the response of the lower critical point to proton irradiation and searched for the signatures of the vortex glass and vortex molasses states in the region below H_{lcp}. Although our specific heat results indicated the presence of a second order phase transition, our scaling attempts were not consistent with the presence of either the vortex glass or vortex molasses states. Therefore, the nature of the vortex matter in this region of the vortex phase diagram remains elusive.

References

[1] U. Welp, J. A. Fendrich, W. K. Kwok, G. W. Crabtree, and B. W. Veal, Phys. Rev. Lett. **76**, 4809-4812 (1996)

[2] A. Schilling, R. A. Fisher, N. E. Phillips, U. Welp, W. K. Kwok, and G. W. Crabtree., Phys. Rev. Lett. **78**, 4833 (1997)

[3] M. Roulin, A. Junod, A. Erb, and E. Walker., Phys. Rev. Lett. **80**, 1722 (1998)

[4] L. M. Paulius, W.-K. Kwok, R. J. Olsson, A. M. Petrean, V. Tobos, J. A. Fendrich, G. W. Crabtree, C. A. Burns, and S. Ferguson, Phys. Rev. B **61**, R11910-R11913 (2000)

[5] A. M. Petrean, L. M. Paulius, W.-K. Kwok, J. A. Fendrich, and G. W. Crabtree, Phys. Rev. Lett. **84**, 5852-5855 (2000)

[6] L. M. Paulius, C. Marcenat, V. Tobos, L. Undreiu, W. K. Kwok, T. Klein and G. W. Crabtree, Physica B, **329**, 1344 (2003)

[7] D. S. Fisher, M. P. A. Fisher, and D. A. Huse., Phys. Rev. B **43**, 130 (1991)

[8] T. Giamarchi and P. Le Doussal., Phys. Rev. B **55**, 6567 (1997)

[9] D. R. Nelson and V. M. Vinokur, Phys. Rev. B **48**, 13060 (1993)

[10] W. K. Kwok, R. J. Olsson, G. Karapetrov, L. M. Paulius, W. G. Moulton, D. J. Hofman, and G. W. Crabtree, Phys. Rev. Lett. **84**, 3706 (2000)

[11] C. Marcenat, F. Bouquet, R. Calemczuk, U. Welp, W. K. Kwok, G. W. Crabtree, N. E. Phillips, R. A. Fisher and A. Schilling, Physica C **341**, 949 (2000)

[12] H. Safar, P. L. Gammel, D. A. Huse, D. J. Bishop, W. C. Lee, J. Giapintzakis, and D. M. Ginsberg, Phys. Rev. Lett. **70**, 3800 (1993)

[13] D. López, L. Krusin-Elbaum, H. Safar, E. Righi, F. de la Cruz, S. Grigera, C. Feild, W. K. Kwok, L. Paulius, and G. W. Crabtree, Phys. Rev. Lett. **80**, 1070-1073 (1998)

[14] F. Bouquet, C. Marcenat, E. Steep, R. Calemczuk, W. K. Kwok, U. Welp, G. W. Crabtree, R. A. Fisher, N. E. Phillips, A. Schilling,

Nature **411**, 448 - 451 (2001)

[15] K. Shibata, T. Nishizaki, T. Sasaki, and N. Kobayashi., Phys. Rev. B **66**, 214518 (2002)

[16] B. Khaykovich, M. Konczykowski, E. Zeldov, R. A. Doyle, D. Majer, P. H. Kes, and T. W. Li , Phys. Rev. B **56**, R517 (1997)

[17] M. Menghini, Y. Fasano, F. de la Cruz, S. S. Banerjee, Y. Myasoedov, E. Zeldov, C. J. van der Beek, M. Konczykowski, and T. Tamegai, Phys. Rev. Lett. **90**, 147001 (2003)

[18] S. S. Banerjee, A. Soibel, Y. Myasoedov, M. Rappaport, E. Zeldov, M. Menghini, Y. Fasano, F. de la Cruz, C. J. van der Beek, M. Konczykowski, and T. Tamegai, Phys. Rev. Lett. **90**, 087004 (2003)

[19] M. P. A. Fisher, Phys. Rev. Lett. **62**, 1415 (1989)

[20] G. Blatter, M. V. Feigel'man, V. B. Geskenbein, A. I. Larkin, and V. M. Vinokur, Rev. Mod. Phys. **66**, 1125 (1994)

[21] P. L. Gammel, L. F. Schneemeyer, and D. J. Bishop, Phys. Rev. Lett. **66**, 953 (1991)

[22] H. Safar, P. L. Gammel, D. J. Bishop, D. B. Mitzi, and A. Kapitulnik, Phys. Rev. Lett. **68**, 2672 (1992)

[23] N.-C. Yeh, W. Jiang, D. S. Reed, A. Gupta, F. Holtzberg, and A. Kussmaul, Phys. Rev. B **45**, 5710 (1992)

[24] J. Herrmann, M. C. de Andrade, C. C. Almasan, R. P. Dickey, M. B. Maple, Wu Jiang, S. N. Mao, and R. L. Greene, Phys. Rev. B **54**, 3610 (1996)

[25] T. Klein, A. Conde-Gallardo, J. Marcus, C. Escribe-Filippini, P. Samuely, P. Szabó, and A. G. M. Jansen, Phys. Rev. B **58**, 12 441 (1998)

[26] J. Kötzler, M. Kaufmann, G. Nakielski, R. Behr, and W. Assmus, Phys. Rev. Lett. **72**, 2081 (1994)

[27] J. M. Roberts, B. Brown, B. A. Hermann, and J. Tate, Phys. Rev. B **49**, 6890 (1994)

[28] L. Hou, J. Deak, P. Metcalf, M. W. McElfresh, and G. Preosti, Phys. Rev. B **55**, 11806 (1997)

[29] L. F. Cohen, and H. J. Jensen, Rep. Prog. Phys. **60**, 1581–1672 (1997)

[30] R. H. Koch, V. Foglietti, W. J. Gallagher, G. Koren, A. Gupta, and M. P. A. Fisher, Phys. Rev. Lett. **63**, 1511-1514 (1989)

[31] C. Dekker, W. Eidelloth, and R. H. Koch, Phys. Rev. Lett. **68**, 3347-3350 (1992)

[32] A. Sawa, H. Yamasaki, Y. Mawatari, H. Obara, M. Umeda, and S. Kosaka, Phys. Rev. B **58**, 2868-2877 (1998)

[33] M. Charalambous, R. H. Koch, T. Masselink, T. Doany, C. Feild, and F. Holtzberg, Phys. Rev. Lett. **75**, 2578-2581 (1995)

[34] M. Friesen, J. Deak, L. Hou, and M. [W.] McElfresh, Phys. Rev. B **54**, 3525 (1996)

[35] K. Moloni, M. Friesen, S. Li, V. Souw, P. Metcalf, and M. McElfresh, Phys. Rev. B **56**, 14 784 (1997)

[36] T. Nojima, T. Ishida, and Y. Kuwasawa, Physica C **263**, 424 (1996)

[37] T. K. Worthington, M. P. A. Fisher, and D. A. Huse, Phys. Rev. B **46**, 11 854 (1992)

[38] A. P. Reyes, X. P. Tang, H. N. Bachman, W. P. Halperin, J. A. Martindale, and P. C. Hammel, Phys. Rev. B **55**, R14 737 (1997)

[39] C. Reichhardt, A. van Otterlo, and G. T. Zimányi, Phys. Rev. Lett. **84**, 1994-1997 (2000).

BIBLIOGRAPHY

A. A. Abrikosov, Sov. Phys. JETP, **5**, 1174 (1957)

A. A. Abrikosov, Zh. Éksp. Teor. Fiz. **32**, 1442 (1957); English translation: Sov. Phys. –JETP **5**, 1174 (1957)

P. W. Anderson, Phys. Rev. Letters **9**, 309 (1962)

P. W. Anderson, Y. B. Kim, Rev. Mod. Phys. **36**, 39–43 (1964)

S. S. Banerjee, A. Soibel, Y. Myasoedov, M. Rappaport, E. Zeldov, M. Menghini, Y. Fasano, F. de la Cruz, C. J. van der Beek, M. Konczykowski, and T. Tamegai, Phys. Rev. Lett. **90**, 087004 (2003)

J. Bardeen, L. N. Cooper, and J. R. Schrieffer, Phys. Rev. **106**, 162 (1957)

J. Bardeen, and M. J. Stephen, Phys. Rev. **140**, A1197 (1965)

M. R. Beasley, R. Labusch, and W. W. Webb, Phys. Rev. **181**, 682–700 (1969)

J. G. Bednorz and K. A. Müller, Z. Phys. B **64**, 189 (1986)

M. A. Beno, L. Soderholm, D. W. Capone, D. G Hinks, J. D. Jorgensen, J. D. Grace, I. K. Schuller, C.U. Segre, and K. Zhang, Appl. Phys. Lett. **51**, 57 (1987)

H. A. Blackstead and G. A. Kapustin, Physica (Amsterdam) **219C**, 109 (1994)

G. Blatter, M. V. Feigel'man, V. B. Geshkenbein, A. I. Larkin, V. M. Vinokur, Rev. Mod. Phys. **66**, 1125 (1994)

F. Bouquet, C. Marcenat, Physics and Materials Science of Vortex States, Flux Pinning and Dynamics. Kluwer Academic Publishers, Dordrecht, p. 743 (1998)

F. Bouquet, C. Marcenat, E. Steep, R. Calemczuk, W. K. Kwok, U. Welp, G. W. Crabtree, R. A. Fisher, N. E. Phillips, and A. Schilling, Nature (London) **411**, 448 (2001)

A. M. Campbell and J. E. Evetts, Adv. Phys. **21**, 199 (1972)

J. J. Capponi, C. Chaillout, A. W. Hewat, P. Lejay, N. Marezio, N. Nguyen, B. Raveau, J. L. Soubeyroux, J. L. Tholence and R. Tournier, Europhys. Lett. **3**, 1301 (1987)

C. Carraro and D. S. Fisher, Phys. Rev. B **51**, 534-538 (1995)

R. J. Cava, B. Batlogg, R. B. v Dover, D. W. Murphy, S. Sunshine, T. Siegrist, J. P. Remeika, E. A. Rietman, S. Zakurak, and G. P. Espinosa, Phys. Rev. Lett. 58, 1676 (1987)

A. M. Chang, H. D. Hallen, H. F. Hess, H. L. Kao, J. Kwo, R. Wolf, J. van der Zeil and T. Y.Chang, Appl. Phys. Lett. **61**, 1974 (1992)

M. Charalambous, J. Chaussy, and P. Lejay, Phys. Rev. B **45**, 5091-5094 (1992)

M. Charalambous, J. Chaussy, P. Lejay, and V. Vinokur, Phys. Rev. Lett. **71**, 436-439 (1993)

M. Charalambous, R. H. Koch, T. Masselink, T. Doany, C. Feild, and F. Holtzberg, Phys. Rev. Lett. **75**, 2578-2581 (1995)

L. Civale, A. D. Marwick, M. W. McElfresh, T. K. Worthington, A. P. Malozemoff, F. H. Holtzberg, J. R. Thompson, M. A. Kirk, Phys. Rev. Lett. **65**, 1164–1167 (1990)

L. Civale, A. D. Marwick, T. K. Worthington, M. A. Kirk, J. R. Thompson, L. Krusin–Elbaum, Y. Sun, J. R. Clem, and F. Holtzberg
Phys. Rev. Lett. **67**, 648-651 (1991)

L. F. Cohen, and H. J. Jensen, Rep. Prog. Phys. **60**, 1581–1672 (1997)

G. W. Crabtree, W. K. Kwok, L. M. Paulius, A. M. Petrean, R. J. Olsson, G. Karapetrov, V. Tobos and W. G. Moulton, Physica C **332**, 71-79 (2000)

R. Cubitt, E. M. Forgan, G. Yang, S. L. Lee, D. McK. Paul, H. A. Mook, M. Yethiraj, P. H. Kes, T. W. Li, A. A. Menovsky, Z. Tarnawski, and K. Mortensen, Nature (London) **365**, 407 (1993)

R.V. Damadian, Science **171**, 1151 (1971)

C. Dekker, W. Eidelloth, and R. H. Koch, Phys. Rev. Lett. **68**, 3347-3350 (1992)

D. Dew-Hughes, *Cryogenics* **28**, 674 (1988)

R. B. van Dover, E. M. Gyorgy, A. E. White, L. F. Schneemeyer, R. J. Felder, and J. V. Waszczak, Phys. Rev. Lett. **56**, 26 (1990)

R. A. Doyle, W. S. Seow, Y. Yan, A. M. Campbell, T. Mochiku, K. Kadowaki, G. Wirth, Phys. Rev. Lett. **77**, 1155 (1996)

D. Ertas and D. R. Nelson, Physica (Amsterdam) **272C**, 79 (1996)

M. V. Feigel'man, Physics A **168**, 319 (1990)

J. A. Fendrich, U. Welp, W. K. Kwok, A. E. Koshelev, G. W. Crabtree, and B. W. Veal, Phys. Rev. Lett. **77**, 2073-2076 (1996)

M. P. A. Fisher, Phys. Rev. Lett. **62**, 1415 (1989)

M. P. A. Fisher and D. H. Lee, Phys. Rev. B **39**, 2756 (1989)

D. S. Fisher, M. P. A. Fisher, and D. A. Huse, Phys. Rev. B **43**, 130-159 (1991)

C. P. Foley; K. E. Leslie; R. Binks; C. Lewis; W. Murray; G. J. Sloggett; S. Lam; B. Sankrithyan; N. Savvides; A. Katzaros; K. -H. Muller; E. E. Mitchell; J. Pollock; J. Lee; D. L. Dart; R. R. Barrow; M. Asten; A. Maddever.; G. Panjkovic; M. Downey; C. Hoffman; R. Turner, Applied Superconductivity **9,** 3786 – 3792 (1999)

J. Frenkel, Kinetic Theory of Liquids, p. 382 (Dover, New York, 1955)

M. Friesen, J. Deak, L. Hou, and M. W. McElfresh, Phys. Rev. B **54**, 3525 (1996)

D. T. Fuchs, E. Zeldov, T. Tamegai, S. Ooi, M. Rappaport, and H. Shtrikman, Phys. Rev. Lett. **80**, 4971 (1998)

D. T. Fuchs, E. Zeldov, D. Majer, R. A. Doyle, T. Tamegai, S. Ooi, and M. Konczykowski, Phys. Rev. B **54**, R796-R799 (1996)

P. L. Gammel, D. J. Bishop, G. J. Dolan, J. R. Kwo, C. A. Murray, L. F. Schneemeyer, and J. V. Waszczak, Phys. Rev. Lett. **59**, 2592–2595 (1987)

P. L. Gammel, L. F. Schneemeyer, and D. J. Bishop, Phys. Rev. Lett. **66**, 953 (1991)

T. Giamarchi, and P. Le Doussal, Phys. Rev. B **52**, 1242 (1995)

T. Giamarchi, and P. Le Doussal, Phys. Rev. B **55**, 6577 (1997)

L. I. Glazman and A. E. Koshelev, Phys. Rev. B **43**, 2835-2843 (1991)

A. Grigorenko, S. Bending, T. Tamegai, S. Ooi, M. Henini, Nature **414**, 728-731 (2001)

H. D. Hallen, R. Seshadri, A. M. Chang, R. Miller, L. N. Pfeiffer, K. West, C. A. Murray, H. F. Hess, Phys. Rev. Lett. **71**, 3007 (1993)

K. Haralda, T. Matsuda, H. Kasai, J. E. Bonevich, T. Yoshida, U. Kawabe, and A. Tonomura, Phys. Rev. Lett. **71**, 3371 (1993)

J. Herrmann, M. C. de Andrade, C. C. Almasan, R. P. Dickey, M. B. Maple, Wu Jiang, S. N. Mao, and R. L. Greene, Phys. Rev. B **54**, 3610 (1996)

H. F. Hess, R. B. Robinson, R. C. Dynes, J. M. Valles, Jr., and J. V. Waszezak, Phys. Rev. Lett. **62**, 214 (1989)

L. Hou, J. Deak, P. Metcalf, M. W. McElfresh, and G. Preosti, Phys. Rev. B **55**, 11 806 (1997)

Y. Imry and M. Wortis, Phys. Rev. B 19, 3580-3585 (1979)

S. E. Inderhees, M. B. Salamon, T. A. Friedmann, D. M. Ginsberg, Phys. Rev. B **36**, 2401 (1987)

Y. Iye, T. Tamegai, H. Takeya and H. Takei, Jpn. J. Appl. Phys. **26**, 1057 (1987)

P. H. Kes, J. Aarts, J. van den Berg, C. J. van der Beek, and J. A. Mydosh, Supercond. Sci. Technol. **1**(5), 242–248 (1989)

B. Khaykovich, M. Konczykowski, E. Zeldov, R. A. Doyle, D. Majer, P. H. Kes, and T. W. Li , Phys. Rev. B **56**, R517 (1997)

R. N. Kleiman, P. L. Gammel, L. F. Schneemeyer, J. V. Waszczak, and D. J. Bishop, Phys. Rev. Lett. **62**, 2331 (1989)

T. Klein, I. Joumard, S. Blanchard, J. Marcus, R. Cubitt, T. Giamarchi, P. Le Doussal, Nature **413**, 404 (2001)

R. H. Koch, V. Foglietti, W. J. Gallagher, G. Koren, A. Gupta, and M. P. A. Fisher, Phys. Rev. Lett. **63**, 1511-1514 (1989)

S. T. Johnson, E. M. Forgan, S. H. Lloyd, C. M. Aegerter, S. L. Lee, R. Cubitt, P. G. Kealey, C. Ager, S. Tajima, A. Rykov, and D. McK. Paul, Phys. Rev. Lett. **82**, 2792 (1999)

J. D. Jorgensen, B. W. Veal, A. P. Paulikas, L. J. Nowicki, G. W. Crabtree, H. Claus, and W. K. Kwok, Phys. Rev. B, **41**, 1863 (1990)

B. D. Josephson, Phys. Lett. **1**, 251 (1962)

A. Junod, M. Roulin, J.-Y. Genoud, B. Revaz, A. Erb, and E. Walker, Physica (Amsterdam) **275C**, 245 (1997)

A. Junod, M. Roulin, J. -Y. Genoud, B. Revaz, E. Walker, A. Erb, C. Marcenat, R. Calemczuk and F. Bouquet, Physica C: Superconductivity, 282-287, Pages 1425-1426 (1997)

D. L. Kaiser, F. Holtzberg, B. A. Scott, T. R. and McGuire, Appl. Phys. Lett., **51**, 1040 (1987)

D. L. Kaiser, F. W. Gayle, R. S. Roth, L. S. Schwartzendruber, J. Mater. Res. **4**, 745 (1989)

W. H. Keesom and J. A. Kok, Comm. Phys. Lab. Leiden **221**, 27 (1932)

D. H. Kim, K. E. Gray, R. T. Kampwirth, and D. M. McKay, Phys.Rev. B **42**, 6249 (1990)

T. Klein, A. Conde-Gallardo, J. Marcus, C. Escribe-Filippini, P. Samuely, P. Szabó, and A. G. M. Jansen, Phys. Rev. B **58**, 12 441 (1998)

T. Klein, I. Joumard, S. Blanchard, J. Marcus, R. Cubitt, T. Giamarchi, P. Le Doussal., Nature 413, 404 (2001)

R. H. Koch, , V. Foglietti, W. J. Gallagher, G. Koren, A. Gupta, and M. P. A. Fisher, Phys. Rev. Lett. **63**, 1511 (1989)

M. Konczykowski, Physica A **168**, 291 (1990)

J. Kötzler, M. Kaufmann, G. Nakielski, R. Behr, and W. Assmus, Phys. Rev. Lett. **72**, 2081 (1994)

J. E. Kunzler, E. Buehler, F. S. L. Hsu, and J. H. Wernick, Phys. Rev. Lett. **6**, 89–91 (1961)

W. K. Kwok, J. Fendrich, S. Fleshler, U. Welp, J. Downey, and G. W. Crabtree, Phys. Rev. Lett. **72**, 1092-1095 (1994)

W. K. Kwok, R. J. Olsson, G. Karapetrov, L. M. Paulius, W. G. Moulton, D. J. Hofman and G. W. Crabtree, Phys. Rev. Lett. **84**, 3706-3709 (2000)

K. K Kwong, J. W. Belliveau, D. A. Chesler, I. E. Goldberg, R. M. Weisskoff, B. P. Poncelet, D. N. Kennedy, B. E. Hoppel, M. S. Cohen, R. Turner, H. -M Cheng, T. J. Brady, B. R. Rosen., Proc. Natl. Acad. Sci. **89,** 5675 (1992)

R. Labusch, Phys. Status Solidi **32**, 439 (1969)

L. D. Landau, E. M. Lifshitz, Statistical Physics, 3rd edition., part **1**, English translation: Pergamon Press, Oxford (1980)

A. I. Larkin, Sov. Phys. JETP **31**, 784-786 (1970)

A. I. Larkin, and Yu. N. Ovchinnikov, J. Low Temp.Phys. **34**, 409–428 (1979)

A. I. Larkin and V. M. Vinokur, Phys. Rev. Lett. **75**, 4666 (1995)

P.C. Lauterbur, Nature **242,** 190-191 (1973)

R. Liang, D. A. Bonn and W. N. Hardy, Phys. Rev. Lett. **76**, 835 (1996)

T. B. Lindemer, J. F. Hunley, J. E. Gates, A. L. Sutton, Jr., J. Brynestad, C. R. Hubbard, P. K. Gallagher, J. Am. Ceram. Soc. **72**(10), 1775 (1989)

F. London and H. London, Proc. Roy. Soc. (London) A **149**, 71 (1935)

D. López, E. F. Righi, G. Nieva, and F. de la Cruz, Phys. Rev. Lett. **76**, 4034–4037 (1996)

D. López, L. Krusin-Elbaum, H. Safar, E. Righi, F. de la Cruz, S. Grigera, C. Feild, W. K. Kwok, L. Paulius, and G. W. Crabtree, Phys. Rev. Lett. **80**, 1070–1073 (1998)

I. Maggio-Aprile, Ch. Renner, A. Erb, E. Walker, and O. Fischer, Phys. Rev. Lett. **75**, 2754–2757 (1995)

A. P. Malozemoff, Mater. Res. Bull. **15**, 50 (1990)

A.P. Malezemoff, J. Mannhart, D. Scalapino, Physics Today **58**, 4 (2005)

C. Marcenat, F. Bouquet, R. Calemczuk, U. Welp, W. K. Kwok, G. W. Crabtree, N. E. Phillips, R. A. Fisher and A. Schilling, Physica C **341**, 949 (2000)

M. C. Marchetti and D. R. Nelson, Phys. Rev. B **42**, 9938-9943 (1990)

E. Maxwell, Phys. Rev. **78**, 477 (1950)

W. Meissner and R. Ochsenfeld, Naturwiss. **21**, 787 (1933)

M. Menghini, Y. Fasano, F. de la Cruz, S. S. Banerjee, Y. Myasoedov, E. Zeldov, C. J. van der Beek, M. Konczykowski, and T. Tamegai, Phys. Rev. Lett. **90**, 147001 (2003)

P. Meuffels, R. Naeven, and H. Wenzl, Physica (Amsterdam) **161C**, 539 (1989)

E. Mezzetti, S. Colombo, R. Gerbaldo, G. Ghigo, L. Gozzelino, B. Minetti, and R. Cherubini, Phys. Rev. B **54**, 3633-3639 (1996)

K. Moloni, M. Friesen, S. Li, V. Souw, P. Metcalf, and M. McElfresh, Phys. Rev. B **56**, 14 784 (1997)

A. Moser, H. J. Hug, I. Parashikov, B. Stiefel, O. Fritz, H. Thomas, A. Baratoff, H.-J. Güntherodt, and P. Chaudhari, Phys. Rev. Lett. **74**, 1847-1850 (1995)

J. Nagamatsu, N. Nakagawa, T. Muranaka, Y. Zenitani, J. Akimitsu, Nature **410** , 63-64 (2001)

D. R. Nelson, Phys. Rev. Lett. **60**, 1973-1976 (1988)

D. R. Nelson and H. S. Seung, Phys. Rev. B **39**, 9153-9174 (1989)

D. R. Nelson and V. M. Vinokur, Phys. Rev. Lett. **68**, 2398 (1992)

D. R. Nelson and V. M. Vinokur , Phys. Rev. B **48**, 13060 (1993)

D. R. Nelson, "Phase Transitions and Relaxation in Systems with Competing Energy Scales", edited by T. Risk and D. Sherrington, Kluwer, Dordrecht, pp. 95–117 (1993)

T. Nishizaki, Y. Onodera, N. Kobayashi, H. Asaoka, and H. Takei, Phys. Rev. B **53**, 82 (1996)

T. Nishizaki, T. Naito, S. Okayasu, A. Iwase and N. Kobayashi, Phys. Rev. B **61**, 3649-3654 (2000)

T. Nojima, T. Ishida, and Y. Kuwasawa, Physica C **263**, 424 (1996)

H. K. Onnes, 120b, 122b, 124c (1911)

M. A. Paesler and P. J. Moyer, "Near-Field Optics: Theory, Instrumentation and Applications," John Wiley and Sons, Inc., New York (1996)

T. T. M. Palstra, B. Batlogg, L. F. Schneemeyer, and J. V.Waszczak, Phys. Rev. Lett. **61**, 1662 (1988)

T. T. M. Palstra, B. Batlogg, R. B. van Dover, L. F. Schneemeyer and J. V. Waszczak, Appl. Phys. Lett. **54**, 763 (1989)

T. T. M Palstra, B. Batlogg, R. B. van Dover, L. F. Schneemeyer, and J. V. Waszczak, Phys. Rev. B **41**, 6621 (1990)

P. D. Panetta, J. E. Ostenson, D. K. Finnemore, and C. L. Snead, Jr., Phys. Rev. B **52**, 15570-15574 (1995)

H. Pastoriza, M. F. Goffman, A. Arribére, and F. de la Cruz., Phys. Rev. Lett. **72**, 2951 (1994)

L. M. Paulius, W.-K. Kwok, R. J. Olsson, A. M. Petrean, V. Tobos, J. A. Fendrich, G. W. Crabtree, C. A. Burns, and S. Ferguson, Phys. Rev. B **61**, R11910-R11913 (2000)

L. M. Paulius, C. Marcenat, V. Tobos, L. Undreiu, W. K. Kwok, T. Klein and G. W. Crabtree, Physica B, **329**, 1344 (2003)

A. M. Petrean, L. M. Paulius, W.-K. Kwok, J. A. Fendrich, and G. W. Crabtree, Phys. Rev. Lett. **84**, 5852-5855 (2000)

D. W. Pohl, W. Denk and M. Lanz, Applied Physics Letters **44**, 651 (1984)

C. Reichhardt, A. van Otterlo, and G. T. Zimányi, Phys. Rev. Lett. **84**, 1994-1997 (2000)

A. P. Reyes, X. P. Tang, H. N. Bachman, W. P. Halperin, J. A. Martindale, and P. C. Hammel, Phys. Rev. B **55**, R14 737 (1997)

C. A. Reynolds, B. Serin, W. H. Wright and L. B. Nesbitt, Phys. Rev. **78**, 487 (1950)

J. M. Roberts, B. Brown, B. A. Hermann, and J. Tate, Phys. Rev. B **49**, 6890-6894 (1994)

S. J. Rothman, J. L. Routbort, U. Welp, and J. E. Baker, Phys. Rev. B **44**, 2326 (1991)

M. Roulin, A. Junod, A. Erb and E. Walker, Phys. Rev. Lett. **80**, 1722 (1998)

A. I. Rykov, S. Tajima, F. V. Kusmartsev, E. M. Forgan, and C. Simon, Phys. Rev. B **60**, 7601 (1999)

S. Ryu, S. Doniach, G. Deutscher, and A. Kapitulnik, Phys. Rev. Lett. **68**, 710-713 (1992)

H. Safar, P. L. Gammel, D. J. Bishop, D. B. Mitzi, and A. Kapitulnik, Phys. Rev. Lett. **68**, 2672 (1992)

H. Safar, P. L. Gammel, D. A. Huse, D. J. Bishop, W. C. Lee, J. Giapintzakis, and D. M. Ginsberg, Phys. Rev. Lett. **70**, 3800-3803 (1993)

A. Sawa, H. Yamasaki, Y. Mawatari, H. Obara, M. Umeda, and S. Kosaka, Phys. Rev. B **58**, 2868-2877 (1998)

A. Schilling, R. A. Fisher, N. E. Phillips, U. Welp, D. Dasgupta, W. K. Kwok, and G. W. Crabtree, Nature (London) **382**, 791 (1996)

A. Schilling, R. A. Fisher, N. E. Phillips, U. Welp, W. K. Kwok, and G. W. Crabtree, Phys.Rev. Lett. **78**, 4833 (1997)

H. Schmid, E. Burkhardt, B. N. Sun, and J. P. Rivera **157**, 555 (1989)

V.V. Schmidt, The Physics of Superconductors, Nauka Publishers, Moskau, ch. 5, (1982)

A. Schilling, R. A. Fisher, N. E. Phillips, U. Welp, W. K. Kwok, and G. W. Crabtree, Phys.Rev. Lett. **78**, 4833 (1997)

T. J. Shaw, J. Clarke, R. B. van Dover, L. F. Schneemeyer, and A. E. White, Phys. Rev. B **54**, 15411-15416 (1996)

K. Shibata, T. Nishizaki, T. Sasaki and N. Kobayashi, Phys. Rev. B **66**, 214518 (2002)

E. R. Soares, K. F. Raihn, A. A. Davis, R. L. Alvarez, P. Marozick and G. L. Hey-Shipton, IEEE Trans. Appl. Supercond., **9** 4018-4021 (1999)

A. Soibel, E. Zeldov, M. Rappaport, Y. Myasoedov, T. Tamegai, S. Ooi, M. Konczykowski, V. B. Geshkenbein, Nature **406**, 282-287 (2000)

A. R. Strnad, C. F. Hempstead, and Y. B. Kim, Phys. Rev. Lett. **13**, 794-797 (1964)

P. F. Sullivan and G. Seidel, Phys. Rev. **173**, 679, (1968)

J. R. Thompson, Yang Ren Sun, F. Holtzberg, Phys. Rev. B **44**,1 (1991)

J. R. Thompson, Y. R. Sun, H. R. Kerchner, D. K. Christen, B. C. Sales, B. C. Chakoumakos, A. D. Marwick, L. Civale, and J. O. Thomson, Appl. Phys. Lett. **60** (18), 2306 (1992)

J. R. Thompson, Y. R. Sun, L. Civale, A. P. Malozemoff, M. W. McElfresh, A. D. Marwick, and F. Holtzberg, Phys. Rev. B **47**, 14440-14447 (1993)

E. V. Thuneberg, J. Kurkijärvi, and D. Rainer, Phys. Rev. B **29**, 3913-3923 (1984)

M. Tinkham, Introduction to Superconductivity (New York: McGraw-Hill) ch 5, (1975)

M. Tinkham, Phys. Rev. Lett. **61**, 1658 (1988)

H. Träuble and U. Essmann, J. Appl. Phys. **25**, 273 (1968)

C. C. Tsuei, J. R. Kirtley, C. C. Chi, Lock See Yu-Jahnes, A. Gupta, T. Shaw, J. Z. Sun, and M. B. Ketchen, Phys. Rev. Lett. **73**, 593–596 (1994)

C. J. van der Beek, M. Konczykowski, V. M. Vinokur, T. W. Li, P. H. Kes, G. W. Crabtree, Phys. Rev. Lett. **74**, 1214 (1995)

L. N. Vu, M. S. Wistrom and D. J. Van Harlingen, Physica B, **194**, 1791-1792 (1994)

U. Welp, M. Grimsditch, H. You, W. -K. Kwok, M. M. Fang, G. W. Crabtree, and J. Z. Liu, Physica C **161**, 1 (1989)

U. Welp, J. A. Fendrich, W. K. Kwok, G. W. Crabtree, and B. W. Veal., Phys. Rev. Lett. **76**, 4809 (1996)

D. Winkler, Supercond. Sci. Technol. **16** 1583-1590 (2003)

T. K. Worthington, M. P. A. Fisher, and D. A. Huse, Phys. Rev. B **46**, 11 854 (1992)

M. K. Wu, J. R. Ashburn, C. J. Torng, P. H. Hor, R. L. Meng, L. Gao, Z. J. Huang, Y. Q. Wang and C. W. Chu, Phys. Rev. Lett. **58**, 908 (1987)

G. C. Xiong, H. C. Li, G. Linker, and O. Meyer, Phys. Rev. B **38**, 240-243 (1988)

[1] N.-C. Yeh, W. Jiang, D. S. Reed, A. Gupta, F. Holtzberg, and A. Kussmaul, Phys. Rev. B **45**, 5710 (1992)

K. Yokota, T. Kura, S. Katayama, M. Ochi, M. Murakami, A. Chayahara, and M. Satho, Phys. Rev. B **45**, 3098-3102 (1992)

J. F. Zeigler, J. P. Biersack, U. Littmark, The Stopping and Range of Ions in Solids vol.1, (Pergamon Press, 1986)

E. Zeldov, D. Majer, M. Konczykowski, V. B. Geshkenbein, V. M. Vinokur, H. Shtrikman, Nature (London) **375**, 373 (1995)